Abstract

Title of Dissertation: EPIGENETICS OF NEURODEGENERATION: QUANTIFICATION OF HISTONE DEACETYLASE ISOFORMS AND POST-TRANSLATIONAL MODIFICATIONS OF HISTONES IN ALZHEIMER'S DISEASE

Kyle Anderson, Doctor of Philosophy, 2015

Dissertation Directed By: Professor Catherine Fenselau
Department of Chemistry and Biochemistry

Dr. Illarion V. Turko
National Institute of Standards and Technology
Institute for Bioscience and Biotechnology Research

Histone post-translational modifications have been implicated in many biological functions and diseases and serve an important role in epigenetic regulation of gene expression. Aberrant modulations in histone post-translational have been suggested to occur in the brain as part of Alzheimer's disease (AD) pathology, consistent with the epigenetic blockade of neurodegeneration. This dissertation details the development and optimization of unique protein standards for quantification, called quantification concatamers, for the absolute quantification of histone deacetylase isoforms in human frontal cortex with AD, human neural retina with AD and age-related macular degeneration, and whole brain hemisphere of a 5XFAD mouse model of AD. Histone deacetylases are enzymes responsible for the deacetylation of histones, which can directly regulate transcription, and have been implicated in AD pathology. In addition to measuring isoforms of histone-modifying enzymes, measurements of post-

translational modifications on histones were also obtained for whole hemispheres of brain from 5XFAD mice and frontal cortex from human donors affected with AD. For the changes in post-translational modifications observed, structural mechanisms were proposed to explain alterations in the DNA-histone affinity in the nucleosome, which can modulate gene expression. Measurements and structural mechanisms were consistent with the global decrease in gene expression observed in AD, which supports the data. This body of work aims to better elucidate the epigenetic pathology of AD and to aid in identification of histone-modifying enzymes involved in AD pathology for drug targets and treatment options. Currently, there are no treatments that prevent, delay, or ameliorate AD, stressing the crucial importance of AD pathology research and the promise of epigenetics as the solution.

EPIGENETICS OF NEURODEGENERATION: QUANTIFICATION OF HISTONE DEACETYLASE ISOFORMS AND POST-TRANSLATIONAL MODIFICATIONS IN ALZHEIMER'S DISEASE

by

Kyle W. Anderson

Dissertation submitted to the Faculty of the Graduate School of the
University of Maryland, College Park in partial fulfillment
of the requirements for the degree of
Biochemistry
2015

Advisory Committee:
Professor Catherine Fenselau, Chair
Dr. Illarion Turko, Co-Chair
Professor David Fushman
Professor Douglas Julin
Professor John Orban
Professor David Mosser, Dean's Representative

© Copyright by
Kyle Anderson
2015

Acknowledgments

I would like to thank my co-advisor Dr. Illarion Turko for providing opportunities to expand my mass spectrometry knowledge and for his guidance in experimental design that helped me become a proficient scientist. Dr. Meiyao Wang was a tremendous source of insight and help, both professionally and personally, and I would like to thank her for her contributions to my development. I would like to thank Dr. Junjun Chen for her assistance with QconCAT design and expression. Dr. Wei Yuan was the first person to teach me mass spectrometry in a laboratory setting and helped me develop a strong understanding of instrumentation, metabolomics, and analytical techniques. Dr. James Edwards was my first advisor in graduate school and provided a solid foundation in mass spectrometry and metabolomics. I also appreciate Dr. Irina Pikuleva for her collaborations. Finally, I would like to thank Dr. Fenselau and my committee for their guidance throughout my graduate studies.

Table of Contents

List of Tables

List of Figures

List of Abbreviations

Abbreviation	Meaning
Aβ	amyloid beta
AD	Alzheimer's disease
AMD	age-related macular degeneration
APP	amyloid precursor protein
CDR	Clinical Dementia Rating
CID	collision induced dissociation
DTT	dithiothreitol
ESI	electrospray ionization
HDAC	histone deacetylase
HPLC	high performance liquid chromatography
LC-MS/MS	liquid chromatography tandem mass spectrometry
m/z	mass to charge ratio
MALDI-TOF	matrix-assisted laser desorption ionization time-of-flight
MRM	multiple reaction monitoring
MS	mass spectrometry
NFT	neurofibrillary tangle
NIST	National Institute of Standards and Technology
PMI	post-mortem interval
PTM	post-translational modification
QTOF	quadrupole time-of-flight
SDS	sodium dodecyl sulfate

Chapter 1: Introduction

1.1 Neurodegeneration

The brain is a complex organ responsible for our learning, memory, motor control, cognition, homeostasis, motivation, and the way we perceive the world around us. The human brain is highly developed relative to other vertebrates; humans have the largest ratio of brain mass to body mass of any vertebrate [1]. A human brain contains approximately 86 billion neurons and trillions of synapses [2], establishing an extensive signaling network. While the human brain is only about 2% of the total body mass, it accounts for nearly 20% of body energy consumption due to the high metabolic demand of the neurons [2]. Despite the capabilities and nourishment of this vital organ, it is susceptible to degenerative conditions that can be debilitating and deadly.

Neurodegeneration is a broad term that describes numerous conditions of deterioration that affect neuronal health. Progressive degeneration of the brain can lead to debilitating problems, most commonly ataxia, dementia, and death. Of the 25 recognized neurodegenerative diseases, the majority are associated with specific protein amyloids or aggregates (Table 1.1) [3]. Diseases caused by protein amyloids or aggregates are protein conformational diseases where misfolding of soluble proteins typically generates highly ordered fibrillar aggregates [4]. When these aggregates are found in the extracellular environment, they are commonly referred to as plaques. Amyloid fibrils may occur within the cell and are referred to as intracellular inclusions, though their structure and morphology may be consistent with those present extracellularly

[5]. About 85% of neurodegenerative diseases are sporadic, such as Alzheimer's disease (AD), while approximately 10% are hereditary and are the result of genetic mutations [4]. Additionally, 5% of neurodegenerative diseases are transmissible, such is the case for spongiform encephalopathies caused by infectious prions [4]. There have also been reports of acceleration of amyloidosis in mice by injection or ingestion of preformed fibrils, suggesting that amyloid formation is increased by the presence of amyloid [6,7].

Table 1.1 - Neurodegenerative diseases [3]

Disease	Protein/Peptide Aggregate
Alzheimer's disease (AD)	amyloid β, tau
Parkinson's disease	α-synuclein
Dementia with Lewy bodies	α-synuclein
Multisystem atrophy	DJ-1
Frontotemporal dementia	tau
Amyotrophic lateral sclerosis	SOD1, DNA/RNA binding proteins co-localizes with TDP-43 and ubiquitin
Frontotemporal lobar degeneration	DNA/RNA binding proteins co-localizes with TDP-43 and ubiquitin
Huntington's disease	Huntingtin
Polyglutamine diseases	ataxins, atrophin-1, androgen receptor
Prion diseases	prion protein
Familial amyloidotic polyneuropathy	transthyretin, apolipoprotein A1, gelsolin
Serpinopathies (familial encephalopathy)	neuroserpin
Neurodegenerative disorders from aging	actin

The primary sequence of a protein generally dictates a specific folded structure that allows for the protein to function. Misfolding of proteins is often mitigated by chaperones under normal conditions. Occasionally, aberrant misfolding of proteins can produce very stable amyloids that are resistant to refolding and degradation [8]. Amyloids possess a β-sheet structure that is usually more thermodynamically stable than the native folded protein [9]. Antiparallel stacking of twisted pleated β-sheets of monomers forms a hydrophobic core along the fibril axis that facilitates formation of higher ordered structures of oligomers and mature fibrils [10]. The heterogeneity of amyloid fibrils varies their toxicity and more recent research has shown that amyloid oligomers may be even more cytotoxic than originally thought [11]. An illustration of heterogeneity in amyloid assemblies is presented in Figure 1.1 [8]. Amyloid plaques can also contain other components in addition to amyloids, including apolipoproteins, collagen, glycosaminoglycans, metal ions, and glycoproteins [12]. Association between plaque constituents and pathology of amyloidosis in disease is another area of study for this reason.

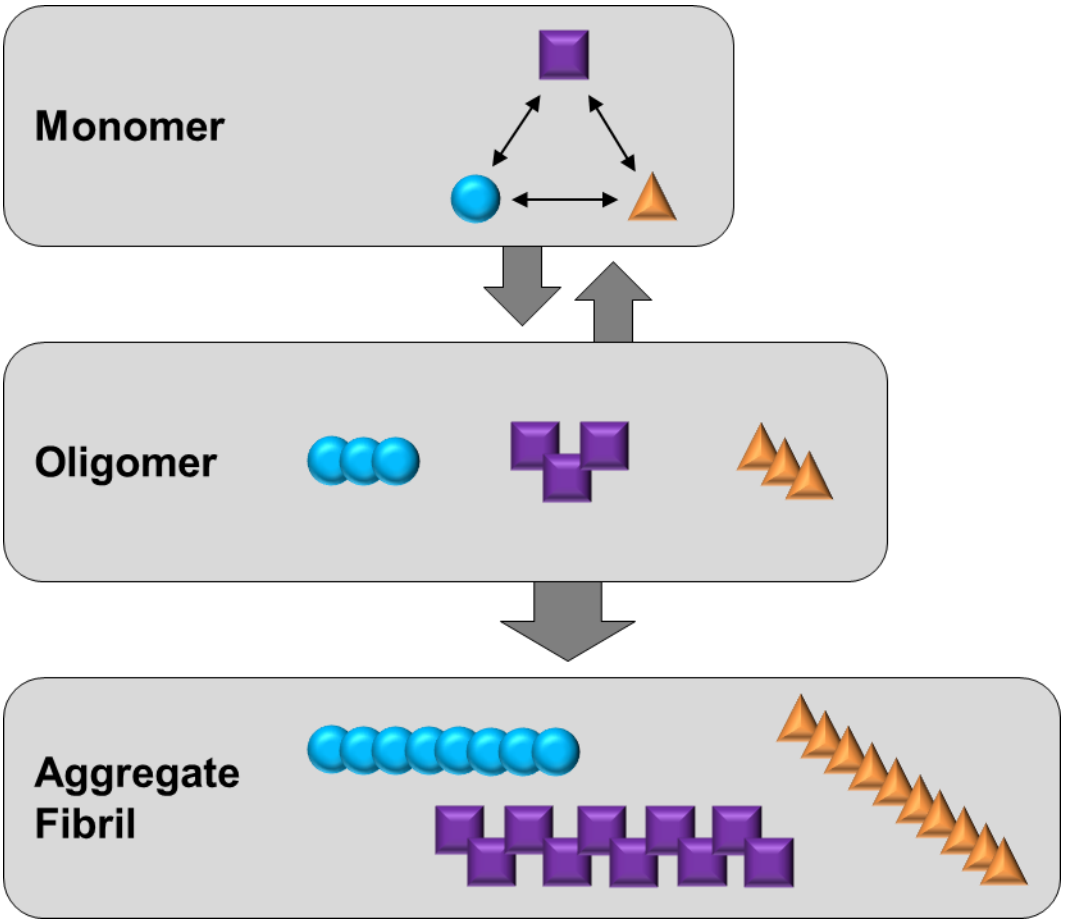

Figure 1.1 - Heterogeneity in amyloid assemblies.
Amyloid monomers are structurally dynamic and adopt several conformers, which may associate into distinct oligomeric structures and aggregates that are structurally stable. Cytotoxicity and other physiological implications vary by amyloid conformer and level of assembly [8].

1.2 Alzheimer's Disease

1.2.1 Prevalence and Impact

Alzheimer's disease (AD) is the leading neurodegenerative disorder and the sixth leading cause of death in the US [13]. AD accounts for over 80% of cases of dementia [13], which most frequently affects the senior population. AD affects approximately 13% of people over the age of 65 years and 45% over 85 [13]. Of the 5.3 million individuals with AD in the US, two-thirds are women [13]. Additionally, Hispanic and black ethnicities are more likely to develop AD than whites [13]. With the increasing population and advancements that have enabled people to live longer, more cases of AD are appearing. If current trends persist, the number of AD cases in the US will triple to 13.8 million in 2050 [13]. Unfortunately, AD is the only cause of death in the top ten in the US that cannot be prevented, slowed, or cured.

In 2015, AD will cost the US $226 billion and is projected to cost $1.1 trillion by 2050 [13]. Two-thirds of the cost for AD is provided by Medicare and Medicaid [13]. AD is the most financially costly disease [13], owing to the long-term care and lack of successful treatments. If a treatment were available now that could delay the onset of AD symptoms for only 5 years, Medicare and Medicaid would save an estimated $42 billion in the year 2020 alone [13]. Currently, for every $310 of Medicare and Medicaid spent on AD, there is only $1 being spent on research at the National Institutes of Health (NIH). The US government is aware of the rising number of cases and the financial burden on the country and, therefore, has created initiatives and increased NIH spending.

The NIH received a $45 million increase in AD research spending in 2013 and another $100 million in 2014. Clearly, the concern for treatment options for AD has been realized. However, the causation of sporadic AD remains unknown, keeping drug targets elusive.

1.2.2 Features of AD

Dementia is a defining symptom of AD that is often, and erroneously, generalized as memory loss. While memory loss is a component of dementia, dementia also includes impairment of cognition and social abilities. On the molecular level, hallmarks of AD are extracellular plaques of Aβ and intracellular neurofibrillary tangles (NFT) of tau protein.

Staging of AD is an important concern when comparing datasets obtained from patients. There are two main methods of staging AD severity in acceptance, Clinical Dementia Rating (CDR) and Braak staging. As the name implies, CDR is focused on the severity of the dementia to assess how advanced the disease is for a patient. For CDR, there are numerous questions in various categories that are answered in a patient interview. The question categories are memory, orientation, judgement and problem solving, community affairs, home and hobbies, and personal care. Answers are scored by category and a composite score is provided using an algorithm [14] to provide a CDR of none (0), questionable (0.5), mild (1), moderate (2), or severe (3). The Braak staging focuses on the degree of NFT of tau as well as the regions of the brain affected as identified by immunohistochemistry. There are six stages for Braak, from I to VI. Braak I/II are characterized by entorhinal NFT distribution, Braak III/IV include

limbic distribution, and Braak V/VI includes neocortical distribution [15]. While Aβ may be a widely known indicator of AD, it is not used to evaluate severity due to the complexity and diversity of Aβ that include diffuse plaques, cored plaques, amyloid lakes, and subpial bands [15]. Additionally, different types of deposits develop in different brain regions, preventing the use of Aβ for assessment of severity [15]. In addition to these two main methods of staging, there are lesser used scoring criteria such as the CERAD score proposed by the Consortium to Establish a Registry for AD, which also uses NFT density and distribution, and the National Institute of Aging's Reagan Institute Criteria, which combines the CERAD and Braak scoring methods to determine the probability that the patient's dementia is attributed to AD. Tissues collected from patients used the patient's score from one of these staging methods to be used to characterize samples for pathology research. While there is not a consensus scoring method established, variation between scoring methods is minimal and tissue from patients ranked with severe AD may be effectively compared to tissue from patients with no detectable indicators to identify notable features of AD pathology.

1.2.3 APP Processing and Aβ

The amyloid precursor protein (APP) is a large transmembrane protein that is expressed in healthy cells, but most abundantly in neurons and concentrated near synapses. Alternative splicing produces three main isoforms of APP, which include the full length canonical sequence with 770 amino acids and two isoforms with 695 and 751 amino acids. APP(770) and APP(751) are primarily found in nonneuronal tissue, while the APP(695) isoform (Figure 1.2B)

is predominately expressed in neurons [16]. In the brain, APP acts as a surface receptor for neuronal adhesion, dendrite growth, axongenesis, mobility, and transcription regulation. Transcription is promoted by APP binding to APBB1 [17] and by binding to Numb to inhibit Notch signaling [18]. However, aberrant processing of APP in neurons (Figure 1.2A) is associated with AD.

APP is translocated into the membrane of the endoplasmic reticulum by the 17-amino acid signal peptide on the N-terminus. During maturation in the secretory pathway, this signal peptide is removed and APP is moved to the plasma membrane of the cell surface. Additionally, APP may be cleaved by α-secretase and secreted as a soluble fragment APP_S-α. Upon cleavage by β-secretase, the extracellular domain of APP is secreted as APPS-β. The remaining portion of APP that contains Aβ can then be cleaved within the membrane by γ-secretase to release Aβ. The intracellular domain (ICD) is then released inside the cell and may act as a signaling molecule. Other transmembrane proteins, such as Notch, CD44, cadherin, low-density lipoprotein-receptor-related protein, and receptor tyrosine kinase ErdB4, can also be cleaved by γ-secretase and their ICDs can act as signaling molecules within the cell [19]. ICDs can activate nuclear signaling pathways, which can result in histone modifications and epigenetic changes [20].

The function of γ-secretase is actually provided by a complex of proteins: presenilin (PS1/PS2), nicasterin (NCT), presenilin enhancer (Pen), and anterior pharynx-defective 1 (Aph). All four proteins are required for γ-secretase activity [21].

A

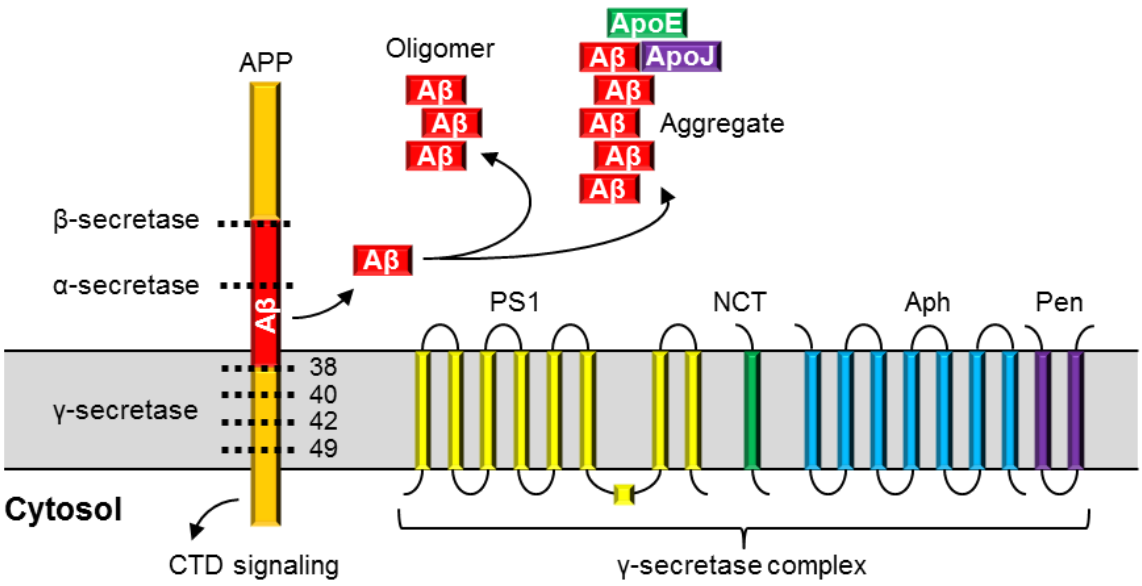

B

APP(695) Sequence:

MLPGLALLLLAAWTARALEVPTDGNAGLLAEPQIAMFCGRLNMHMNVQNGKWDS
DPSGTKTCIDTKEGILQYCQEVYPELQITNVVEANQPVTIQNWCKRGRKQCKTHPH
FVIPYRCLVGEFVSDALLVPDKCKFLHQERMDVCETHLHWHTVAKETCSEKSTNLH
DYGMLLPCGIDKFRGVEFVCCPLAEESDNVDSADAEEDDSDVWWGGADTDYADG
SEDKVVEVAEEEEVAEVEEEEADDDEDDEDGDEVEEEAEEPYEEATERTTSIATTT
TTTTESVEEVVRVPTTAASTPDAVDKYLETPGDENEHAHFQKAKERLEAKHRERM
SQVMREWEEAERQAKNLPKADKKAVIQHFQEKVESLEQEAANERQQLVETHMAR
VEAMLNDRRRLALENYITALQAVPPRPRHVFNMLKKYVRAEQKDRQHTLKHFEHV
RMVDPKKAAQIRSQVMTHLRVIYERMNQSLSLLYNVPAVAEEIQDEVDELLQKEQN
YSDDVLANMISEPRISYGNDALMPSLTETKTTVELLPVNGEFSLDDLQPWHSFGAD
SVPANTENEVEPVDARPAADRGLTTRPGSGLTNIKTEEISEVKMDAEFRHDSGYEV
HHQKLVFFAEDVGSNKGAIIGLMVGGVVIATVIVITLVMLKKKQYTSIHHGVVEVDAA
VTPEERHLSKMQQNGYENPTYKFFEQMQN

Figure 1.2 - APP processing and Aβ in AD.
(A) Presenilin (PS1/PS2), nicasterin (NCT), anterior pharynx-defective 1 (Aph), and presenilin enhancer (Pen) together form the γ-secretase complex, which cleaves APP within the membrane region. Aβ is released after β- and γ- secretase cleavage, and can associate into soluble oligomers or aggregate into insoluble amyloid plaques. Other APP cleavage products act as signaling molecules. **(B)** The sequence of APP(695) is shown with the Aβ region shown in red.

The site of cleavage by γ-secretase is variable, with the most frequently cleaved site in healthy tissue yielding Aβ1-38. However in AD, Aβ1-42 is predominately produced and is more prone to aggregation and oligomerization than Aβ1-38, which is likely due to the additional hydrophobic residues 39-42 [11]. Mutations in APP and processing enzymes can affect the preference for Aβ1-42 production and its pathogenicity. Mutations in APP flanking the Aβ sequence can favor Aβ1-42, while mutations within Aβ can directly augment the ability to form oligomers and aggregates [11]. Similarly, mutations in PS1/PS2, the component of the γ-secretase complex that contains the proteolytic domain, can also increase APP processing. While not all cases of AD contain mutations in proteins associated with APP processing, identified mutations are inheritable and have been implemented in animal models of amyloidogenesis.

1.2.4 Sporadic and Familial AD

In the vast majority of cases of AD, the disease is considered sporadic or late-onset, which the cause is not known. In about 5% of cases, AD can be caused by specific point mutations in the genome, known as familial or early-onset AD. Familial AD was recognized in families where members developed AD around the age of forty, noticeably younger than late sixties and older as is common in sporadic AD. Observed families had mutations in either APP or PS1/PS2 which led to an increased production of Aβ1-42. Several of the mutations were named after the location of the families carrying the mutation, for example the substitution of isoleucine for valine at position 716 on APP is called the Florida mutation. Other common familial mutations are APP K670N/M671L

(Swedish), APP V717I (London), PS1 M146L, and PS1 L286V. While specific mutations have been identified in familial AD, it is not known what causes AD in sporadic cases. There are also polymorphisms in apolipoprotein E (ApoE) that are linked to an increased predisposition of AD. However, unlike mutations in APP and PS1, ApoE polymorphisms are not indicators of disease, but rather increase the propensity of developing AD [16]. However, amyloid production is consistent in both sporadic and familial AD, which indicates similarities in pathology, while exact etiology may vary by individual. Similar to the heterogeneity of cancer, heterogeneity in AD etiology makes AD research more complex. The complexity is compounded by difficulty in acquisition of neuronal samples from humans. It is not feasible to collect brain biopsies throughout an individual's life to monitor disease pathology, therefore only post-mortem brain tissue is available. Due to limitations in acquisition of human brain tissue for studying the pathology of AD, animal models are a common tool used to simulate AD in humans.

1.2.5 Animal Models of Amyloidosis

Mouse models are the most popular animal models for amyloidosis and AD. Mice do not naturally develop AD-like disease, due to either their relatively short longevity or murine biology; therefore transgenic mice are created specifically to develop AD. Common models include overexpression of human proteins with mutations associated with familial AD in humans. One common mouse model of AD is called 5XFAD, so called for its five mutations of familial AD [22]. 5XFAD mice coexpress two transgenes, yielding high levels of mutant

human APP and PS1 in neurons. The transgenes are placed under control of the mouse *Thy1* promoter, which normally expresses the Thy1 cell surface antigen in mature neurons. Mutant APP and PS1 proteins contain the following mutations: APP(695) with Swedish (K670N, M671L), Florida (I176V), and London (V717I) and PS1 with M146L and L286V. 5XFAD mice preferentially produce Aβ1-42 and rapidly develop senile plaques beginning at 1.5 months [22]. Tau neurofibrillary tangles are not present in 5XFAD mice. Gliosis begins when mice reach 2 months and mice also develop extensive neuronal loss. Additionally, these mice exhibit severe cognitive impairment, which includes impaired spatial memory, stress-related memory, and remote memory stabilization [22].

A benefit to using brain from mice rather than humans is that mice may be sacrificed quickly by decapitation or cervical dislocation and brain tissue can be rapidly collected and flash frozen. This is of particular importance when studies are to be performed on PTMs or target molecules that may be degraded shortly after death in the presence of heat and the milieu of biological reactions occurring in the body. The post-mortem interval, defined as the time between death and the tissue being cryopreserved, is typically in the range from several hours to a day. Labile PTMs and target molecules may be lost during this time, potentially leading to high variability and inaccuracy in measurements. Additionally, the quick method of sacrificing mice ensures tissue is not stressed in the process, which may happen during the process of death in humans and can contribute to inadvertent changes in targets.

Nonhuman primate models of AD have demonstrated that they may be potentially better at modeling AD pathology. Macaques can develop amyloid plaques naturally late in life near 30 years of age. However, considering the time for primates to reach advanced age and the percentage of the population that will actually display amyloidosis, it is not practical to allow primates to naturally develop amyloidosis [23]. Similar to mouse models, injection of Aβ oligomers into the brain may be performed to evaluate pathological features. An interesting observation is that primate models administered Aβ oligomers develop tau phosphorylation and neurofibrillary tangles, which are not present in mice unless tau mutants are expressed [24]. Primate studies may be more biologically revelant than mouse studies, however, primate studies can be prohibitively expensive and mouse models are a more economical approach. Despite animal models simulating disease pathology in humans, they are limited to carrying familial AD mutations or administration of amyloids, which may have deviances from sporadic AD pathology. The majority of research in AD has been performed using mouse models, which is ideal for early exploration of disease pathology. However, the importance of measurements from human donors with AD should be considered to validate observations in animal models.

1.2.6 Treatments and Therapies

There are currently no available treatments that can cure or stop the progression of AD. A range of clinical trials have been made that include, immunotherapy targeting Aβ, small molecule inhibition of Aβ production and aggregation, anti-inflammatory drugs, and inhibition of epigenetic alterations. For

immunotherapy, antibodies may be produced either by Aβ-peptide vaccination [25] or by passive infusion of anti-Aβ antibodies [26]. Glycosaminoglycans and glycolipids associated with aggregation of Aβ have been targeted by small molecules and have been shown to reduce plaques in mice [27,28]. Inhibition of APP processing enzymes, such as γ-secretase, has also been explored. However, due to the role of APP in normal physiology, direct inhibition of γ-secretase was shown to be deleterious [29]. Anti-inflammatory drugs, such as NSAID derivative R-flurbiprofen, have been shown to reduce inflammation associated with AD and indirectly reduce γ-secretase activity [30]. Another class of drug candidates that are not directly related to Aβ is HDAC inhibitors. Epigenetic changes have been discovered in AD, namely deacetylation of histone tails, which affect gene expression. Inhibition of histone deacetylases has been shown to reduce cognitive impairment and may be a promising treatment [31]. Currently, therapeutic HDAC inhibitors target many HDAC isoforms, a particularly detrimental approach when HDAC isoforms are known to have different and specialized functions. While many AD therapies are focused on Aβ, Aβ may very well be a side product of detrimental intracellular signaling. Moreover, sporadic AD does not appear to be caused by mutations in genes encoding proteins in APP processing, turning the focus toward intracellular signaling and epigenetic regulation.

1.3 Epigenetics and the Histone Code

1.3.1 PTMs and Regulation

DNA is packaged into the eukaryotic nucleus as chromatin, a structure comprised of nucleosomes formed by 146 base pairs of DNA wrapped around an octamer of duplicates of histones H2A, H2B, H3, and H4. These histones are dynamically modified by post-translational modifications (PTMs), known as the “histone code”, which can regulate gene expression. Disruption of these PTM codes through the use of inhibitors can affect cell cycle, alter gene expression, and induce apoptosis [32]. Studies on monozygous twins suggest that AD may be caused by epigenetic factors, an explanation for different outcomes when the DNA sequence is conserved [33]. Once acquired, epigenetic factors, such as DNA methylation and histone PTMs, can be passed on to offspring cells [34]. The most common PTMs in histones are acetylation, methylation, phosphorylation, and ubiquitination (Figure 1.3). Histone PTMs are classified into two main mechanisms of function: *cis* and *trans*. *Cis* mechanisms modify interactions within and between nucleosomes, while *trans* mechanisms act as signals for other proteins to assist in alteration of gene expression, chromatin, or other cellular functions [34]. Histone PTMs alter chromatin structure by dictating histone-DNA and inter-nucleosome interactions [35]. Changes in chromatin structure regulation have been linked to neurodegeneration and AD, giving credence to focusing on epigenetic targets for treatment of neurodegeneration [36–38].

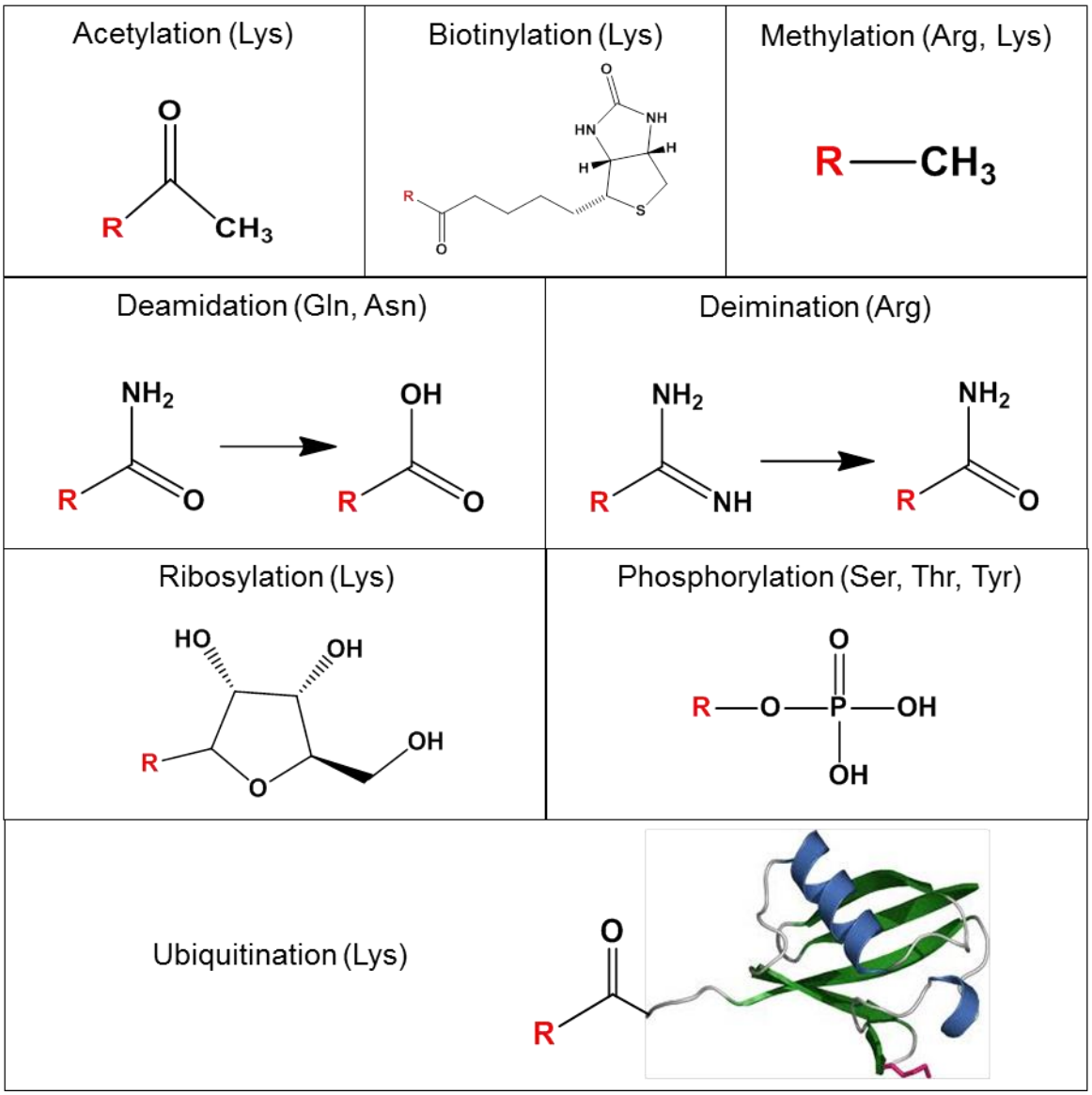

Figure 1.3 - Common histone PTMs.
There are several PTMs found in histones with acetylation, methylation, and phosphorylation being the most abundant.

1.3.2 Acetylation

One of the most common PTMs in histones is acetylation. Histone acetylation can occur on the primary amine of lysine residues and is catalyzed by histone acetyltransferase (HAT) and removed by various histone deacetylases (HDACs). The major region of acetylation occurs on the tail region of histones. The N-terminal tails of histones extend beyond the nucleosome and are very flexible. Additionally, they are rich in positively charged lysine and arginine residues. When the histone tail is not hypoacetylated, the positively charged tail interacts with the negatively charged backbone of DNA, forming a tighter nucleosome structure. The tight nucleosome facilitates packaging into dense chromatin, which is less transcriptionally active. Hyperacetylated tails have the opposite effect; acetylation neutralizes the charge on the tail region and the histone tails act as spacers between nucleosomes, characteristic of transcriptional activity. There is strong evidence that HDACs, rather than HATs, have significant role in the pathology of neurodegeneration [31]. There are 11 main isoforms of HDAC with a total of 38 variants in humans. Inhibition of HDACs is currently performed with broad inhibitors that affect many or all isoforms of HDACs. More studies need to be conducted on HDACs to determine which isoforms are associated with disease pathology so that HDAC inhibitors could be better targeted for improved safety and efficacy.

1.3.3 Methylation

Lysine residues may be mono-, di-, or tri-methylated and arginine residues may be mono- or di-methylated, with arginine demethylation being symmetric or

asymmetric. Methylation was originally thought to be an irreversible modification; however, it has been shown to be reversible with trimethylation being less dynamic than dimethylation and monomethylation. The degree of histone methylation often relates to the epigenetic function, but it is not absolute. For example, monomethylation is frequently a mark of transcription activation, while trimethylation is frequently associated with transcription repression [34]. Methylation of histones is catalyzed by histone methyltransferases (HMTs) and removal is catalyzed by histone demethylases (HDMs). The demethylase families identified predominately act on lysine and are the lysine-specific demethylases (LSD/KDM) and the jumonji C-domain-containing iron-dependent dioxygenases (JMJD). Despite efforts by others, arginine demethylases are not well characterized [39]. Methylation is involved in important biological functions including transcriptional regulation, chromatin remodeling, DNA repair, RNA processing, signal transduction [34]. The complexity of functions and related enzymes stresses the importance of identifying specific sites of methylation in histones. Additionally, combinatorial effects from histone PTMs are common with methylation [40]. Unlike histone acetyltransferases, histone methyltransferases are considerably more site specific and often are responsible for modifying only a single site on histones. Thus it is important to identify the specific sites of histone methylation and their changes relevant to pathology.

1.3.4 Phosphorylation

Phosphorylation can occur on serine, threonine, and tyrosine residues. Histone phosphorylation has been linked to activation and repression of genes

based on site of modification and condition of cells [41–43]. The kinases and phosphatases that regulate histone phosphorylation are diverse and each site is often modified by a single enzyme [44]. Phosphorylation can regulate histone by two mechanisms. One method is the phosphorylation mark acts as signal for regulatory enzymes to perform a function on the phosphorylated nucleosome complex. Another mechanism is the modulation of electrostatic charges on the histone. Introduction of phosphate groups increases the negative charge in the local environment. Attraction between the negative charge on the phosphorylated residue and a neighboring positively charged residue, lysine or arginine, could facilitate structural changes. Likewise, negatively charged amino acid residues and the phosphate backbone of DNA would be repulsed by the phosphorylated residue. It is possible that nucleosome stability could be directly influenced by phosphorylation events on the DNA-histone interface.

1.3.5 Other Histone PTMs

There are several other less common PTMs found in histones. Ubiquitination is less common than the previously described PTMs, which is likely owing to the relatively large size of ubiquitin. The bulky 8.5 kDa protein is restricted to modification sites and is mostly found on linker H1 and to a lesser extent on the exposed histone core away from the DNA-histone interface. Monoubiquitination is the dominant form of histone ubiquitination as polyubiquitination is typically associated with degradation. Ubiquitination of histone residues has the potential to alter the affinity of histone-histone interactions within the nucleosome [45], indicate the presence of DNA damage

[46,47], and be a marker for other functional roles. While ubiquitin is 8.5 kDa, only its two glycines from the C-terminus remain on modified lysines after digestion with trypsin, the most common enzyme for MS proteomics. The diglycine modification yields a mass increment of 114.043 Da. Polyubiquitin chains are not easily observed in proteomics analysis of histones as the diglycine modification is the only remnant of ubiquitination and does not indicate the degree of ubiquitination.

Other less frequent histone PTMs are deamidation, deamination, biotinylation, and ribosylation. Deamidation of glutamine and asparagine residues is mainly localized to histone H1 variants and is linked to aging [48].. Deimination, often called citrullination, of arginine residues is catalyzed by peptidylarginine deiminases and this modification is thought to prevent other PTMs from occurring on the deiminated arginine [49]. Deimination causes the mass to increase by 0.984 Da, which is difficult to distinguish from isotopic peaks when using MS. Biotinylation of lysine residues is catalyzed by holocarboxylase synthetase and removed by biotinidase. Biotinylation has been implicated in gene silencing by changing the nucleosome structure [50]. Ribosylation is of very low abundance in histones and is typically not detectable with MS, therefore ribosylation studies are usually performed using more sensitive methods, such as Western blotting or radioactivity assays [34]. In rare cases, instances of glutathionylation [51] and propionylation [52] have been reported on H3.

1.4 Mass Spectrometry

1.4.1 Proteomics and Mass Spectrometry

Mass spectrometry (MS) is a powerful technique for characterization and quantification of biological molecules. In simple terms, MS is the measurement of mass to charge (*m/z*) of an ionized analyte and the associated abundance. MS has become an essential tool in proteomics, which is the study of all proteins in a biological system. This is because proteomics is more challenging than genomics and transcriptomics, due to the dynamic range in protein expression and complexity from PTMs, which MS is equipped to address. MS excels in mass accuracy, resolution, sensitivity, dynamic range, and speed. Mass accuracy is important to correctly identify analytes and resolution is important to observe isotopes and modifications with small mass increments, such as deamidation. The sensitivity and dynamic range facilitate the measurement of lowly abundant proteins, such as HDAC [53], and highly abundant proteins, such as Aβ [54], in a single acquisition. MS also allows for rapid analysis and can perform subsecond quantifications [55].

MS measurements can be performed on the protein level, called top-down, or on the peptide level, called bottom-up. Bottom-up analysis typically involves fragmentation of the peptide, which can yield various ions that differ by the site of fragmentation and localization of charge. The most commonly observed ions for peptides fragmented with collision induced dissociation (CID) are y-ions, which are formed by fragmentation of amide bonds with the charge localized on the C-terminus, and b-ions, which are the result of amide bond

fragmentation with charge localized on the N-terminus. Multiple fragments from a single peptide enable sequencing of the amino acids residues. While this feat is too labor intensive to perform manually for large data sets, there are many peptide database search engines that can compile fragmentation data and provide a list of peptides and associated proteins and the confidence of the peptide identities by fragmentation sequencing and mass accuracy. Peptides perform better than proteins in the mass spectrometer because they ionize more easily and their relatively small size generates less possible charge states, which correlates to greater signal intensity. By contrast, proteins are larger and have a much greater heterogeneity in charge states upon ionization, which correlates to lower signal for individual charge states when the protein abundance is divided among them. A benefit to using top-down is that multiple PTMs can be observed on the same protein molecule, permitting a combinatorial assessment of PTMs. This is not possible on the peptide level unless both PTMs are present on the same peptide, which is not often the case. Depending on the application, it is important to use a suitable type of MS instrumentation.

1.4.2 Instrumentation

While MS has been around since the early 1900s, it was not until advances in instrumentation in the 1950s and 1960s did MS begin to take shape as the powerful analytical method we know today. There are various ionization methods, mass analyzers, and detectors used in MS. Of the methods of ionization, the most popular for peptides and proteins is electrospray ionization (ESI) for several reasons. The majority of MS analyses of complex mixtures

involve separation of the peptides or proteins prior to entering the mass spectrometer. Liquid chromatography (LC) is most commonly employed for peptides and proteins, while gas chromatography and capillary electrophoresis are alternatives. LC requires desolvation and ionization, which is provided by ESI. When voltage is applied to the solvent containing the sample before or at the spray emitter, a voltage of the opposite polarity is applied to the source plate to direct the aerosol spray toward the source. The droplets in the aerosol are reduced in size by application of a drying gas and heat, which causes the droplets to have a reduced volume and concentrated charge. When the concentrated charge approaches the Rayleigh limit, the droplets undergo fission and iterative cycles of this yield desolvated analytes.

Analytes that have entered the mass spectrometer may be separated by various mass analyzers. The mass analyzer and parameters used vary based on the intended application. Quantification may be performed on any mass spectrometer, however, triple quadrupoles and hybrid Qtraps are the preferred mass analyzers of choice for targeted quantification. A triple quadrupole consists of an initial quadruple which uses Rf frequencies and voltages to isolate a narrow window of ions with m/z values near the targeted analyte, while other ions are filtered out. The isolated ions, referred to as precursor ions, are then moved to a second quadrupole. In the second quadrupole, ions undergo fragmentation by CID, which is the bombardment of ions with N_2, resulting in increased vibrational energy leading to fragmentation of labile bonds. Fragment ions, referred to as product ions, are then moved to the last quadrupole which functions as another

mass analyzer to isolate only the ions selected for the detector. This platform is used for multiple reaction monitoring (MRM), which consists of multiple transitions (pairs of product ions and their respective precursor ions) generated from CID reactions. MRM is robust and high throughput because the first quadrupole may be selecting precursor ions, while the last quadrupole is selecting product ions from the previous precursor ion, simultaneously. In addition to high throughput, the nature of the acquisition selecting one analyte at a time results in greater stability in ion signal, which results in more reproducible and accurate quantification. Moreover, the selectivity of MRM reduces complexity of ions reaching the detector, preferably to only the target analyte, which results in improved sensitivity as low as the attomole level [56]. One disadvantage of performing MRM on a triple quadrupole is that the mass accuracy is lower than other analyzers. Validation of the identity and retention time of an analyte using mass analyzers with greater mass accuracy prior to MRM on a triple quadrupole is beneficial when investigating a target in a complex mixture.

Characterization of PTMs and determination of intact masses of proteins benefits from MS instrumentation with high mass accuracy and resolution. There are several mass spectrometers in this category, namely Orbitraps and QTOFs, which were included in the work herein. These instruments have the ability to measure an analyte with an error in mass of less than 1 ppm. In addition, the ability to resolve isotopic peaks and discern between unmodified and deamidated peaks can prove highly beneficial depending on the application of the work. Orbitraps inject ions into a large barrel-shaped analyzer with a spindle along the

axis of the barrel's length. Ions are injected perpendicular to the spindle and undergo harmonic oscillations along the spindle, as a result of the applied frequencies, and signals are Fourier transformed for data output. Orbitraps are advantageous in their space-to-charge capacity, which accommodates more ions for improved signal and increases the dynamic range. Smaller *m/z* ions have greater amplitude of oscillations, which generates larger signal intensity. Conversely, large *m/z* ions have lower signal intensity than observed in other mass analyzers, like QTOFs. QTOFs combine a quadrupole with a time-of-flight (TOF) analyzer to separate ions by their time to travel a fixed distance. TOF analyzers can more easily accommodate larger masses than an Orbitrap, however, they are typically not as sensitive.

1.4.3 Methods of Quantification

There are several methods for quantification of proteins in MS, including stable isotope dilution, labeling, and label-free approaches. The most common and widely preferred methods involve the use of stable isotopes. Incorporation of heavy, stable isotopes of carbon, nitrogen, oxygen, or hydrogen can be used to increase the mass of a standard or analyte so that it is distinguishable from an unlabeled or differently labeled analyte by MS. A labeled and an unlabeled peptide have nearly identical chemical properties, which yields consistent ionization efficiency for MS and consistent retention time in chromatography. This is preferable to using a single reference peptide or protein, as is common with Western blotting, for normalization of all target measurements. Labeling of peptides can be performed during proteolysis in the presence of ^{18}O from $H_2{}^{18}O$

in the reaction mixture. ^{18}O incorporates into the carboxylic acid group on the terminus of all proteolytic peptides and ^{18}O-labeled peptides can be mixed with unlabeled peptides with naturally occurring ^{16}O to obtain an isotopic ratio [57]. Isobaric tagging reagents, which also allow multiplexing, can also be used to modify specific functional groups [55]. An alternate to schemes involving modification of proteins or peptides after translation, stable isotopes may be incorporated into proteins or peptides during translation. Synthesized peptides or proteins expressed in cell-free expression systems can have heavy-labeled amino acids incorporated by replacing specific free unlabeled amino acids with labeled amino acids during synthesis. Proteins may also be fully-labeled with ^{15}N when expressed in media with ^{15}N as the sole source of nitrogen. Full-length labeled proteins are likely the best standards for protein quantification because the amino acid sequence flanking a proteolytic digestion site is conserved between the biological protein and the full-length labeled standard protein, resulting in a consistent rate of cleavage. Moreover, supplementing a sample with a full-length protein standard means that all of the measureable peptides are contained in the same standard and variations in peptide abundancies are due strictly to the inherent cleavage fidelity and ionization efficiency for each peptide, not the error in amount of peptide added as seen with individual peptide standards. Additionally, protein standards may be added early in the sample preparation scheme and are processed in parallel to the protein targets. This accounts for sample loss and other errors that may arise during sample preparation that are not reflected when supplementing sample with peptide

standards near the end of a sample processing scheme. More recently, a hybrid between peptide and full-length standards has been developed called a quantification concatamer (QconCAT) [58–60]. QconCATs are novel multiplexing standards that combine multiple peptides for measurement from many proteins and express them as one recombinant protein standard, which benefits from the advantages of full-length protein standards without the need to express many proteins.

Chapter 2: Optimization of QconCAT Technology

This chapter contains published work [61].

2.1 Introduction

Multiple reaction monitoring (MRM) mass spectrometry is commonly used for targeted protein quantification in complex biological samples. Quantification in MRM assay typically relies on stable isotope-labeled internal standard added to the biological sample. In 2005, a new technology was proposed to produce isotopically labeled internal standard for MRM mass spectrometry by genetic engineering [59,62] and was termed QconCAT. QconCAT stands for quantification concatamer and is an artificial protein expressed from a synthetic gene and composed of multiple tryptic peptides (called Q-peptides) from proteins targeted for quantification. As originally proposed [59,62], Q-peptides are directly concatenated in the QconCAT. A pitfall of direct concatenation is that natural amino acid sequences surrounding the sites of trypsin-catalyzed cleavage are not identical in the QconCAT and the target protein [58]. The efficiency of tryptic digestion is likely to be influenced by other residues in close proximity to the cleavage site [63–66]. Therefore, differences in the sequence composition around the cleavage site in QconCATs and target proteins can cause an error in quantification. To avoid potential quantitative discrepancy, the QconCATs with original natural flanking sequences for every Q-peptide were first proposed by Kito et al. [67] and then further used by others [68–71]. Nearly identical efficiency of trypsin digestion for the target protein and QconCAT with flanking sequences

was validated using recombinant clusterin and ^{15}N-labeled clusterin QconCAT [69]. Four- or six-amino acid residues flanking sequences were used by different researchers [67–71]. Flanking sequences can unfortunately occupy a large portion of the QconCAT in addition to the essential Q-peptides. Therefore, it is important to determine experimentally the shortest necessary size of flanking sequences that guarantee identical rates of proteolytic excision of the peptides from the QconCAT and target protein.

In the present study, we selected seven Q-peptides from recombinant human clusterin and supplemented these peptides with natural flanking sequences ranging from none (+0) to six amino acid residues (+6). These peptides were assembled into seven QconCATs in a way that only one specific Q-peptide with only one specific length of natural flanking sequence appears in each QconCAT. MRM measurements on 1:1 molar mixture of clusterin and individual QconCATs demonstrate that more amino acids included into the flanking region may be beneficial for reliable quantification to overcome the effect differences in amino acid composition near the cleavage site.

2.2 Methods

2.2.1 Expression, Purification, and Characterization of QconCATs

Synthetic genes encoding seven QconCATs were synthesized by Biomatik Corporation (Cambridge, Ontario, Canada). The design of these QconCATs includes seven tryptic peptides (Q-peptides) from human clusterin with their natural flanking sequences on both sides of the Q-peptides. Length of the natural flanking sequences ranges from 0 to 6 amino acid residues for each

Q-peptide. Each QconCAT has only one copy of a specific Q-peptide with specific length of the natural flanking sequence. The synthetic genes were cloned into the NdeI/HindIII restriction sites of pET21a expression vector in-frame to the C-terminal His6-tag. For expression, the plasmid was transformed into One Shot BL21(DE3) and cells were cultivated at 37 °C in M9 minimum medium containing 1 g/L $^{15}NH_4Cl$ (Cambridge Isotope Laboratories, Andover, MA) as the sole nitrogen source. Initial inoculation started with 5 mL of LB media and the cells were grown for 6-8 h at 37 °C. Cells were collected by centrifugation at 20,000 g for 20 min and washed once by 10 mL of $^{15}NH_4Cl$-containing M9 medium. Cells were then transferred to 50 mL of $^{15}NH_4Cl$-containing M9 medium and grown for 12-14 h at 37 °C. Cells were collected by centrifugation at 20,000 g for 20 min and washed twice by 100 mL of $^{15}NH_4Cl$-containing M9 medium. Cells were then transferred to 500 mL of $^{15}NH_4Cl$-containing M9 medium. The expression was induced with 1 mmol/L isopropyl β-D-1-thiogalactopyranoside at OD_{600} of 0.6-0.8 and incubated for an additional 3 h at 37 °C. Cells were divided into 10 portions and harvested by centrifugation at 20,000 g for 30 min. One portion of cells was resuspended in 20 mL of lysis buffer (50 mmol/L Tris•HCl, pH 7.5). Cells were disrupted by sonication and centrifuged at 20,000 g for 30 min. The supernatant was discarded. The pellet was resuspended in 3 mL of urea buffer (7 mol/L urea/100 mmol/L NaH_2PO_4/10 mmol/L Tris•HCl, pH 8.0) and ^{15}N-labeled QconCAT was purified on nickel-nitrilotriacetic acid resin (Qiagen, Valencia, CA) in batch mode. The protein concentration of purified ^{15}N-labeled QconCAT was measured using the DC Protein Assay kit and bovine serum

albumin as a standard. The purified ^{15}N-QconCAT was then aliquoted and kept frozen at -80 °C.

To determine the molecular mass of QconCATs, liquid chromatography-mass spectrometry (LC-MS) analyses were performed in positive ion mode with an Agilent 6550 QTOF (Santa Clara, CA) coupled with an Agilent 1200 HPLC (Santa Clara, CA). The QconCAT was eluted from an Agilent ProtID C18 nanochip (75 µm x 150 mm, 300 nm) over a 10-min gradient from 20% to 80% acetonitrile containing 0.1% formic acid at a flow rate of 400 nL/min. Acquisition method in positive mode used capillary temperature 275 °C, fragmentor 180 V, capillary voltage 1950 V, and a 500 m/z to 2000 m/z mass window. Mass deconvolution was later performed using MagTran 1.0 software.

2.2.2 Processing of Samples

20 pmol of human recombinant clusterin (purity > 95%, ProSpec-Tany TechnoGene Ltd, Ness Ziona, Israel), 20 pmol of individual QconCAT, and 20 µg of bovine serum albumin were mixed in 25 mmol/L NH_4HCO_3 buffer/1% SDS/10 mmol/L DTT. The mixture was incubated at room temperature for 60 min to allow reduction of cysteines and was then treated with 55 mmol/L iodoacetamide for another 60 min to alkylate the reduced cysteines. Alkylated samples were precipitated with chloroform/methanol [72] to deplete salts, urea, and SDS from the samples. Protein pellets were then sonicated in 100 µL of 25 mmol/L NH_4HCO_3/0.1% RapiGest and treated with trypsin for 15 h at 37 °C. The substrate/trypsin ratio was 10:1 (w/w). After trypsin digestion, the peptide samples were treated with 0.5% trifluoroacetic acid for 30 min at 37 °C and

centrifuged at 106,000 g for 30 min. After centrifugation, the supernatants were dried using a vacuum centrifuge (Vacufuge, Eppendorf AG, Hamburg, Germany).

2.2.3 LC-MS/MS Analysis

Dried peptides were reconstituted in 30 µL of 3% acetonitrile/97% water containing 0.1% formic acid and 5 µL were used for a single LC-MS/MS run. Instrumental analyses were performed on an Agilent Zorbax Eclipse Plus C18 RRHD column (2.1 mm x 50 mm, 1.8 µm particle) coupled to Agilent 6460 Triple Quadrupole LC/MS system (Santa Clara, CA). Peptides were eluted over a 35-min gradient from 5% to 50% acetonitrile containing 0.1% formic acid at a flow rate of 200 µL/min. The gradient settings were: 5% to 10% solvent B in 5 min, 10% to 30% solvent B in 25 min, 30% to 50% solvent B in 5 min, then returned to 5% solvent B in 5 min. Solvent A was water containing 0.1% formic acid and solvent B was 95% acetonitrile, 5% water, and 0.1 % formic acid. Acquisition method used the following parameters in positive mode: fragmentor 135 V, electron multiplier 500 V, and capillary voltage 3500 V. Collision energy was optimized for each peptide using the default equation from Agilent, CE = 0.036 m/z - 4.8. Dwell time for all transitions was set at 50 ms.

2.3 Results and Discussion

2.3.1 Design of QconCATs

Selection of Q-peptides has size and composition restraints. Peptides that contain less than eight amino acids are typically omitted because of small m/z values. Peptides with Cys or Met are also avoided due to the existence of

various oxidation entities, which could introduce variations in the quantification. In the present study, human clusterin (apolipoprotein J) was selected as a model protein because this secreted protein has an average mass (52.5 kDa) and multiple Cys/Met but allows selection of up to 9 tryptic peptides, which comply with Q-peptide selection criteria. As a first step, the abundance of these Q-peptides in the tryptic digest of recombinant clusterin was determined and 7 Q-peptides were selected based on signal intensity. These 7 Q-peptides were named by Q1 (EIQNAVNGVK), Q2 (TLLSNLEEAK), Q3 (SGSGLVGR), Q4 (IDSLLENDR), Q5 (ASSIIDELFQDR), Q6 (ELDESLQVAER), and Q7 (VTTVASHTSDSDVPSGVTEVVVK). They were then supplemented with natural flanking sequences ranging from 0 to 6 amino acid residues on both sides of each Q-peptide and were arranged in 7 QconCATs in a way that only one specific Q-peptide with only one specific length of natural flanking sequence appears in each QconCAT (Table 2.1).

Table 2.1 - QconCAT sequences, Q-peptides, and natural flanking sequences.
Color codes are: (i) Q-peptides are shown in red, natural flanking sequences are shown in black, an extra N-terminal sequence for improved QconCAT expression is shown in blue, and C-terminal sequence for His_6-tag is shown in blue.

QconCAT #1

MEVWTQRLHGGSAPLPQDRGFLVKEIQNAVNGVKRKTLLSNLEEAKKVCRSG
SGLVGRQLNGDRIDSLLENDRQQTDHFSRASSIIDELFQDRFFTRQAKLRRELD
ESLQVAERLTRKYEDQYYLRVTTVASHTSDSDVPSGVTEVVVKLFDSDPKLAAA
LEHHHHHH

Q-peptide	Sequence	Flanking sequence length
Q1	EIQNAVNGVK	0
Q2	TLLSNLEEAK	1
Q3	SGSGLVGR	2
Q4	IDSLLENDR	3
Q5	ASSIIDELFQDR	4
Q6	ELDESLQVAER	5
Q7	VTTVASHTSDSDVPSGVTEVVVK	6

QconCAT #2

MEVWTQRLHGGSAPLPQDRGFLVNKEIQNAVNGVKQERKTLLSNLEEAKKKR
VCRSGSGLVGRQLEMNGDRIDSLLENDRQQTHQDHFSRASSIIDELFQDRFFT
RESQAKLRRELDESLQVAERLTRKYNRVTTVASHTSDSDVPSGVTEVVVKKLA
AALEHHHHHH

Q-peptide	Sequence	Flanking sequence length
Q1	EIQNAVNGVK	1
Q2	TLLSNLEEAK	2
Q3	SGSGLVGR	3
Q4	IDSLLENDR	4
Q5	ASSIIDELFQDR	5
Q6	ELDESLQVAER	6
Q7	VTTVASHTSDSDVPSGVTEVVVK	0

QconCAT #3

MEVWTQRLHGGSAPLPQDRGFLVVNKEIQNAVNGVKQIEERKTLLSNLEEAKK
KKARVCRSGSGLVGRQLEEWMNGDRIDSLLENDRQQTHMQDHFSRASSIIDEL
FQDRFFTREPRELDESLQVAERLRVTTVASHTSDSDVPSGVTEVVVKLKLAAAL
EHHHHHH

Q-peptide	Sequence	Flanking sequence length
Q1	EIQNAVNGVK	2
Q2	TLLSNLEEAK	3
Q3	SGSGLVGR	4
Q4	IDSLLENDR	5
Q5	ASSIIDELFQDR	6
Q6	ELDESLQVAER	0
Q7	VTTVASHTSDSDVPSGVTEVVVK	1

QconCAT #4

MEVWTQRLHGGSAPLPQDRGFLVYVNKEIQNAVNGVKQIKNEERKTLLSNLEE
AKKKKEYARVCRSGSGLVGRQLEEFWMNGDRIDSLLENDRQQTHMLRASSIID
ELFQDRRELDESLQVAERLYLRVTTVASHTSDSDVPSGVTEVVVKLFKLAAALE
HHHHHH

Q-peptide	Sequence	Flanking sequence length
Q1	EIQNAVNGVK	3
Q2	TLLSNLEEAK	4
Q3	SGSGLVGR	5
Q4	IDSLLENDR	6
Q5	ASSIIDELFQDR	0
Q6	ELDESLQVAER	1
Q7	VTTVASHTSDSDVPSGVTEVVVK	2

QconCAT #5

MEVWTQRLHGGSAPLPQDRGFLVKYVNKEIQNAVNGVKQIKTNEERKTLLSNL
EEAKKKKEDFYARVCRSGSGLVGRQLEEFLRIDSLLENDRSRASSIIDELFQDRF
LRRELDESLQVAERLTYYLRVTTVASHTSDSDVPSGVTEVVVKLFDKLAAALEH
HHHHH

Q-peptide	Sequence	Flanking sequence length
Q1	EIQNAVNGVK	4
Q2	TLLSNLEEAK	5
Q3	SGSGLVGR	6
Q4	IDSLLENDR	0
Q5	ASSIIDELFQDR	1
Q6	ELDESLQVAER	2
Q7	VTTVASHTSDSDVPSGVTEVVVK	3

QconCAT #6

MEVWTQRLHGGSAPLPQDRGFLVSKYVNKEIQNAVNGVKQIKTLKTNEERKTL
LSNLEEAKKKKEDARSGSGLVGRDRIDSLLENDRQFSRASSIIDELFQDRFFKLR
RELDESLQVAERLTRQYYLRVTTVASHTSDSDVPSGVTEVVVKLFDSKLAAALE
HHHHHH

Q-peptide	Sequence	Flanking sequence length
Q1	EIQNAVNGVK	5
Q2	TLLSNLEEAK	6
Q3	SGSGLVGR	0
Q4	IDSLLENDR	1
Q5	ASSIIDELFQDR	2
Q6	ELDESLQVAER	3
Q7	VTTVASHTSDSDVPSGVTEVVVK	4

QconCAT #7

MEVWTQRLHGGSAPLPQDRGFLVGSKYVNKEIQNAVNGVKQIKTLIKTLLSNLE
EAKCRSGSGLVGRQGDRIDSLLENDRQQHFSRASSIIDELFQDRFFTAKLRREL
DESLQVAERLTRKDQYYLRVTTVASHTSDSDVPSGVTEVVVKLFDSDKLAAALE
HHHHHH

Q-peptide	Sequence	Flanking sequence length
Q1	EIQNAVNGVK	6
Q2	TLLSNLEEAK	0
Q3	SGSGLVGR	1
Q4	IDSLLENDR	2
Q5	ASSIIDELFQDR	3
Q6	ELDESLQVAER	4
Q7	VTTVASHTSDSDVPSGVTEVVVK	5

2.3.2 Characterization of QconCATs

Purity of QconCATs was estimated by SDS-PAGE (Figure 2.1A) and considered to be nearly 100% pure. No correction for protein concentration of QconCATs was made for further MRM analysis and total protein concentration determined for the purified QconCATs was used as mg/mL concentration.

^{15}N isotope incorporation was determined based on MALDI spectra of Q-peptides by Isotopic Enrichment Calculator (www.nist.gov/mml/bmd/bioanalytical/isoenrichcalc.cfm) [73]. Figure 2.1B shows representative MALDI spectra for two Q-peptides from QconCAT #1. The MALDI spectra for these Q-peptides from other QconCATs (from #2 to #7) are summarized in Figure 2.2. Both peptides yielded consistent results and the mean value based on two peptides and three analytical replicates was higher than 99% for each QconCAT (Table 2.2). These values were accepted as complete labeling and no correction was applied to data.

To determine the molecular mass of QconCATs, LC–MS analyses were performed in positive ion mode with an Agilent 6550 QTOF. Figure 2.1C shows a representative spectrum and deconvolution for QconCAT #1. The related spectra for other QconCATs (from #2 to #7) are summarized in Figure 2.3. Overall, observed mass of each QconCAT was consistent with calculated mass (Table 2.2), indicating full-length expression of QconCAT. Accordingly, the calculated average molecular mass was used to convert mg/mL concentration of QconCAT into the mol/L concentration, which was further used to mix QconCAT and recombinant clusterin at 1:1 molar ratio.

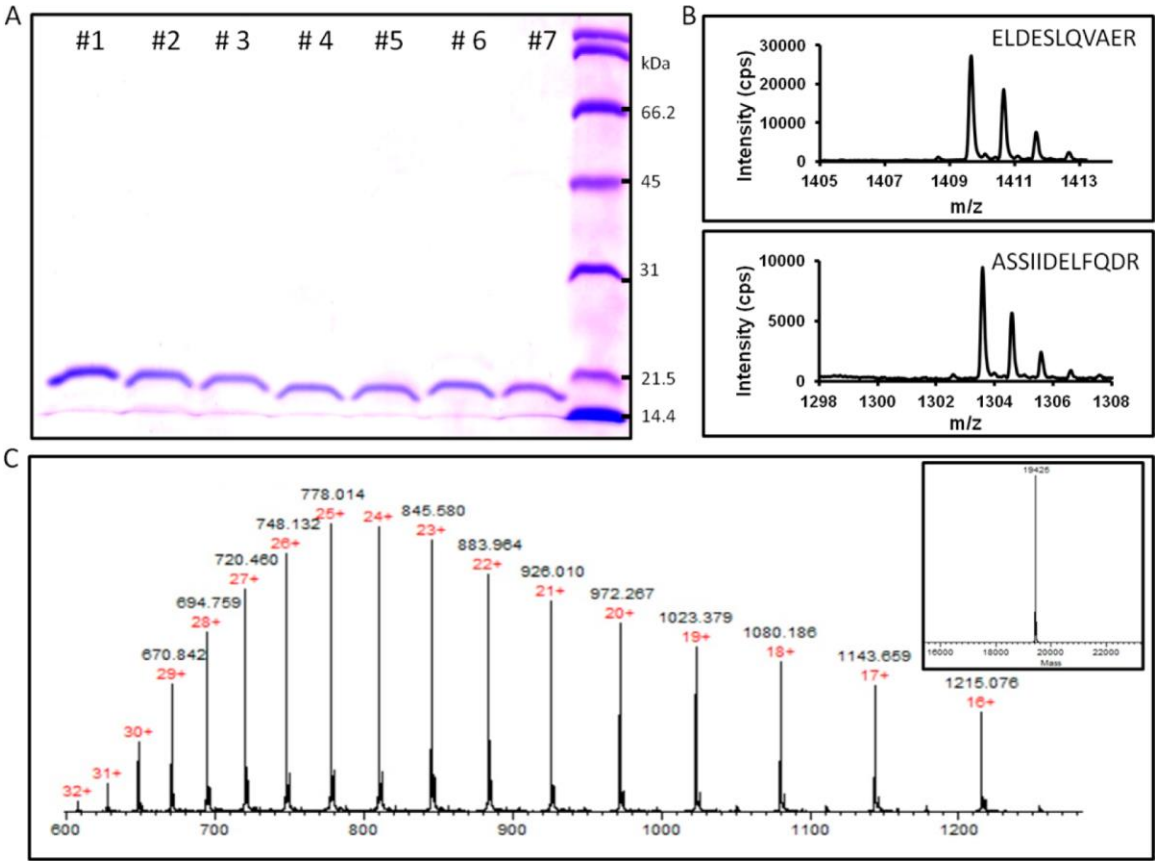

Figure 2.1 - Characterization of QconCATs.
(A) 100 pmol of purified QconCATs (from #1 to #7) were separated on 12.5% SDS-PAGE. The molecular mass standards are shown on the right. **(B)** MALDI spectra for two Q-peptides from QconCAT #1, which were used to calculate ^{15}N-incorporation by Isotopic Enrichment Calculator (http://www.nist.gov/mml/analytical/organic/isoenrichcalc.cfm). The MALDI spectra for other QconCATs (from #2 to #7) are summarized in Figure 2.2. **(C)** Full-size QconCAT expression was confirmed using Agilent 6550 QTOF instrument. ESI mass spectrum of QconCAT #1 is shown. The insert shows deconvoluted spectrum with observed average molecular mass of QconCAT #1. The spectra for other QconCATs (from #2 to #7) are summarized in Figure 2.3.

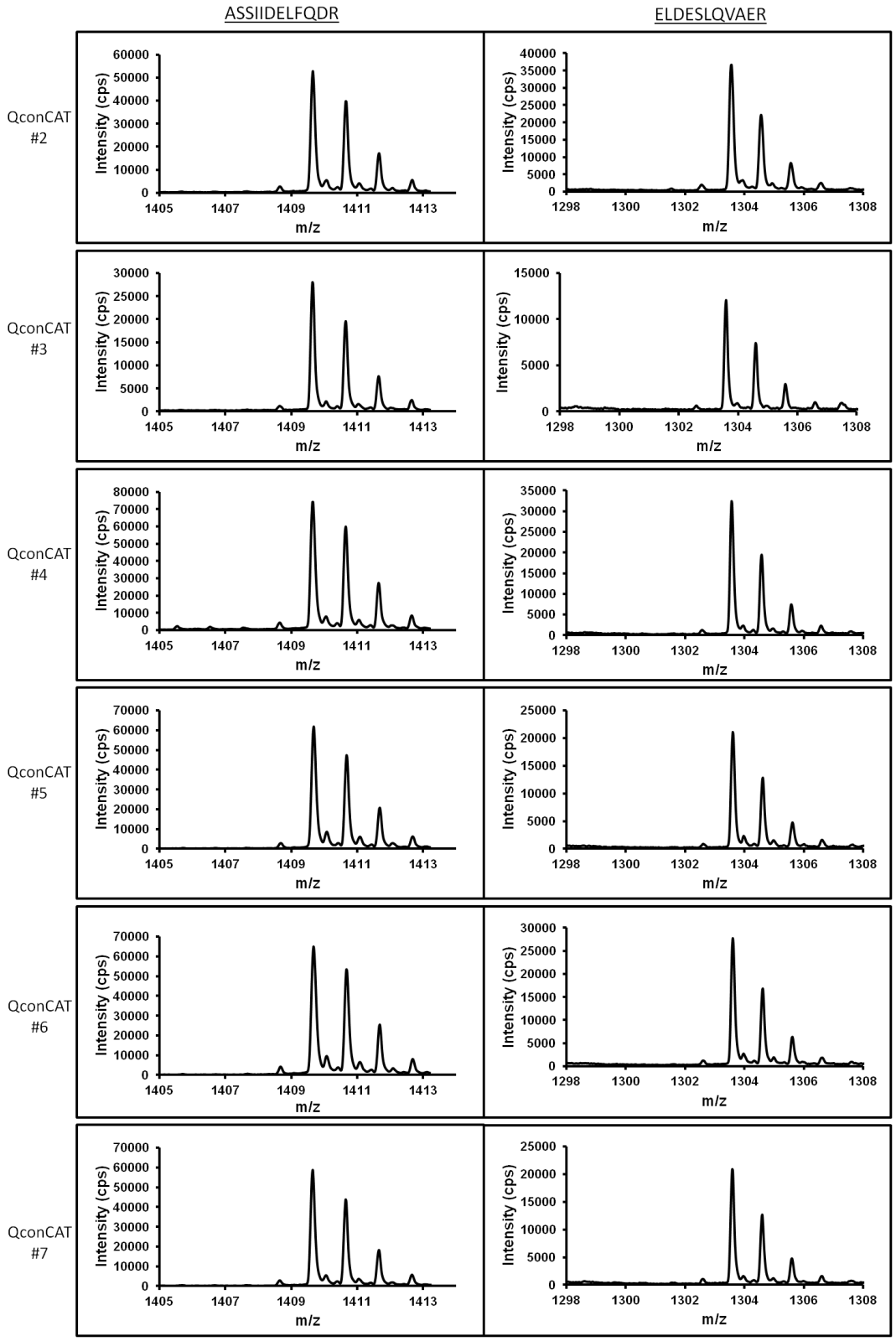

Figure 2.2 - MALDI spectra used to calculate ^{15}N incorporation.
Two Q-peptides (Q5 and Q6) were chosen to determine percentile of ^{15}N incorporation. Data presented as mean ± SD are summarized in the Table 2.2.

Table 2.2 - Properties of QconCATs.

QconCAT	^{15}N incorporation (%)	Calculated mass (Da)	Observed mass (Da)	Error (ppm)
#1	99.7 ± 0.08	19427	19425	103
#2	99.6 ± 0.08	19459	19425	1747
#3	99.6 ± 0.08	19301	19382	4197
#4	99.7 ± 0.04	19286	19365	4096
#5	99.7 ± 0.08	19430	19471	2110
#6	99.7 ± 0.14	19472	19472	N/A
#7	99.5 ± 0.51	19265	19231	1765

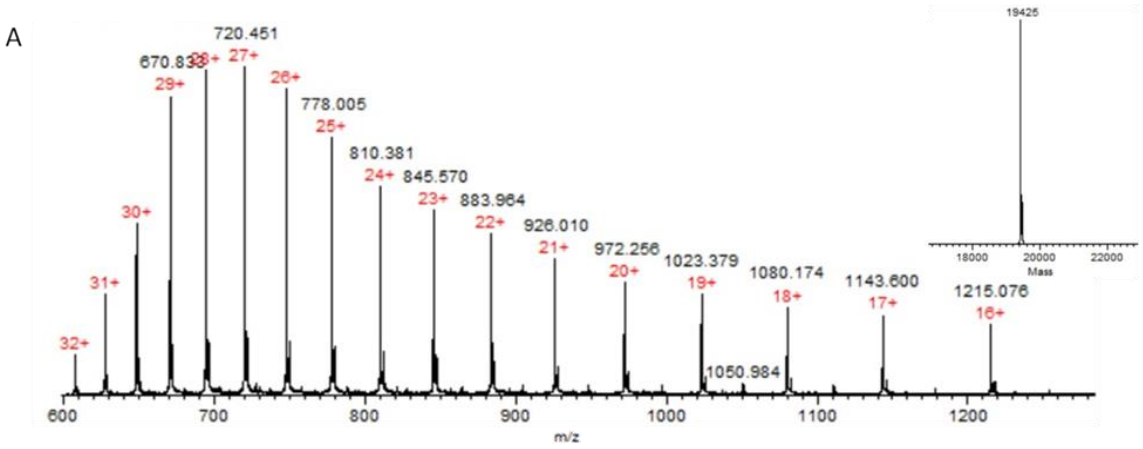
A
720.451
670.833
29+
28+
27+
26+
778.005
25+
810.381
24+
845.570
23+
883.964
22+
926.010
21+
972.256
20+
1023.379
19+
1080.174
18+
1143.600
17+
1215.076
16+
30+
31+
32+
1050.984
600
700
800
900
1000
1100
1200
m/z
19425
18000
20000
22000
Mass

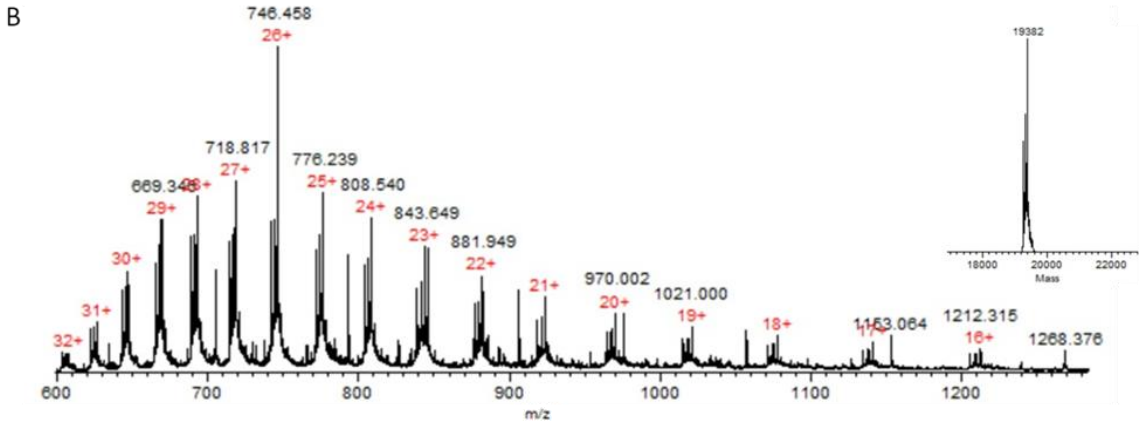
B
746.458
26+
718.817
27+
776.239
25+
808.540
24+
843.649
23+
881.949
22+
970.002
21+
1021.000
20+
19+
18+
1153.064
17+
1212.315
16+
1268.376
669.34
29+
30+
31+
32+
600
700
800
900
1000
1100
1200
m/z
19382
18000
20000
22000
Mass

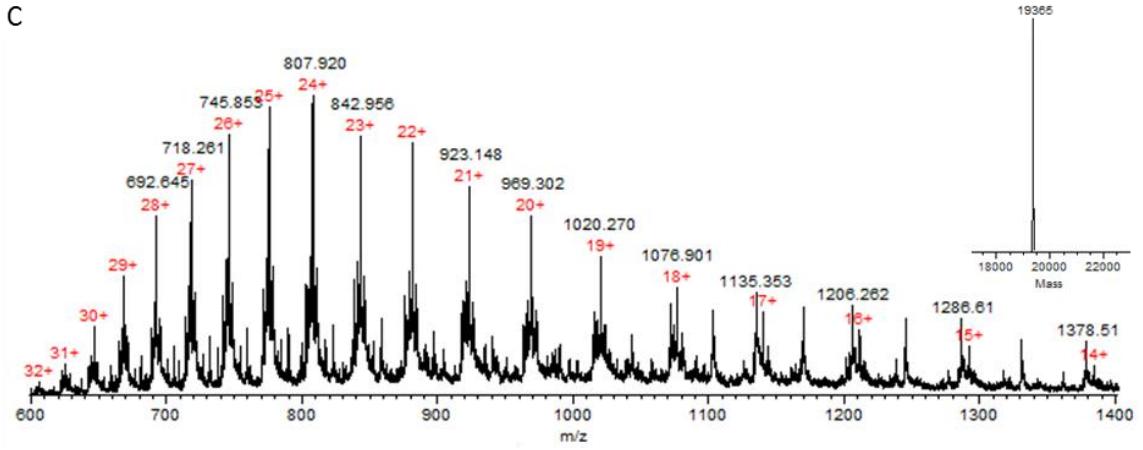
C
807.920
24+
745.859
25+
26+
842.956
23+
22+
718.261
27+
923.148
21+
692.645
28+
969.302
20+
1020.270
19+
1076.901
18+
1135.353
17+
1206.262
16+
1286.61
15+
1378.51
14+
29+
30+
31+
32+
600
700
800
900
1000
1100
1200
1300
1400
m/z
19365
18000
20000
22000
Mass

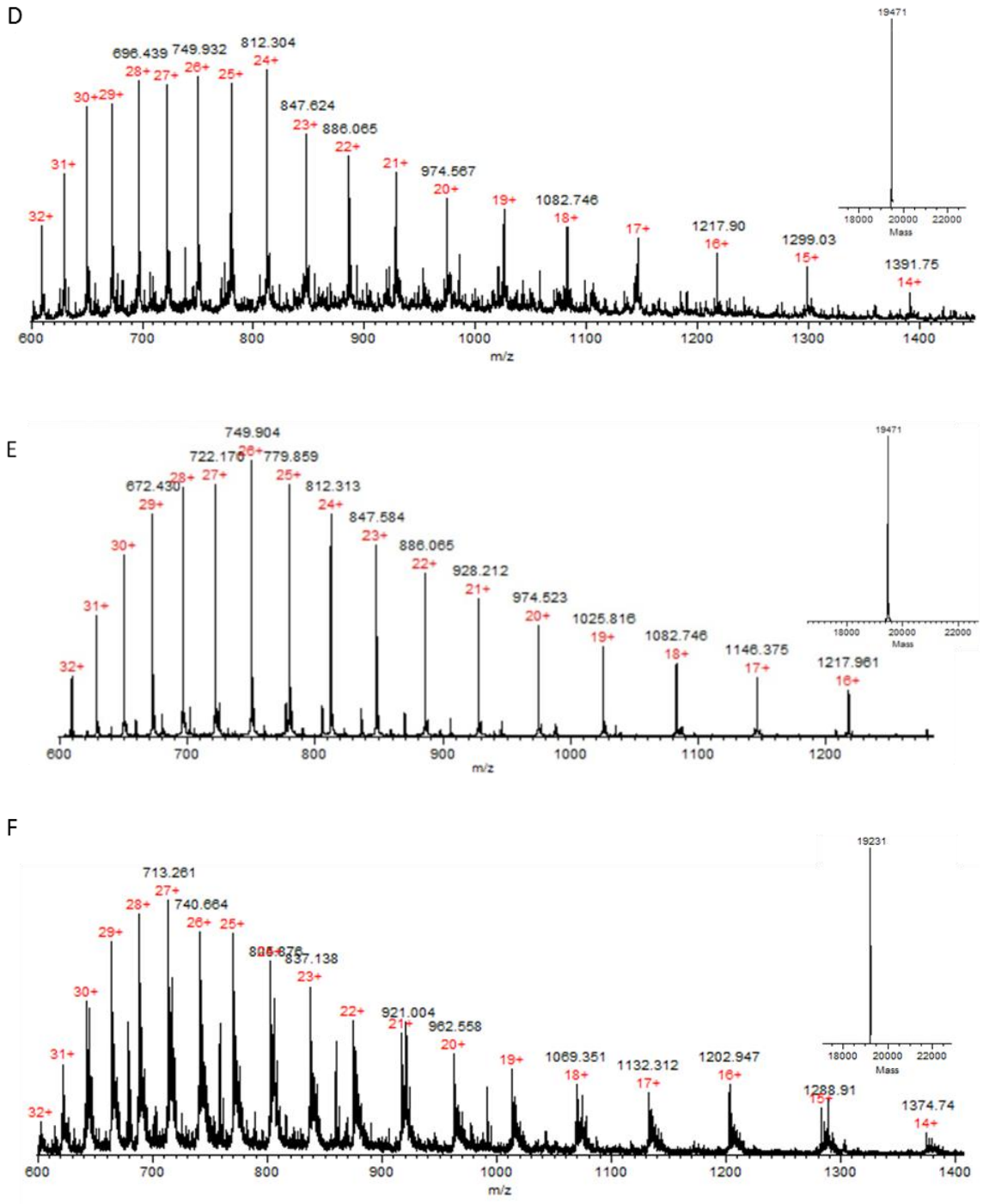

Figure 2.3 - Spectra of intact QconCATs.
Full-size QconCAT expression was confirmed using Agilent 6550 QTOF instrument. The insert shows the spectrum deconvoluted with MagTran 1.0 with observed average molecular mass. Observed mass of QconCAT #2 **(A)** was 19425 Da (19459 Da calculated), QconCAT #3 **(B)** was 19382 Da (19301 Da calculated), QconCAT #4 **(C)** was 19365 Da (19286 Da calculated), QconCAT #5 **(D)** was 19471 (19430 Da calculated), QconCAT #6 **(E)** was 19472 Da (19472 Da calculated), and QconCAT #7 **(F)** was 19231 (19265 Da calculated).

2.3.3 Measured Ratios as a Function of Length of Natural Flanking Sequences

Three MRM transitions for each Q-peptide were selected as previously described [74] and are tabulated in Table 2.3. These transitions were treated as independent measurements, each resulting in a ratio value for the corresponding Q-peptide. Measurements were performed with three analytical replicates for each of two biological replicates, resulting in the total n = 18. The average value for each natural flanking sequence variant of a Q-peptide was normalized to the value obtained for the respective 6 amino acid natural flanking sequence of that Q-peptide. Normalization was performed to simplify evaluation of the effect of flanking sequence length on each Q-peptide as well as to allow for comparison between Q-peptides. Data in Figure 2.4 are presented as a mean ± SD and plotted versus the length of natural flanking sequence for all seven Q-peptides. Recombinant clusterin and QconCAT were mixed at 1:1 molar ratio. If the presence of natural flanking sequence is not essential for accurate quantification, then all measured ratios should be around 1.0 with CV up to 30% (shown with blue dashed lines in Figure 2-4A). CV of 30% range is typical for MRM assay of proteins [75,76] and covers uncertainties associated with measurements of total protein concentrations, pipetting during analyte/standard mixing, and biological and analytical replicates. Some data presented herein fit well in this range. For example, Q7 shows little ratio variation associated with the length of natural flanking sequences and even absence of natural flanking sequence has the ratio (1.05 ± 0.13) similar to the ratio measured for the presence of 6 amino acid residues natural flanking sequence (1.0 ± 0.10).

Table 2.3 - Transitions used for quantification.

Q-peptide	Analyte precursor (m/z)	Analyte product (m/z)	Internal standard precursor (m/z)	Internal standard product (m/z)	Ion product
Q1	536.293	829.453 701.394 587.351	543.273	841.417 711.364 595.327	1+, y8 1+, y7 1+, y6
Q2	559.309	790.394 703.362 589.319	565.291	799.367 711.338 595.301	1+, y7 1+, y6 1+, y5
Q3	366.704	588.346 501.314 444.293	372.775	299.164 255.149 226.140	1+, y6 1+, y5 1+, y4
Q4	537.775	846.432 759.400 646.315	544.256	857.399 769.370 655.289	1+, y7 1+, y6 1+, y5
Q5	697.352	1035.511 807.400 678.357	705.328	1047.475 817.370 687.330	1+, y8 1+, y6 1+, y5
Q6	644.823	802.442 715.410 602.326	652.300	813.409 725.380 611.299	1+, y7 1+, y6 1+, y5
Q7	772.064	1014.583 773.477 507.795	780.705	1025.550 781.453 513.279	1+, y10 1+, y7 2+, y10

A

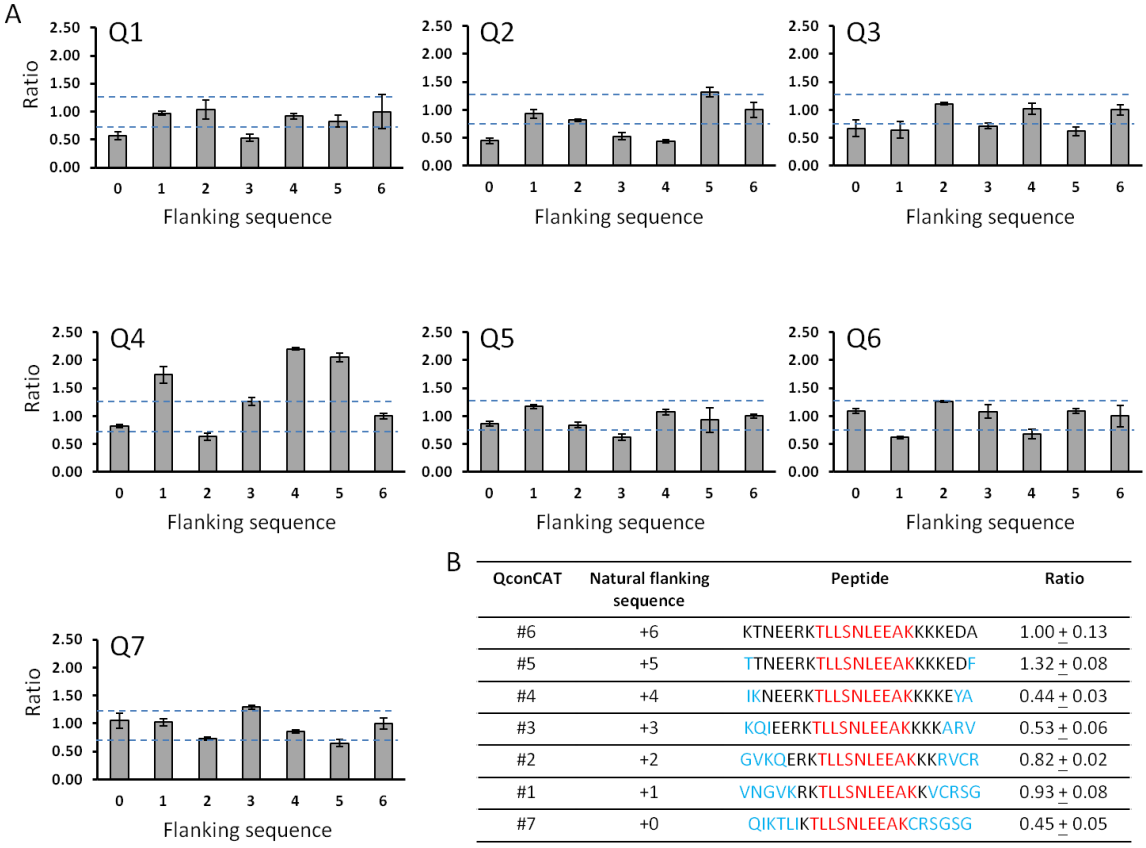

B

QconCAT	Natural flanking sequence	Peptide	Ratio
#6	+6	KTNEERKTLLSNLEEAKKKKEDA	1.00 ± 0.13
#5	+5	TTNEERKTLLSNLEEAKKKKEDF	1.32 ± 0.08
#4	+4	IKNEERKTLLSNLEEAKKKKEYA	0.44 ± 0.03
#3	+3	KQIEERKTLLSNLEEAKKKARV	0.53 ± 0.06
#2	+2	GVKQERKTLLSNLEEAKKRVCR	0.82 ± 0.02
#1	+1	VNGVKRKTLLSNLEEAKKVCRSG	0.93 ± 0.08
#7	+0	QIKTLIKTLLSNLEEAKCRSGSG	0.45 ± 0.05

Figure 2.4 - Measured ratios.
Recombinant human clusterin was mixed with individual QconCATs at 1/1 (pmol/pmol) ratio resulting in seven separate samples. MRM assay for these samples was used to determine actual measured ratios for each individual Q-peptide with different length of natural flanking sequences. **(A)** Measured ratios (mean ± SD, n = 18) are plotted versus the length of natural flanking sequence for all seven Q-peptides. Blue dashed lines border a section of plot for ratios in the range of 1.0 ± 30%. **(B)** Data for Q2 (shown in red) are used as a representative example to demonstrate how shorter natural flanking sequences (shown in black) cause an appearance of random non-original amino acid residues (shown in blue) in the close proximity to trypsin cleavage sites. Related data presentation for all of other Q-peptides is summarized in Table 2.4.

Table 2.4 – Measured ratios.
The three transitions from each peptide were treated as independent measurements, each resulting in a ratio value for the corresponding peptide. Measurements were performed with three analytical replicates for each of two biological replicates resulting in the total n = 18. Data are presented as a mean ± SD normalized to the +6 natural flanking sequence mean value for respective Q-peptide.

QconCAT	Natural flanking sequence	Q1	Ratio
#7	+6	GSKYVNKEIQNAVNGVKQIKTLI	1.00 ± 0.31
#6	+5	VSKYVNKEIQNAVNGVKQIKTLK	0.83 ± 0.11
#5	+4	LVKYVNKEIQNAVNGVKQIKTTN	0.92 ± 0.05
#4	+3	FLVYVNKEIQNAVNGVKQIKNEE	0.53 ± 0.06
#3	+2	GFLVVNKEIQNAVNGVKQIEERK	1.03 ± 0.17
#2	+1	RGFLVNKEIQNAVNGVKQERKTL	0.97 ± 0.04
#1	+0	DRGFLVKEIQNAVNGVKRKTLLS	0.57 ± 0.07

QconCAT	Natural flanking sequence	Q2	Ratio
#6	+6	KTNEERKTLLSNLEEAKKKKEDA	1.00 ± 0.13
#5	+5	TTNEERKTLLSNLEEAKKKEDF	1.32 ± 0.08
#4	+4	IKNEERKTLLSNLEEAKKKEYA	0.44 ± 0.03
#3	+3	KQIEERKTLLSNLEEAKKKARV	0.53 ± 0.06
#2	+2	GVKQERKTLLSNLEEAKKRVCR	0.82 ± 0.02
#1	+1	VNGVKRKTLLSNLEEAKKVCRSG	0.93 ± 0.08
#7	+0	QIKTLIKTLLSNLEEAKCRSGSG	0.45 ± 0.05

QconCAT	Natural flanking sequence	Q3	Ratio
#5	+6	FYARVCRSGSGLVGRQLEEFL	1.00 ± 0.09
#4	+5	EYARVCRSGSGLVGRQLEEFF	0.62 ± 0.08
#3	+4	KKARVCRSGSGLVGRQLEEWM	1.02 ± 0.10
#2	+3	KKKRVCRSGSGLVGRQLEMNG	0.71 ± 0.05
#1	+2	EAKKVCRSGSGLVGRQLNGDR	1.11 ± 0.02
#7	+1	LEEAKCRSGSGLVGRQGDRID	0.64 ± 0.15
#6	+0	KKKEDARSGSGLVGRDRIDSL	0.67 ± 0.15

QconCAT	Natural flanking sequence	Q4	Ratio
#4	+6	FWMNGDRIDSLLENDRQQTHML	1.00 ± 0.05
#3	+5	EWMNGDRIDSLLENDRQQTHMM	2.05 ± 0.08
#2	+4	LEMNGDRIDSLLENDRQQTHQD	2.20 ± 0.02
#1	+3	RQLNGDRIDSLLENDRQQTDHF	1.26 ± 0.07
#7	+2	VGRQGDRIDSLLENDRQQHFSR	0.63 ± 0.06
#6	+1	GLVGRDRIDSLLENDRQFSRAS	1.74 ± 0.15
#5	+0	QLEEFLRIDSLLENDRSRASSI	0.82 ± 0.03

QconCAT	Natural flanking sequence	Q5	Ratio
#3	+6	MQDHFSRASSIIDELFQDRFFTREP	1.00 ± 0.04
#2	+5	HQDHFSRASSIIDELFQDRFFTRES	0.93 ± 0.22
#1	+4	QTDHFSRASSIIDELFQDRFFTRQA	1.07 ± 0.05
#7	+3	RQQHFSRASSIIDELFQDRFFTAKL	0.62 ± 0.06
#6	+2	NDRQFSRASSIIDELFQDRFFKLRR	0.84 ± 0.05
#5	+1	LENDRSRASSIIDELFQDRFLRREL	1.17 ± 0.03
#4	+0	QQTHMLRASSIIDELFQDRRRELDE	0.86 ± 0.04

QconCAT	Natural flanking sequence	Q6	Ratio
#2	+6	SQAKLRRELDESLQVAERLTRKYN	1.00 ± 0.19
#1	+5	RQAKLRRELDESLQVAERLTRKYE	1.09 ± 0.04
#7	+4	FTAKLRRELDESLQVAERLTRKDQ	0.68 ± 0.08
#6	+3	RFFKLRRELDESLQVAERLTRQYY	1.08 ± 0.12
#5	+2	QDRFLRRELDESLQVAERLTYYLR	1.26 ± 0.02
#4	+1	LFQDRRRELDESLQVAERLYLRVT	0.62 ± 0.02
#3	+0	FFTREPRELDESLQVAERLRVTTV	1.09 ± 0.04

QconCAT	Natural flanking sequence	Q7	Ratio
#1	+6	EDQYYLRVTTVASHTSDSDVPSGVTE VVVKLFDSDP	1.00 ± 0.10
#7	+5	KDQYYLRVTTVASHTSDSDVPSG VTEVVVKLFDSDK	0.65 ± 0.06
#6	+4	TRQYYLRVTTVASHTSDSDVPSGVTE VVVKLFDSKL	0.86 ± 0.03
#5	+3	RLTYYLRVTTVASHTSDSDVPSGVTE VVVKLFDKLA	1.29 ± 0.04
#4	+2	AERLYLRVTTVASHTSDSDVPSGVTE VVVKLFKLAA	0.73 ± 0.03
#3	+1	QVAERLRVTTVASHTSDSDVPSGVTE VVVKLKLAAA	1.02 ± 0.06
#2	+0	LTRKYNRVTTVASHTSDSDVPSGVTE VVVKKLAAAL	1.05 ± 0.13

However, we have also observed multiple examples when measured ratios strongly deviate from expected 1.0 ± 30% (Figure 2.4). These deviations did not simply correlate with the length of the natural flanking sequence itself. This observation encouraged us to analyze the actual amino acid sequences surrounding trypsin cleavage sites because shorter natural flanking sequences brought random amino acid residues into close proximity to the trypsin cleavage sites. As a representative case, the data for Q2 are shown in Figure 2.4B. Related data for all other QconCATs is summarized in Table 2.4. Figure 2.4B allows side-by-side comparison of the ratios for Q2 and these ratios depend on the changing pattern of amino acid residues surrounding trypsin cleavage sites, with natural flanking residues shown in black and random residues shown in blue. In general, these random amino acid residues can have negative, positive, or no effect for trypsin digestion. Indeed, +1 and +2 flanking combinations for Q2 do not differ from +6 pure natural flanking sequence. However, +0 and +6 combinations have approximately 2-fold difference. The same is correct for +4 and +6 combinations. Some of these deviations can be explained based on so-called Keil rules (reviewed in [58,77]). For example, if to compare +6 (KTNEERKTLLSNLEEAKKKKEDA) to +0 (QIKTLIKTLLSNLEEAKCRSGSG), it is apparent that omitting most of positive- and negative-charged residues on both sides of Q2 in +0 combination improves rate of trypsin digestion and results in high yield of Q2 from QconCAT versus yield of Q2 from recombinant clusterin. Overall, it gives a measured ratio 0.45 ± 0.05 for +0 combination. However, measured ratios for many other combinations cannot be so simply explained.

For example, the difference in flanking sequences between +4 and +5 combinations is small and hard to be related to Keil rules while the difference in ratios is approximately 3-fold.

Sequence-based analysis of other Q-peptides (Table 2.4) concurs well with trends described here for Q2 and can be summarized in two assumptions: (i) inclusion of +6 residues natural flanking sequences on Q-peptide mimics well the close proximity of trypsin cleavage sites and provides for the most accurate quantification of target protein; (ii) shorter natural flanking sequences still could be quantitative, in some occasions, such as Q4, Q5, Q6, and Q7, even no natural flanking sequences at all (+0 combination) performed quantitatively well (Figure 2.4A). However this is not a guarantee since random residues brought into close proximity of trypsin cleavage sites can have unpredictable effect on efficiency of trypsin digestion. Work by others has attempted to provide structural effects on cleavage sites as a rationale for deviations from expected Keil rules, such as greater trypsinolysis of exposed sites within loop structures and decreased trypsin cleavage fidelity near negatively-charged pockets created by bringing acidic residues into close proximity in the folded conformation rather than proximity within linear amino acid sequence [77]. These contradictions to Keil rules on a structural basis cannot be applied to our observations because both clusterin and QconCATs were denatured with SDS, thereby reducing structural effects on trypsinolysis. While a minor degree of secondary structures may be present due to incomplete denaturation by SDS, it is unlikely that it is significant enough to impact cleavage by trypsin and, therefore, our observations can be

described as being caused by the primary amino acid sequence. Since variation between trypsin cleavage fidelity in native protein and QconCAT is not completely predictable, several precautionary steps may be considered to reduce inconsistencies in quantification. First, and perhaps the most simple method to avoid error in measurement, is to include more natural amino acid residues on both sides of every Q-peptide. Simple inclusion of more natural amino acids will enable more reliable relative quantification to near absolute quantification appropriate for measurements within similar samples performed by consistent protocols. Second, and perhaps more laborious, is to optimize natural flanking sequence length by conducting experiments similar to those provided herein to determine the appropriate length of the natural flanking sequence to yield consistent 1:1 ratio between QconCAT and analyte for each Q-peptide. Optimization would be preferred for QconCATs produced for inter-laboratory comparisons and comparisons of protein concentrations between tissues or species where more accurate quantitative data is imperative.

An important observation in the present study is that the randomly occurring error of quantification associated with shorter than +6 natural flanking sequences was not greater than approximately 2-fold. Although the wording “absolute” quantification is broadly used, MRM quantification with QconCATs is often used for “relative” comparison of two (or more) biological samples. Acquiring quantification with up to ±2-fold error in both biological samples will not change their relative comparison in side-by-side experiments and can justify support of QconCATs without natural flanking sequences. However, there are

several applications where truly absolute quantification is important. For example, inter-laboratory comparisons, discovery of post-translational modifications, comparison of protein expression levels in different tissues/species, and others. For all of these applications, it would be recommended to use more amino acid residues in the natural flanking sequences of every Q-peptide to be included into the QconCAT.

2.4 Conclusions

Although natural flanking sequences for Q-peptides are not directly used for quantification and occupy a large portion of the QconCAT, it appears that including more natural amino acid flanking residues is better for reliable quantification. It is evident from our observations that trypsin cleavage is not solely dependent on the length of natural amino acid flanking sequence in the +0 to +6 amino acid residue range, but rather on the properties of amino acids residues found within that range. Furthermore, effects of amino acid composition within the flanking sequence cannot be predicted entirely by Keil rules of trypsin cleavage. I suggest performing experiments similar to those performed herein to optimize each Q-peptide flanking sequence to confirm accurate quantification or to simply include additional natural amino acid flanking residues. When it is necessary to have a large number of Q-peptides, it is practical to select an appropriate number of amino acids, such as four, in the flanking sequence to obtain a desirable QconCAT size.

Chapter 3: Quantification of Histone Deacetylase Isoforms

This chapter contains published work [53].

3.1 Introduction

One of the most common PTMs in histones is acetylation. Removal of acetyl groups from histone tails is chiefly catalyzed by histone deacetylases (HDACs). HDACs are categorized into eleven main isoforms, which are further broken into thirty-eight sequence variants by truncations, deletions, and substitutions of the canonical sequence [78]. Several HDACs have been linked to memory impairment and dementia [79,80], a hallmark of AD, and it has been demonstrated that global deacetylation of histones and overall activity of HDACs is increased in AD [81]. In addition to histones, HDACs are also known to modify over 50 non-histone proteins [81]. The majority of information on effects of HDAC isoforms comes from overexpression and knockouts of HDACs in murine models of AD. While mice may be more practical for neurodegeneration research involving manipulation of HDACs, it is still a non-human model for familial, early-onset AD. Most AD cases are considered sporadic or late onset, and while they may have the same key characteristics like dementia and protein aggregation, pathogenesis may vary from familial AD [82]. A connection between HDACs and AD has been established in mouse models; however, little information exists on changes in specific isoforms and the significance of their effects on AD pathology in humans.

HDAC inhibitors (HDIs) have shown improvement of AD-related symptoms; however, these are broad class HDIs, which do not target specific isoforms. If a long-term regimen of broad class HDIs were prescribed to prevent or stop the progression of AD, there may be deleterious side effects in other HDAC-associated pathways. For example, HDIs in mouse models have demonstrated improvement in memory [79,83,84], yet deficiency of either HDAC4 or HDAC5 impairs memory [85,86]. Specific knowledge of isoforms directly related to AD is imperative for treatment specificity and safety [31].

Various methods for assessment of HDAC levels have been reported, including quantitative real-time polymerase chain reaction [87,88], *in situ* hybridization [89], Western blotting [87,88], and immunohistochemical staining [90]. However, these semi-quantitative methods are unable to provide absolute quantitative data on the protein level of HDAC isoforms and isoform-specific quantification of HDACs remains elusive. Mass spectrometry (MS) provides the potential to perform targeted absolute quantification of protein isoforms. Synthetic peptides and full-length proteins labeled with stable isotopes are commonly used in MS-based protein quantification. Due to the large number of HDAC isoforms, it is less practical to use synthetic peptides or express full-length protein for each isoform. An alternative is performing quantitative measurements using QconCATs as internal standards [58,60]. QconCATs are standard proteins comprised of proteolytic peptides used for quantification and they may include the respective natural flanking sequences from targeted proteins. Previous work has shown applicability of QconCATs for measurement of abundant proteins in

neural tissues, such as amyloid precursor protein [91], apolipoprotein E [92], clusterin [69], PICALM [93], and ubiquitin carboxy-terminal hydrolase L1 [71]. QconCATs used in this study exceed past number of proteins measured and cover 25 sequence variants of HDACs, proteins with significantly lower abundance than those previously reported.

The goal of the present study was to determine whether multiplexing QconCAT technology could be applied to quantification of HDAC isoforms in different neural tissues in normal and disease state. Using QconCAT technology [60], three ^{15}N-labeled standard proteins were produced to measure all selected HDAC variants. Human and mouse brain and human retina samples were supplemented with these standard proteins and protocols for sample processing were optimized and analytically characterized. Measurements in human frontal cortex and human retina give insight into abundance of particular isoforms in different neural tissues in normal and disease states. Mouse brain, a common model for neurodegenerative phenotypes, shows HDAC profiles in comparison to human tissue. Quantification of HDAC isoforms in AD-affected human brain and age-matched controls also contributes to our knowledge of disease-associated isoforms that may be of value for HDIs therapies for AD. Furthermore, the developed analytical approach is broadly applicable to quantitative analysis of HDAC variants in various tissues and disease models.

3.2 Methods

3.2.1 Expression, Purification, and Characterization of QconCATs

Tryptic peptides for all HDAC isoforms were predicted and 64 HDAC-specific peptides with respective four-amino acid long natural flanking sequences were compiled into three QconCAT proteins (Figure 3.1 and Tables 3.1, 3.2, 3.3). Amino acid sequences were translated into cDNA and cloned into pET21a expression vectors with NdeI/HindIII restrictions sites by Biomatik Corporation (Cambridge, ON, Canada). Expression vector, which included His_6-tag expressed on C-terminus of the protein, was transformed into One Shot BL21(DE3) *E. coli* and cells were cultivated at 37 °C in M9 minimal medium containing 1 g/L $^{15}NH_4Cl$ as the sole nitrogen source. Initial inoculation began with 5 mL LB media and cells were grown for 6 h at 37 °C. Cells were pelleted by centrifugation at 20,000 *g* for 20 min and washed with 10 mL of $^{15}NH_4Cl$-containing M9 medium. Cells were then transferred to 50 mL $^{15}NH_4Cl$-containing M9 medium and grown for 12 h to 14 h at 37 °C. Cells were collected by centrifugation at 20,000 *g* for 20 min and washed twice by 100 mL $^{15}NH_4Cl$ M9 medium. Cells were then transferred to 500 mL $^{15}NH_4Cl$ M9 medium. Expression was induced with 1 mmol/L IPTG at OD_{600} of 0.6 to 0.8 and incubated for an additional 3 h at 37 °C. Cells were divided into 10 portions and harvested by centrifugation at 20,000 *g* for 30 min. One portion of cells was resuspended in 20 mL of lysis buffer (50 mmol/L Tris, pH 7.5). Cells were lysed by sonication and centrifuged at 20,000 *g* for 30 min; supernatant was discarded.

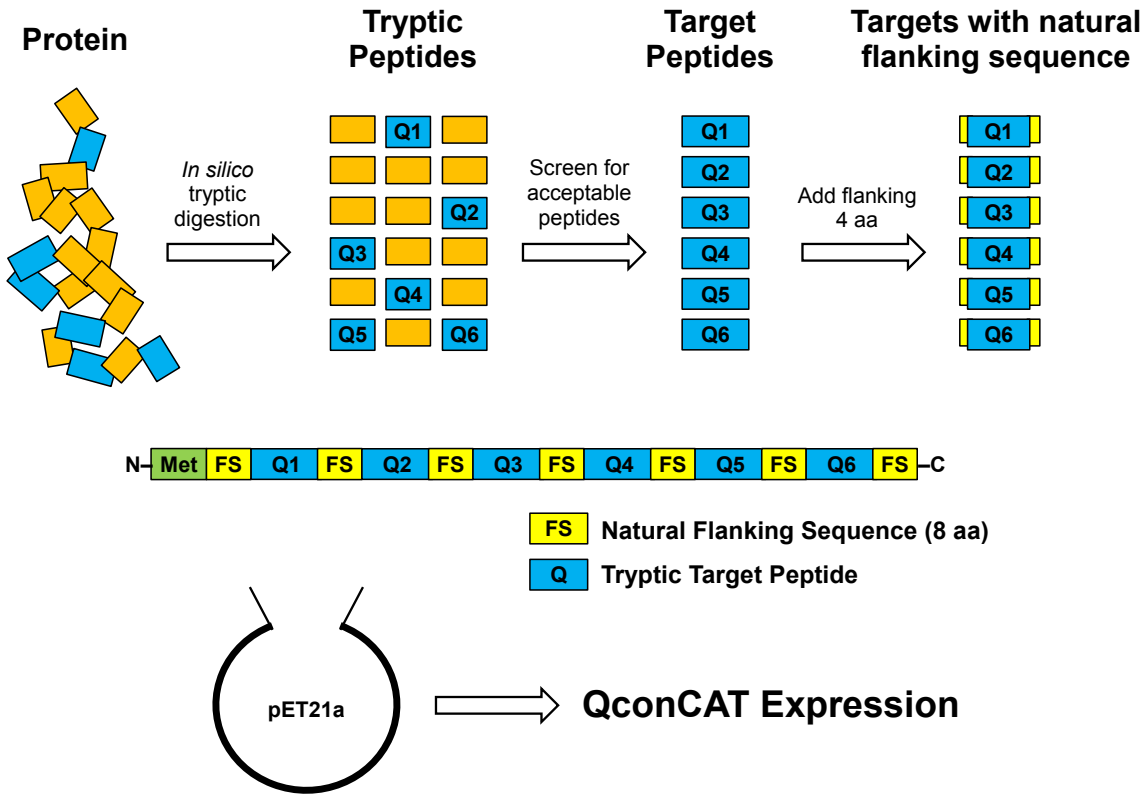

Figure 3.1 - QconCAT design overview.
Tryptic peptides from HDACs were predicted and screened for peptides suitable for MRM quantification. Natural flanking sequences consisting of four amino acids on each side of tryptic Q-peptides were included. A cDNA construct encoding the concatamer of these peptides was inserted into pET21a expression vector by Biomatik. BL21 (DE3) cells were transformed with plasmid and QconCATs were expressed with His_6-tag and purified by nickel-nitrilotriacetic (Ni-NTA) acid resin.

Table 3.1 - HDAC QconCAT#1 sequence and peptides for quantification.

HDAC QconCAT #1

MEMTKYHSDDYIKFLRSGKGKYYAVNYPLRDGIDSFHKYGEYFPGTGDLRDIGAEMTK
YHSDEYIKFLRSDMCRFHSEDYIDFLQRVSPTFCSRYTGASLQGATQLNNKICDIVPLRD
GIDDQSYKHLFQTYDRTDEADAEERGPEELSGRDQPVELLNPARVNHMMDLRLDHQF
SLPVAEPALREQQLLAMKHQQELLEHQRKLEREKGKESAVASTEVKMKLQQMNKIIPK
PSEPARQPESEELREHQALLDEPYLDRLPGQPGQKEAHAQAGVQVKKQEPPGQRQP
SEQELLFRQQALGMCKVAINWSGGWHHAKKDEAGKGRYYSVNVPIQDGIQDEKYYQI
SVLKEVYQAFNPKAVVLERHRIQQILNYIKGNLKKLAAALEHHHHHH

Sequence	**Isoforms**
EMTKYHSDDYIKFLRS	HDAC1
GKGKYYAVNYPLRDGID	HDAC1
SFHKYGEYFPGTGDLRDIGA	HDAC1, 2
EMTKYHSDEYIKFLRS	HDAC2
DMCRFHSEDYIDFLQRVSPT	HDAC3(all)
FCSRYTGASLQGATQLNNKICDI	HDAC3(all)
VPLRDGIDDQSYKHLFQ	HDAC3(all)
TYDRTDEADAEERGPEE	HDAC3(all)
LSGRDQPVELLNPARVNHM	HDAC4
MDLRLDHQFSLPVAEPALREQQL	HDAC4
LAMKHQQELLEHQRKLER	HDAC4
EKGKESAVASTEVKMKLQ	HDAC4
QMNKIIPKPSEPARQPES	HDAC4
EELREHQALLDEPYLDRLPGQ	HDAC4
PGQKEAHAQAGVQVKKQEP	HDAC4
PGQRQPSEQELLFRQQAL	HDAC4
GMCKVAINWSGGWHHAKKDEA	HDAC8(1-3, 5)
GKGRYYSVNVPIQDGIQDEKYYQI	HDAC8(1-2, 4-5)
SVLKEVYQAFNPKAVVL	HDAC8(1, 4)
ERHRIQQILNYIKGNLK	HDAC8(1, 4)

Molecular weight: 45547.3 Da ^{14}N (46125.6 Da ^{15}N)
Grand average of hydropathicity (GRAVY): -0.885 (hydrophilic)

Table 3.2 - HDAC QconCAT#2 sequence and peptides for quantification.

HDAC QconCAT #2

MSGREPSLEILPRTSLHVELRGALVGSVDPTLREQQLHLTRQHEVQLQKHLKQPSYKL
PLPGPYDSRDDFPASPKLSTQQEAERQALQGGMKSPPDQPVKHLFTIWSRLQETGLLS
KCERIDSKKLLGPISQKMYAVHAIKEQLIQEGLLDRCVSFSVLRLVDAVLGAEIRNGMAA
GGKLILSLEGGYNLRALAEIMCRLEELGLAGRCLTLVAARHAQTISGHALRILIVALERTV
HPNSPGIPYRTLEPIPYRTLEPLETEGATRSMLSPLRKTVSEPNLKLRYKTTERLSGSGL
HWPLSRTRSELEHRELGHGQPEARGPAPRGRKASLEELQSVHSERHVLLHSERHVLL
YGTNPLSRLKLDDNGKLAGLLAQRMFVMNAARWAAGSVTDLAFKVASRLGNRVDPLS
EEGWKQKPNKLAAALEHHHHHH

Sequence	**Isoforms**
MSGREPSLEILPRTSLH	HDAC5(all)
VELRGALVGSVDPTLREQQL	HDAC5(all)
HLTRQHEVQLQKHLKQ	HDAC5(all)
PSYKLPLPGPYDSRDDFP	HDAC5(all)
ASPKLSTQQEAERQALQ	HDAC5(all)
GGMKSPPDQPVKHLFT	HDAC5(all)
IWSRLQETGLLSKCERI	HDAC5(1, 3)
DSKKLLGPISQKMYAV	HDAC5(1, 3)
HAIKEQLIQEGLLDRCVSF	HDAC6
SVLRLVDAVLGAEIRNGMA	HDAC6
AGGKLILSLEGGYNLRALAE	HDAC6
IMCRLEELGLAGRCLTL	HDAC6
VAARHAQTISGHALRILIV	HDAC6
ALERTVHPNSPGIPYRTLEP	HDAC7(1, 3-8)
IPYRTLEPLETEGATRSMLS	HDAC7(1, 3-8)
PLRKTVSEPNLKLRYK	HDAC7(1, 3-8)
TTERLSGSGLHWPLSRTRSE	HDAC7(1, 3-8, 10)
LEHRELGHGQPEARGPAP	HDAC7(1, 3-8, 10)
RGRKASLEELQSVHSERHVLL	HDAC7(all)
HSERHVLLYGTNPLSRLKLD	HDAC7(all)
DNGKLAGLLAQRMFVM	HDAC7(all)
NAARWAAGSVTDLAFKVASR	HDAC7(all)
LGNRVDPLSEEGWKQKPN	HDAC7(all)

Molecular weight: 48288.6 Da ^{14}N (48929.7 Da ^{15}N)
Grand average of hydropathicity (GRAVY): -0.435 (hydrophilic)

Table 3.3 - HDAC QconCAT#3 sequence and peptides for quantification.

HDAC QconCAT #3

MQIQKQLLIAEFQKQHENNLTRQHQAQLQEHIKELLAGRERAVASTEVKQKLQPSYKYT
LPGAQDAKDDFPQEDRAPSSGNSTRSDSSIWSRLQETGLLNKCERILDPRILLGDDSQ
KFFSSVIGKDLAPGFVIKVIIGCCRIFPDGVAGREQLLVAGREQLLAQQRMHSMPFLRES
DADAVGRGQGLQSARAAQAPHWKSLQQSLAREEALTALGKLLYLAVRRGLSHGAQRL
LCVMYLRGQLEPQWKMLQCPASRDPGPGAEWRGTSPETRWPIVYSPRYNITGLEKLH
PFDAGKWGKVVEARREASEEDLLVVHTRRYLNGISRATIIDLDAHQGNGHERDFMDEGD
RLGGLSISPAGIVKRDELKLAAALEHHHHHH

Sequence	**Isoforms**
QIQKQLLIAEFQKQHEN	HDAC9(all)
NLTRQHQAQLQEHIKELLA	HDAC9(all)
GRERAVASTEVKQKLQ	HDAC9(all)
PSYKYTLPGAQDAKDDFP	HDAC9(all)
QEDRAPSSGNSTRSDSS	HDAC9(1, 3-8)
IWSRLQETGLLNKCERI	HDAC9(1-2, 4-7)
LDPRILLGDDSQKFFSS	HDAC9(1-2, 4-7)
VIGKDLAPGFVIKVII	HDAC9(3, 8)
GCCRIFPDGVAGREQLL	HDAC9(8)
VAGREQLLAQQRMHSM	HDAC9(8)
PFLRESDADAVGRGQGL	HDAC10(all)
QSARAAQAPHWKSLQQ	HDAC10(all)
SLAREEALTALGKLLYL	HDAC10(1-2, 4)
AVRRGLSHGAQRLLCV	HDAC10(1-2, 4)
MYLRGQLEPQWKMLQC	HDAC10(1-2)
PASRDPGPGAEWRGTS	HDAC10(4)
PETRWPIVYSPRYNIT	HDAC11(1)
GLEKLHPFDAGKWGKV	HDAC11(all)
VEAREASEEDLLVVHTRRYLN	HDAC11(all)
GISRATIIDLDAHQGNGHERDFMD	HDAC11(all)
EGDRLGGLSISPAGIVKRDEL	HDAC11(all)

Molecular weight: 42602.3 Da ^{14}N (43166.6 Da ^{15}N)
Grand average of hydropathicity (GRAVY): -0.551 (hydrophilic)

Pellet was resuspended in 3 mL urea buffer (7 mol/L urea; 0.1 mol/L NaH_2PO_4; 0.01 mol/L Tris•HCl; pH 8.0) and ^{15}N-labeled QconCAT was purified on nickel-nitrilotriacetic (Ni-NTA) acid resin (Qiagen, Valencia, CA). Purified ^{15}N-labeled QconCAT was loaded onto a SpinTrap G-25 spin column (GE Healthcare, Waukesha, WI) to exchange buffer into 25 mmol/L NH_4HCO_3 with 1% SDS. Protein concentration was measured in presence of 1% SDS using detergent-compatible DC Protein Assay kit and bovine serum albumin as standard. Final QconCATs were aliquoted and stored at -80^oC. Purity was estimated by 10% sodium dodecyl sulfate-polyacrylamide gel electrophoresis (SDS-PAGE) and ImageJ software (http://www.imagej.nih.gov/ij/).

Intact masses of QconCATs were determined experimentally using an Agilent 6550 QTOF and mass deconvolution with MagTran 1.0 software. QconCATs were eluted from an Agilent ProtID C18 nanochip (75 µm x 150 mm, 300 nm) over 10 min gradient from 20% to 80% acetonitrile containing 0.1% formic acid at a flow rate of 400 nL/min. Acquisition method in positive mode used capillary temperature 275 °C, fragmentor 180 V, capillary voltage 1950 V, and a 500 m/z to 2000 m/z mass window. QconCAT characterization on the peptide level was performed using an Applied Biosystems 4700 Proteomic Analyzer (Framingham, MA). For sequence confirmation, 50 pmol of each QconCAT was digested for 15 h at 37 °C with trypsin (50:1, mass ratio) in 25 mmol/L NH_4HCO_3. Tryptic peptides were mixed with α-cyano-4-hydroxycinnamic acid matrix and analyzed by reflector mode and all expected peptides were observed. To determine level of ^{15}N incorporation, peptide spectra were acquired

in reflector mode which provided isotopic peaks used to calculate percent ^{15}N with Isotopic Enrichment Calculator [73]. Representative short and long peptides were chosen for each QconCAT to determine percent ^{15}N (Figure 3.2). HDAC6 full-length protein was used as standard protein for calibration curves and lower limit of quantification (LLOQ) of HDAC6 peptides present in QconCAT#2.

3.2.2 Human Tissues

Frozen frontal cortex was obtained from the Washington University School of Medicine Alzheimer's Disease Research Center (St. Louis, MO). Eyes were acquired, characterized and dissected as described [94] at Case Western Reserve University (Cleveland, OH). Information regarding the acquisition and approval of human tissues is provided in Appendix A1.3 and demographic information of the de-identified donors is summarized in Table 3.4.

3.2.3 *Human Frontal Cortex Processing*

Minced frontal cortex tissue was homogenized in 25 mmol/L NH_4HCO_3 by sonication at 30 W using five 10 s continuous cycles (Sonicator 3000, Misonix Inc., Farmingdale, NY). Homogenates were centrifuged for 5 min at 2,000 *g* to remove debris. Resulting supernatant was measured for total protein concentration using detergent-compatible DC protein assay kit in the presence of 1% SDS and bovine serum albumin as a standard. Homogenates were stored at -80 °C. Pools of 20 mg total protein were prepared from equal amounts of each AD (n=5) and normal (n=5) donors. Samples were centrifuged at 106,000 *g* for 1 h at 4 °C. Supernatant, which contained soluble protein and HDAC, was supplemented with 10 pmol of each QconCAT , 20 mmol/L DTT , and 1% SDS.

Table 3.4 - Donor information.

Donor ID	Age (y)	Gender	Frontal cortex and retina status
1	90	F	frontal cortex, normal
2	91.3	M	frontal cortex, normal
3	87	M	frontal cortex, normal
8	91.5	M	frontal cortex, normal
9	92.1	F	frontal cortex, normal
11	79	M	frontal cortex, severe AD
12	73.6	F	frontal cortex, severe AD
14	82	F	frontal cortex, severe AD
17	72	M	frontal cortex, severe AD
19	76	F	frontal cortex, severe AD
PM032	68	M	neural retina, normal
PM038	79	M	neural retina, normal
PM039	82	M	neural retina, normal
PM049	69	F	neural retina, normal
PM028	86	M	neural retina, AMD-affected
PM033	86	M	neural retina, AMD-affected
PM040	80	M	neural retina, AMD-affected
PM051	86	F	neural retina, AMD-affected
PM030	76	M	neural retina, normal, history of AD
PM041	77	F	neural retina, normal, history of AD
PM045	81	M	neural retina, normal, history of AD

Alzheimer's disease (AD) in frontal cortex was evaluated by Clinical Dementia Rating with no dementia representing normal brain and severe dementia representing severe AD brain. Retina status was assessed by fellowship trained vitreo-retinal specialist and information about AD was in the clinical history provided by the eye bank.

After 1 h incubation at room temperature to reduce cysteines, 55 mmol/L iodoacetamide was added and incubated for an additional 1 h to alkylate cysteines. Protein was isolated by chloroform/methanol precipitation. Protein pellets were sonicated in 1 mL 25 mmol/L NH_4HCO_3 and 0.1% RapiGest SF (Waters, Milford, MA) then treated in 25:1 mass ratio with trypsin overnight at 37 °C. Following trypsinolysis, 0.5% TFA was added and incubated at 37 °C for 1 h to cleave acid-labile RapiGest. Samples were then centrifuged at 179,000 *g* for 30 min at 4 °C to remove precipitated surfactant. Supernatants were dried using a Vacufuge (Eppendorf AG, Hamburg, Germany).

3.2.4 Human Retina Tissue Processing

Three pools of post-mortem neural retina from human donors were prepared: normal retina from AD-unaffected (n=4) and affected (n=3) donors and retina from donors (n=4) with age-related macular degeneration (AMD). Pools with total protein amounts of 7.6 mg for normal retina, 8.8 mg for AMD, and 12.3 mg for AD were supplemented with 5 pmol to 7 pmol of QconCAT standards. Samples were further processed similar to human frontal cortex. Protein pellets after chloroform/methanol precipitation were sonicated in 400 µL 25 mmol/L NH_4HCO_3 and 0.1% RapiGest then treated in 25:1 mass ratio with trypsin overnight at 37 °C. After trypsinolysis, 0.5% TFA was added and incubated at 37 °C for 1 h. Samples were then centrifuged at 179,000 *g* for 30 min at 4 °C and supernatants were dried using a Vacufuge. Samples were reconstituted in 300 µL 50% acetonitrile and centrifuged again at 65,000 *g* for 1 h at 4 °C to remove insoluble material before final drying in Vacufuge.

3.2.5 Mice

Animal handling procedures and approvals are provided in Appendix A1.4. 5XFAD mice were obtained by crossing 5XFAD hemizygous males on B6SJL background (purchased from the Jackson laboratory) with wild type B6SJL females (also from The Jackson Laboratory). Only F1 males homozygous with respect to the transgene were used. Age-matched males on C57BL/6J background served as controls. Mice were housed in the Animal Resource Center at Case Western Reserve University and maintained in a standard 12 h light/12 h dark cycle environment. Water and food were provided *ab libitum*. Mice

were sacrificed by cervical dislocation at the age of 4 months, and their brains were immediately isolated with the left hemisphere used for quantifications.

3.2.6 Mouse Brain Processing

Left hemispheres of the brain from 5XFAD male mice [22] (n=4) and age- and sex-matched wild type controls (n=2) were prepared similar to human frontal cortex and total protein was measured. Mouse brains were processed individually with no sample pooling. Five mg total protein of each mouse brain sample was supplemented with 5 pmol of QconCATs. Further sample processing was consistent with that of human brain. BLAST search of human-derived HDAC peptides in QconCATs was performed for mice and peptides present in mice were used in analysis of mouse brain samples.

3.2.7 LC-MS/MS Analysis

Dried peptides were reconstituted in 3% acetonitrile, 97% water, and 0.1% formic acid. Separation and MRM analysis was performed on an Agilent Zorbax Eclipse Plus C18 RRHD column (2.1 mm x 50 mm, 1.8 µm particle) coupled to Agilent 6490 Triple Quadrupole LC/MS system with iFunnel technology (Santa Clara, CA). Peptides were eluted over 30 min gradient from 15% to 35% acetonitrile containing 0.1% formic acid at a flow rate of 200 µL/min. Acquisition method used following parameters in positive mode: fragmentor 380 V, cell accelerator 4 V, electron multiplier 500 V, and capillary voltage 3500 V. Collision energy was optimized for each peptide using the default equation from Agilent, CE = 0.036 m/z - 4.8 [95]. Dwell times were varied based on complexity of samples being analyzed and were in 80 ms to 120 ms range.

3.2.8 Data Analysis

MRM transitions were predicted using OrgMassSpecR (http://orgmassspecr.r-forge.r-project.org/) and 2+ charge precursor ions were selected. Transitions were screened in digest of QconCATs to obtain the 3 or 4 most intense transitions, which were further used for quantification (Figure 3.5). Relative signal ratios of transitions for quantification were similar in both the standard QconCAT digest and when QconCATs were added into tissue homogenates, indicating no obvious interference from biological matrices on the quantification using selected transitions. Ratio of peak areas for unlabeled biological peptides to fully-labeled ^{15}N standard peptides was performed using MassHunter (Agilent) and pmol/mg concentrations were calculated based on known picomoles of standard and milligrams of total protein. Protein concentrations represent the mean ± standard deviation (SD) of transitions and peptides associated with each protein. Statistical significance of mean differences was determined by two-tailed Student's *t*-test.

3.3 Results and Discussion

3.3.1 Design of QconCATs

Tryptic peptides were predicted for all HDAC isoforms. Peptides that contained less than eight amino acids were removed to avoid small m/z values. Long peptides were excluded because they tend to have lower signal intensities and more charge states with electrospray ionization. In addition to size constraints, peptides containing methionine were avoided due to oxidation and cysteines were avoided due to potential disulfide bonds and oxidation, which

would interfere with quantification. Finally, sequences were screened with BLAST to ensure Q-peptides were unique in the human proteome. Q-peptides and their natural flanking sequences were assembled into QconCATs. The purpose of including natural flanking sequences is to reduce disparity in efficiency of tryptic digestion between endogenous protein and QconCAT.[58] Additionally, a His_6-tag was included on the C-terminal end, which ensured QconCATs purified by Ni-NTA column would be full-length and not include truncated forms. An overview of design and expression is shown in Figure 3.1 and QconCAT sequences are presented in Tables 3.1, 3.2, and 3.3.

3.3.2 Characterization of ^{15}N QconCAT Internal Standard

Purity of QconCATs was estimated by SDS-PAGE (Figure 3.2A) and ImageJ software to be nearly 100% for QconCAT#1, ≥95% for QconCAT#2, and ≥97% for QconCAT#3. No correction for protein concentration was made for analysis. Intact mass of each QconCAT was consistent with expected mass, indicating full-length expression of protein. Figure 3.2B shows a representative spectrum and deconvolution for QconCAT#1. Deconvoluted mass for QconCAT#1 was 46126.7 (46125.6 Da theoretical), QconCAT#2 was 48931.2 Da (48929.7 Da theoretical), and QconCAT#3 was 43167.8 Da (43166.6 Da theoretical).

Table 3.5 - Transitions used for quantification.

Isoform	Peptide	Species		Precursor (m/z)	Product Ions (m/z)		
					1	2	3
HDAC1,2	YGEYFPGTGDLR	human/mouse	L	687.8	715.4 (y_7)	862.4 (y_8)	1025.5 (y_9)
			H	695.3	725.3 (y_7)	873.4 (y_8)	1037.5 (y_9)
HDAC3	YTGASLQGATQLNNK	human/mouse	L	783.4	845.4 (y_8)	973.5 (y_9)	1173.6 (y_{11})
			H	793.4	857.4 (y_8)	987.5 (y_9)	1189.6 (y_{11})
HDAC4	ESAVASTEVK	human/mouse	L	510.8	563.3 (y_5)	634.3 (y_6)	733.4 (y_7)
			H	516.2	569.3 (y_5)	641.3 (y_6)	741.4 (y_7)
	DQPVELLNPAR	human/mouse	L	626.3	683.4 (y_6)	812.5 (y_7)	1008.6 (y_9)
			H	634.3	693.4 (y_6)	823.4 (y_7)	1021.5 (y_9)
HDAC5	LSTQQEAER	human/mouse	L	510.8	632.3 (y_5)	760.4 (y_6)	861.4 (y_7)
			H	531.3	641.3 (y_5)	771.3 (y_6)	873.4 (y_7)
	GALVGSVDPTLR	human	L	592.8	601.3 (y_5)	787.4 (y_7)	844.5 (y_8)
			H	600.3	609.3 (y_5)	797.4 (y_7)	855.4 (y_8)
HDAC6	EQLIQEGLLDR	human/mouse	L	657.4	702.4 (y_6)	830.4 (y_7)	943.5 (y_8)
			H	665.3	711.4 (y_6)	841.4 (y_7)	955.5 (y_8)
	LEELGLAGR	human	L	479.3	586.4 (y_6)	715.4 (y_7)	844.5 (y_8)
			H	485.3	595.3 (y_6)	725.4 (y_7)	855.4 (y_8)
HDAC7	TLEPLETEGATR	human	L	658.8	763.4 (y_7)	876.4 (y_8)	1102.5 (y_{10})
			H	666.3	773.3 (y_7)	887.4 (y_8)	1115.5 (y_{10})

Transitions are listed for both unlabeled, light (L) and fully ^{15}N-labeled, heavy (H) peptides. All precursor ions were +2 charge and product ions were +1 charge. Additionally, y-ion information is included for reference.

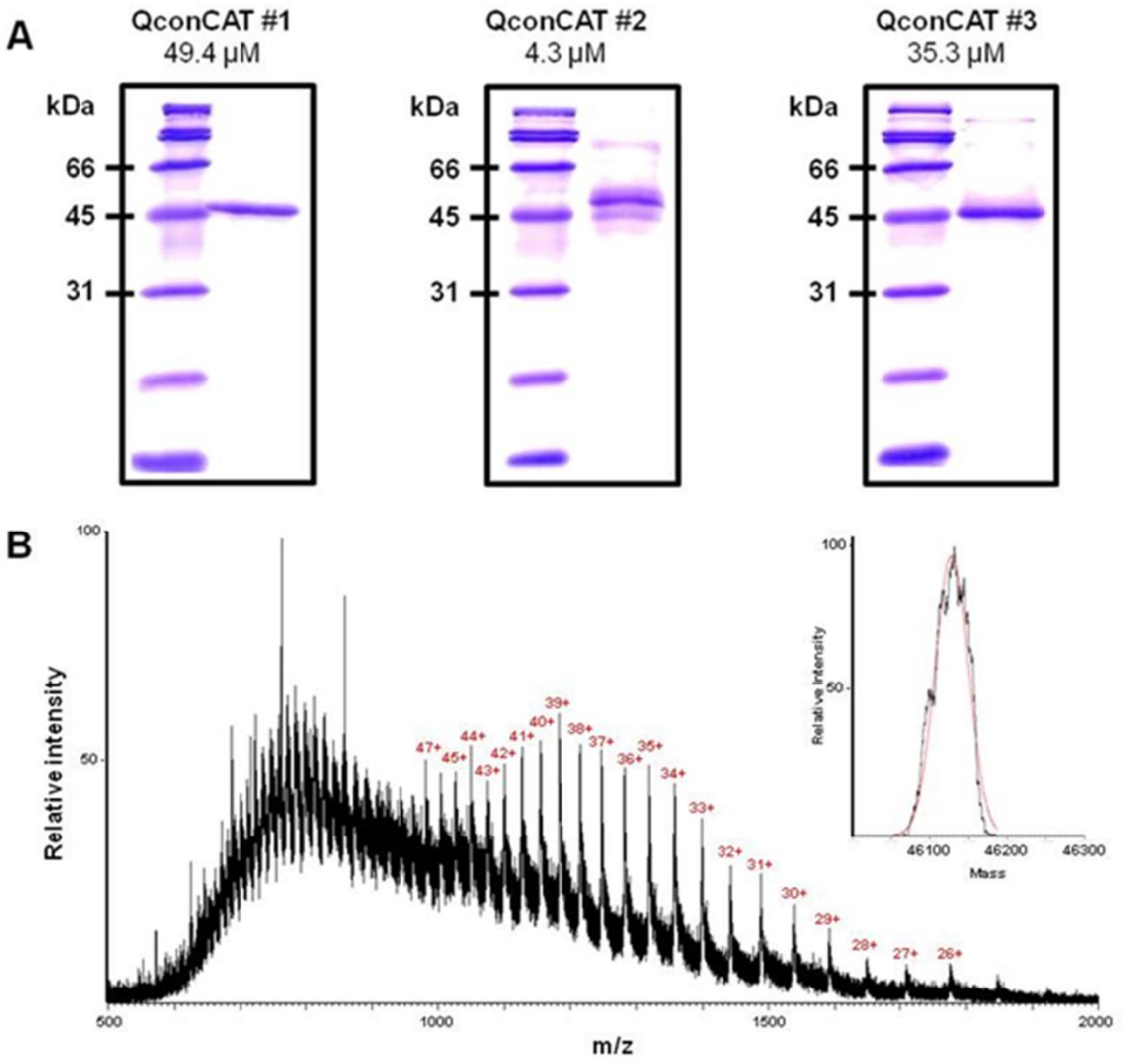

Figure 3.2 - Purity and size of QconCATs.
(**A**) Purified QconCATs (30 pmol of QconCAT#1, 22 pmol of QconCAT#2, and 25 pmol of QconCAT#3) were separated on 10% SDS-PAGE and ImageJ software was used for estimation of purity. Purity was nearly 100% for QconCAT#1, ≥95% for QconCAT#2, and ≥97% for QconCAT#3. Protein concentrations were determined by DC Protein Assay. (**B**) Charge state masses were collected for all QconCATs (representative spectrum of QconCAT#1 shown) with an Agilent 6550 QTOF and deconvoluted with MagTran 1.0 (insert) to confirm protein mass was congruous with expected mass based on sequence. Observed mass of QconCAT#1 was 46126.7 Da (46125.6 Da theoretical), QconCAT#2 was 48931.2 Da (48929.7 Da theoretical), and QconCAT#3 was 43167.8 Da (43166.6 Da theoretical).

^{15}N isotope incorporation (Figure 3.3) was determined using a relatively short and long peptide for each QconCAT and both peptide lengths yielded consistent results. Incorporation was 99.3% for QconCAT#1, 99.3% for QconCAT#2, and 99.4% for QconCAT#3. These values were accepted as complete labeling and no correction was applied to data. Calibration curves were performed using variable amounts of unlabeled HDAC6 mixed with a fixed amount of QconCAT#2, which contained HDAC6 peptides. Calibration curves showed linearity of Q-peptides in the 0.125 pmol to 2.5 pmol HDAC6 range tested; Figure 3.4 shows a representative calibration curve for peptide LEELGLAGR. Lower limit of quantification (LLOQ) was defined as the lowest point of calibration curve that could be measured with a coefficient of variance less than 20%. LLOQ for HDAC6 peptide LEELGLAGR was 0.05 pmol in mixture of HDAC6 standard and QconCAT#2 internal standard. A representative chromatogram and spectrum of a Q-peptide is shown in Figure 3.5.

3.3.3 Human Frontal Cortex

The outermost portion, or cortex, of the frontal lobe was used for sample preparation. Cortex is commonly referred to as gray matter and consists primarily of neural cell bodies with few myelinated axons. Measurements in frontal cortex present a challenge due to the high lipid content, approximately 40% of dry weight [96]; therefore sample processing is important. Two methods of fractionation were used to reduce sample complexity while maintaining the same ratio of analyte to internal standard.

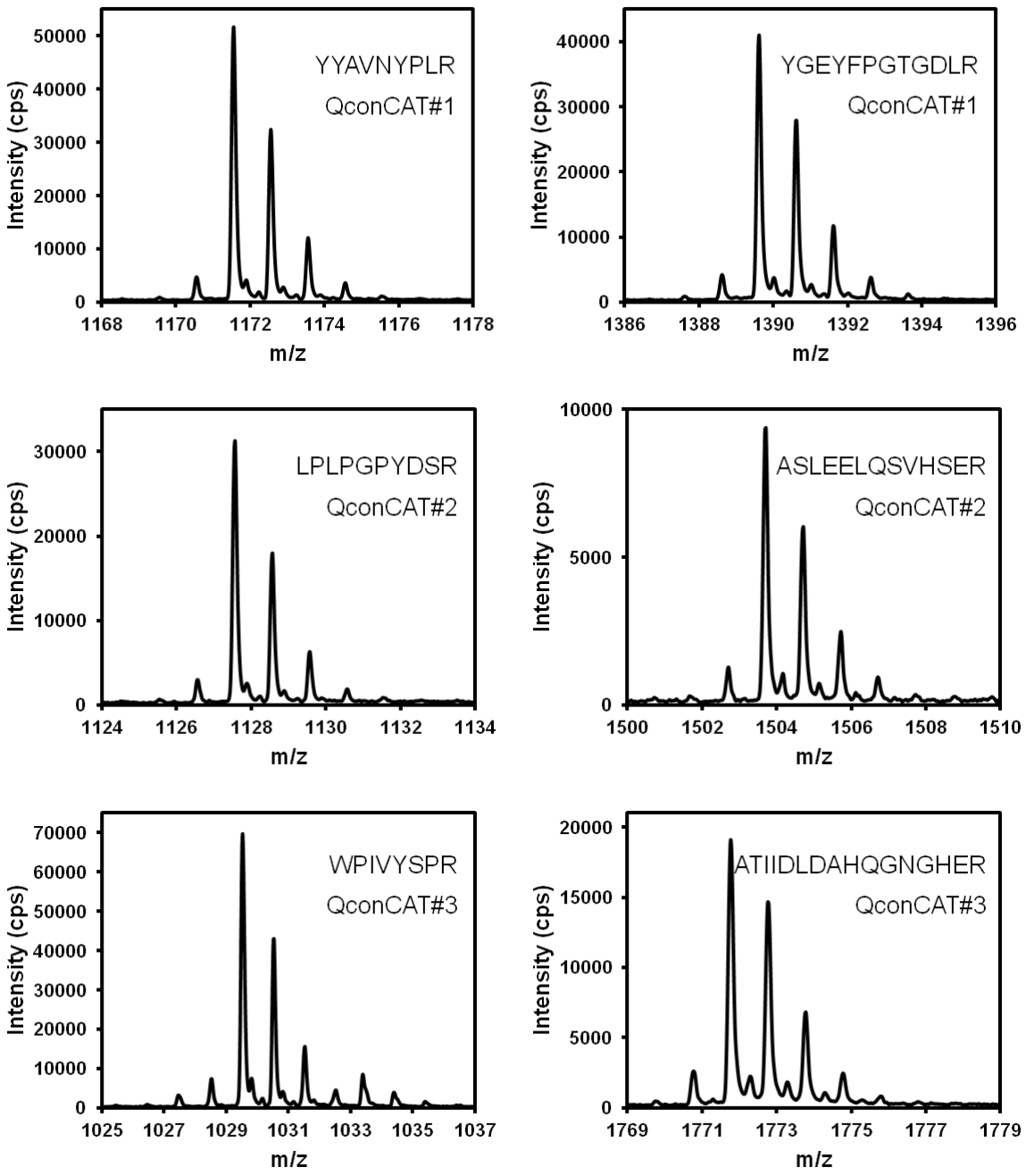

Figure 3.3 - ^{15}N incorporation in QconCATs.
MALDI spectra of QconCAT peptides were used to calculate ^{15}N incorporation with Isotopic Enrichment Calculator (www.nist.gov/mml/analytical/organic/isoenrichcalc.cfm). Incorporation of ^{15}N was determined to be 99.3% for QconCAT#1, 99.3% for QconCAT#2, and 99.4% for QconCAT#3.

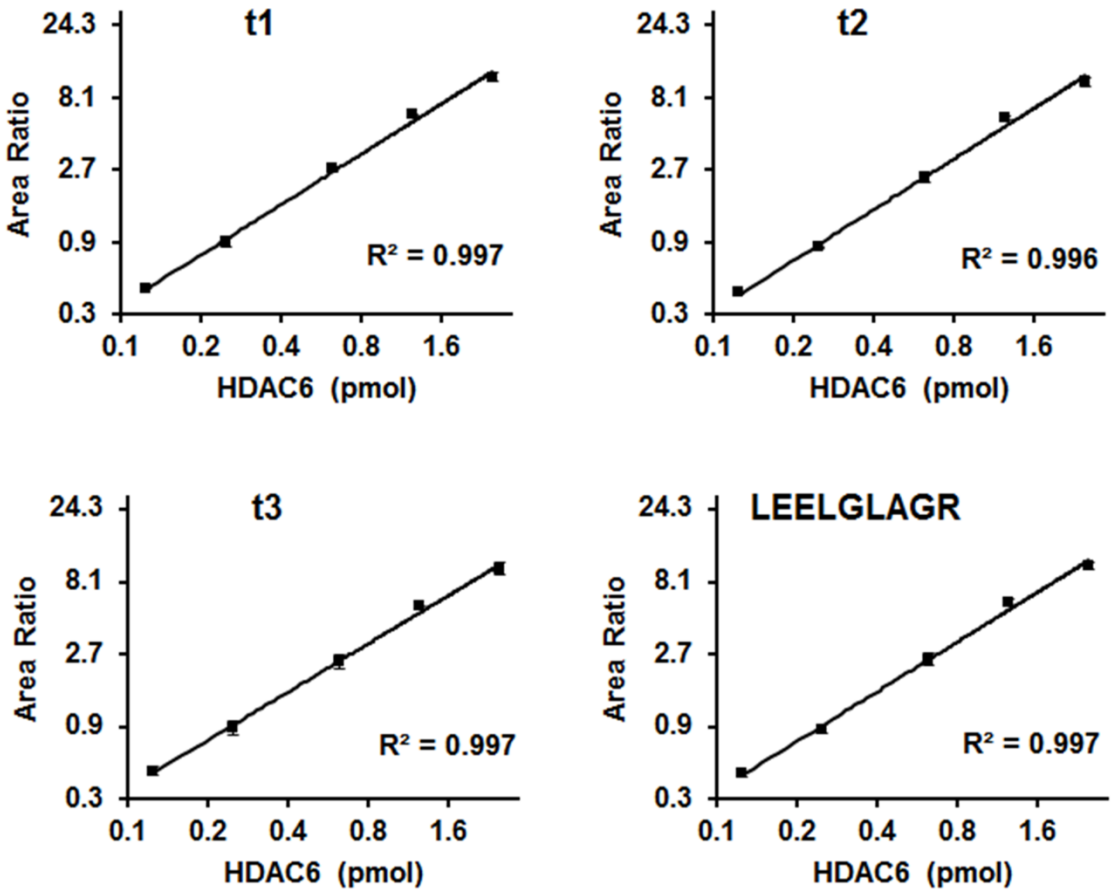

Figure 3.4 - Calibration curves.
Calibration for quantification of peptide LEELGLAGR from HDAC6 standard using ^{15}N-labeled peptide from QconCAT#2 as internal standard. Area ratio of ^{14}N-LEELGLAGR to ^{15}N-LEELGLAGR for each of the three transitions for quantification was plotted versus pmol of HDAC6 standard. Individual transitions shown are (t1) 479.3/586.4 and 485.3/595.3, (t2) 479.3/715.4 and 485.3/725.4, (t3) 479.3/586.4 and 485.3/595.3. Three replicates for each were collected and presented as mean ± SD. Consensus for t1-t3 is represented in LEELGLAGR graph.

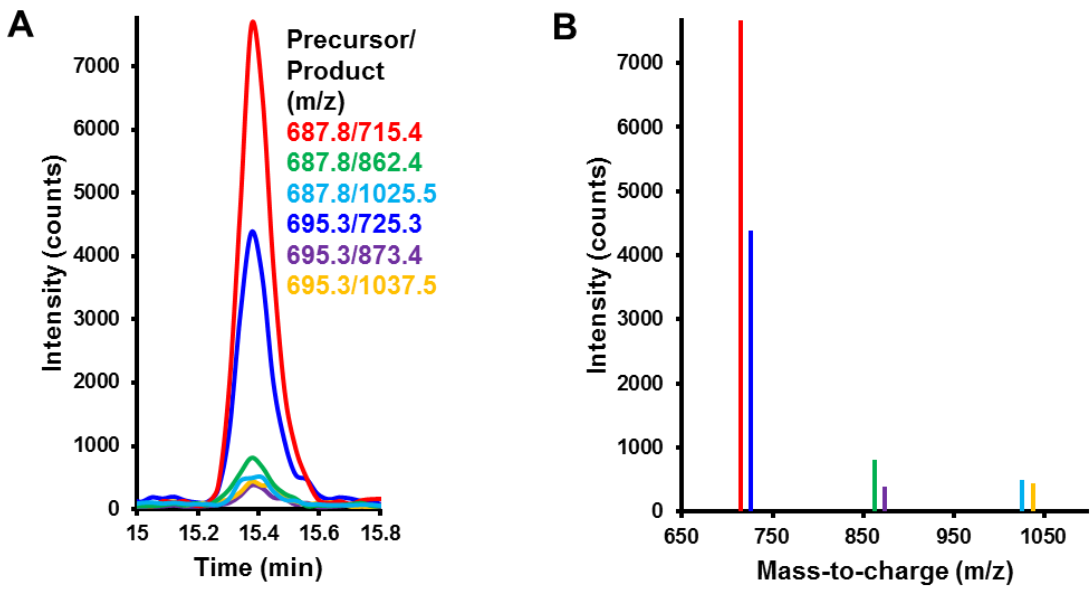

Figure 3.5 - Representative chromatogram and spectrum.
Transitions for HDAC1,2 peptide YGEYFPGTGDLR in 5XFAD mouse brain hemisphere are shown as a **(A)** chromatogram and **(B)** spectrum. Chromatogram peaks of transitions are representative of data for other peptides in neural tissue. Peak areas were used for quantification.

High speed centrifugation at 106,000 *g* was performed which separated membrane associated proteins and some lipids from soluble proteins and HDACs. Additionally, chloroform/methanol precipitation was performed which removed SDS, by-products of cysteine alkylation, remaining lipids, and salts. These two fractionation steps are important for the success of the mass spectrometry method of quantification, improving chromatographic performance and reducing ion suppression effects.

Measurements were performed on pooled samples from AD (n=5) and normal (n=5) human frontal cortex. The purpose of using pooled tissue samples is to minimize the effects of donor-to-donor variation while maintaining the biological variation between donor groups, allowing for evaluation of substantive characteristics of the donor population. This research functions as a feasibility study, demonstrating the applicability of QconCAT technology with MRM MS to conduct protein quantification in a complex biological matrix, such as brain. While our study findings are based on pools from five donors in each sample group, our method can easily be applied to a large number of individual donor samples, if a larger number of samples are available. HDAC isoforms detected in human frontal cortex are summarized in Table 3.6. Out of the 11 isoforms, we detected HDAC1,2, HDAC5, and HDAC6 only. Other HDAC isoforms are either (i) not significantly expressed in human frontal cortex or (ii) expressed at levels in human frontal cortex that are below the limit of quantification of our MRM assay, which is approximately 5 fmol/mg total protein. Concentration of HDAC1,2 decreased 32% from 1.10 pmol/mg in control to 0.746 pmol/mg in AD.

Table 3.6 – Summary of human frontal cortex HDAC concentrations.

	pmol/mg tissue protein[a]	
Isoform	Control	AD
HDAC1,2	1.10 ± 0.14	0.746 ± 0.071[c]
HDAC5	0.083 ± 0.016	0.122 ± 0.025[b]
HDAC6	0.106 ± 0.015	0.139 ± 0.015[c]

[a]Measurements were performed on supernatant of frontal cortex from age-matched control (n=5) and severe AD (n=5) human donor pools (Table 3.4) supplemented with QconCAT standard after high-speed centrifugation. Concentrations were calculated for three biological replicates and with three transitions per Q-peptide. Q-peptide transitions are summarized in Table 3.5. Data presented as mean ± SD. [b], $p < 0.01$; [c], $p < 0.001$.

HDAC1,2 measurement was based on a peptide in both isoforms because HDAC1 and HDAC2 have similar sequences and unique peptides included in QconCATs did not produce signals sufficient for detection or quantification. Therefore, we were not able to ascertain whether both HDAC1 and HDAC2 decreased but were able to determine the sum of their concentrations decreased in AD. HDAC5 and HDAC6 both showed an increasing trend of 47% and 31%, respectively. Work by others has shown that HDAC5 is correlated to repression of angiogenesis [97] and HDAC6 is correlated with protein aggregation [81,98,99] in mouse models. Conversely, decreases in HDAC5 can impair memory, which is a function of the hippocampus and temporal lobe, suggesting HDAC isoforms may vary by brain regions.

Immunohistochemical staining of cerebral cortex in The Human Protein Atlas (www.proteinatlas.org) shows HDAC2 is highly abundant, and when combined with less expressed HDAC1, they would be among the most abundant of the HDACs. They report HDAC5 is present at medium levels and HDAC6 at

low levels. While our concentrations of HDAC5 and HDAC6 are within a similar range and in a specific portion of the cerebral cortex, called the frontal cortex, the qualitative levels on these HDACs available in The Human Protein Atlas are similar to our profile. Additionally, quantitative polymerase chain reaction assays by Jakovceoski et al. have shown transcript levels of HDAC1, 2, 5, and 6 are nearly identical in frontal cortex [100], which is consistent with our findings given that HDAC1 and 2 are combined. HDAC6 has been shown to increase in AD brain [101], as we have shown. However, it has been reported that HDAC2 increases and HDAC1 remains normal in AD brain and cortex [102,103], counter to our observed trends.

3.3.4 Human Retina

Neural retina is a specialized extension of the central nervous system (CNS) connected to the occipital lobe of the brain. We selected neural retina to test our protocol of HDAC quantification in a different biological matrix and to gain insight into AD changes in other functionalized portions of the CNS. Sample processing procedures for frontal cortex were also applied to retina, enabling quantification of HDACs in this tissue (Table 3.7). Similarity in HDAC coverage acquired in frontal cortex demonstrates this procedure is also appropriate for neural retinal tissue matrix. Retina samples were obtained from AD-affected and AMD donors to evaluate changes in HDACs in these disease states. AMD retina was included because it is another degenerative disease associated with aging and has several clinical similarities with AD, including amyloid deposition and stress stimuli [93,104,105]. HDAC concentrations in retina are summarized in

Table 3.7. A decrease in concentration was observed for all detected HDAC isoforms in normal retina from AD-affected donors compared to normal retina from AD-unaffected donors. HDAC1,2 decreased similarly in both AD-affected tissue types of retina and frontal cortex and showed a slight decrease in AMD retina. HDAC5 and HDAC6 showed a decrease in AMD retina and a greater decrease in retina from AD-affected donors, counter to the increasing trend observed in frontal cortex. HDAC7 did not appear to change in concentration in AMD retina but was nearly reduced in half in retina from AD-affected donors.

In addition to trends in concentration of retinal HDACs and their comparison to those in frontal cortex in disease state, overall profile of HDAC isoforms was also different in retina and frontal cortex. HDAC1,2 and HDAC5 had similar levels of concentration in both frontal cortex and retina tissues while HDAC6 in retina was approximately five-fold greater than the concentration in control frontal cortex.

Table 3.7 - HDAC concentrations in human neural retina.

	pmol/mg tissue protein[a]		
Isoform	Control	AD	AMD
HDAC1,2	1.63 ± 0.12	0.743 ± 0.065[c]	1.14 ± 0.19[c]
HDAC5	0.106 ± 0.014	0.0393 ± 0.0077[c]	0.074 ± 0.017[b]
HDAC6	0.558 ± 0.081	0.298 ± 0.062[c]	0.415 ± 0.032[c]
HDAC7	0.078 ± 0.020	0.0251 ± 0.0068[c]	0.069 ± 0.017

[a]Measurements were performed on supernatant of retina from control (n=4), AD-affected (n=3), and AMD (n=4) human donor pools (Table 3.4) supplemented with QconCAT standards after high-speed centrifugation. Concentrations were calculated for three experimental replicates and with three transitions per Q-peptide. Q-peptide transitions are summarized in Table 3.5. Data presented as mean ± SD. [b], $p < 0.01$; [c], $p < 0.001$.

Additionally, HDAC 7 was detected in retina in concentrations comparable to HDAC5 in retina but was not detected in frontal cortex. Disparity in changes in retina from those in frontal cortex is an interesting pathological phenomenon that may suggest importance of HDAC isoforms and their respective roles in specialized tissues. HDAC1, 3, and 6 have been shown by Western blot to decrease in concentration in retina as it ages, while HDAC2 and 5 remain unchanged [106]. We also observed a decrease in HDAC1,2 and in HDAC6 in disease-affected retina, perhaps indicative of their decreased abundance in aging tissue.

3.3.5 Mouse Brain

Whole hemisphere of brain was analyzed for several reasons. Firstly, whole hemisphere of mouse brain was homogenized during sample preparation and HDAC concentrations reflect inclusive averages for the entire brain rather than a specific, functionalized portion of human brain, such as frontal cortex. Secondly, tissue matrix varies from human frontal cortex, which mainly contains only gray matter, to the brain hemisphere of mice, which includes white matter rich in myelinated axons. Lipids are a concern in brain tissue analysis and whole brain tissue contains more lipids than gray matter of frontal cortex due to the abundance of myelin, which is 80% lipid by dry weight [96]. Thirdly, and perhaps most important for AD pathology, HDAC profiles in mouse models may be compared to that of human frontal cortex. There are two main points to consider in comparing mouse and human HDAC profiles for AD: species variation and familial versus sporadic AD. While the eleven main isoforms of HDACs are

present in both mice and humans, there are some differences in the amino acid sequences that had to be taken into account. Accordingly for mouse sample analysis, BLAST was used to refine human peptides present in expressed QconCATs to those for both human and mouse isoforms, approximately half of total human peptides. Thus, not all peptides measured in human were used to obtain HDAC concentrations in mice. Additionally, HDAC isoform concentrations could be dictated by levels of HDAC regulation in mice different from that in humans. Another important caveat to using animal models for AD research is that mice may only be produced as models of familial AD via known mutations. The vast majority of AD cases in humans are considered sporadic AD and cannot be predicted. While clinical indicators of AD, such as amyloid aggregation, may be present in both sporadic and familial AD, pathogenesis may vary. In this study, 5XFAD transgenic mouse models of rapid brain amyloidosis were used. 5XFAD mice overexpress two mutant human proteins: presenilin 1 with familial AD (FAD) mutations M146L and L286V and β-amyloid precursor protein (APP695) with Swedish (K670N, M671L), Florida (I716V), and London (V717I) FAD mutations. Mixed wild type B6SJLF1/J mice are used for the production of 5XFAD transgenic mice and therefore provide an appropriate background strain of wild-type mice, which were used as our control.

HDAC isoform concentrations in both control and 5XFAD mice are summarized in Table 3.8. HDAC1,2 had no change in 5XFAD mice but decreased by 1.5-fold in AD human frontal cortex (Table 3.6). Since HDAC1,2 measurements were based on a conserved peptide, we were unable to

determine the contribution of isoforms HDAC1 and HDAC2 to the reported measurements. HDAC3 had a slight increase of 50%, HDAC4 also increased by 63%, and HDAC5 and HDAC6 did not show significant change in 5XFAD mouse model. Of the HDAC isoforms reported for both mouse and human profiles, HDAC1,2 was most abundant in both. However, HDAC3 and HDAC4 were within the concentration range of other isoforms in HDAC profile in mouse model yet not detected in human. Inconsistency in observed HDAC profiles of human and mouse brains may be for several reasons, such as differences in expression of HDACs between species, differences in functionalization of frontal cortex to whole brain hemisphere, and post-translational modification of peptides used for quantification. Additionally, due to sampling limitations, small portions of frontal cortex tissue were excised from human donors at random by support pathologists. It may be possible that patterning of HDACs varies across the frontal cortex region of the brain. While our pilot study highlights specific HDAC changes, future studies using our MRM assay could be performed on many sites across a particular donor to address variability in HDAC concentrations within frontal cortex. Mouse models allow for knockout and overexpression studies for disease pathology but our work suggests HDAC findings in mouse models should not be over interpreted without evaluation of human tissue.

HDAC profiles in mouse brain were evaluated by Broide et al. [89] using *in situ* hybridization and they found that HDAC3, 4, and 5 were close in abundance with HDAC6 being less abundant and the sum of HDAC1 and 2 being more abundant, consistent with our observations. Wang et al. performed

Table 3.8 - HDAC concentrations in whole hemisphere of mouse brain.

	pmol/mg tissue protein[a]	
Isoform	WT	5XFAD
HDAC1,2	1.010 ± 0.074	1.02 ± 0.23
HDAC3	0.131 ± 0.010	0.196 ± 0.024[b]
HDAC4	0.230 ± 0.029	0.375 ± 0.023[c]
HDAC5	0.154 ± 0.015	0.143 ± 0.023
HDAC6	0.0149 ± 0.0039	0.0171 ± 0.0022

[a]Measurements were performed on supernatants of whole left hemispheres of mouse brains from 5XFAD (n=4) and wild type (n=2) mice supplemented with QconCAT standards after high-speed centrifugation. Three transitions per Q-peptide were used to calculate concentration for each mouse. Wild type (n=2) and 5XFAD (n=4) mice concentrations were averaged and data is presented as mean ± SD of each sample group. Q-peptide transitions are summarized in Supporting Information S5 Table. [b], $p < 0.05$; [c], $p < 0.01$.

autoradiography with a radioactive isotopologue to an inhibitor of HDAC1-3 and 8 to measure pmol/mg concentrations *ex vivo* in mouse brain [107]. They were unable to detect HDAC8, as we were unable to, which was confirmed by Western blot. They reported the sum of HDAC1-3 concentrations to be 12.9 pmol/mg within mouse brain, more than our measurement of 1.14 pmol/mg. While their method was able to provide pmol/mg concentrations, this was based on binding to an inhibitor shared between multiple HDACs and individual HDAC measurements would have to be derived by using Western blot intensities of HDAC1, 2, and 3 performed in parallel to account for contribution of each HDAC isoform bound to the labeled inhibitor.

Measurements for HDAC5 and 6 in human tissues and HDAC4 in mouse tissue were performed using two peptides for each isoform (Table 3.5). When measured individually, peptides were in close agreement with the other

respective peptide for the isoform (Table 3.9). This demonstrates that the peptide-to-peptide variability in measurement was not statistically significant using the MRM assay with QconCATs as internal standards.

Table 3.9 - Comparison of individual Q-peptide and protein measurements.

Mouse brain (control)	pmol/mg
ESAVASTEVK	0.229 ± 0.028
DQPVELLNPAR	0.231 ± 0.034
HDAC4 (total)	**0.230 ± 0.029**

Human frontal cortex (control)	pmol/mg
GALVGSVDPTLR	0.085 ± 0.020
LSTQQEAER	0.080 ± 0.010
HDAC5 (total)	**0.083 ± 0.016**
EQLIQEGLLDR	0.102 ± 0.010
LEELGLAGR	0.112 ± 0.018
HDAC6 (total)	**0.106 ± 0.015**

Three transitions for each Q-peptide (Supporting Information S5 Table) were used for measurements in biological replicate samples of control human frontal cortex (n=5) and whole hemispheres of control mice (n=2). For HDACs 4, 5, and 6, two Q-peptides were used for quantification of each protein. Concentrations of mean ± SD for individual peptides are presented for comparison to mean ± SD for protein measurements, which include a total of both peptides (bold). Student t-test was performed and concentrations of peptides for the same protein were not statistically different in comparison to each other, indicating a consensus in peptide measurements.

3.4 Conclusions

Concentrations of several HDAC isoforms were obtained in three different tissues: human frontal cortex, human retina, and whole mouse brain. We demonstrated that our method of protein quantification is suitable in different types of tissues, particularly in challenging matrices with high lipid content. In human frontal cortex, observed HDAC isoforms had different changes in control to AD with HDAC1,2 decreasing, HDAC5 increasing, and HDAC6 having negligible change in concentration. In human retina, reduction in concentration of detected HDACs was observed in both AMD retina and retina from AD donors in comparison to control retina. Mouse brain depicted a slightly different HDAC profile from humans with variance in overall HDAC3 and HDAC4 abundance being greater in mouse. Additionally, HDAC1,2 concentrations in AD-affected donors decreased compared to control in both human frontal cortex and retina but showed no change in mouse hemisphere. Mouse models are widely used for neurodegenerative research and our data indicates some disparity in HDAC profiles and changes in disease state compared to human frontal cortex tissue.

However, limitations in Q-peptides suitable for MRM did restrict our HDAC profile in tissues examined. Many HDAC isoforms have similar sequences and therefore selecting unique sequences that meet MRM criteria, such as length and no post-translational modifications, restricts availability of Q-peptides. Furthermore, some peptides do not perform well either in ionization efficiency or reproducibility of transitions. Once unsuitable peptides are excluded, HDAC isoform profiles were further restricted to isoforms that can be observed in

biological sample. Some HDACs may be present at very low levels precluding their detection via MRM and may require more sensitive approaches, such as an enzyme-linked immunosorbent assay (ELISA). While the QconCAT MRM method may have shortcomings, it is able to multiplex protein quantification, reduce analysis time, and accounts for loss during sample processing compared to synthetic labeled peptides and ELISA [60].

Our feasibility study demonstrates the value of MRM mass spectrometry and QconCAT technology to perform multiplexed, quantitative measurements of HDAC isoforms in various tissues. Moreover, our measurements show that changes in concentrations of HDACs have different trends in frontal cortex and neural retina in AD and that mouse hemisphere and human frontal cortex HDAC profiles differ. This method may be applied to other tissues and disease conditions to obtain concentrations of HDAC isoforms, a practical and useful tool for investigation of disease pathology.

Chapter 4: Phosphorylation of Histone H3 Ser57 and Thr58

This chapter contains published material [54].

4.1 Introduction

One common PTM on histones is phosphorylation of serine (Sp) and threonine (Tp) residues, which has been linked to activation and repression of genes based on site of modification and condition of cells [41–43]. Serine phosphoacceptor sites are found on the tail regions of all core histones [108]. Phosphorylation of S10 on histone H3 (H3S10p) has been extensively studied for its roles in condensation of chromatin during mitosis [42,43] and to a lesser extent in neurodegenerative disorders, such as AD [109]. While many types of PTMs on histone tails have been associated with disease, little information exists on PTMs in the core region of histones. It is suggested that phosphorylation of H3 may be particularly meaningful compared to other core histones [41,110]. Specifically in the core region of H3, there are several potential threonine and serine phosphorylation sites, but exploration of their significance has been minimal. H3T45p is directly correlated with apoptosis [111], H3T80p is increased in mitosis [112], and H3T118p destabilizes the nucleosome [113]. However, little is known about H3S57 and H3T58 phosphorylation roles in normal biological functions and there is no information to date describing changes in these phosphorylation sites in AD brain. H3S57p has been detected in mammalian cells and may have implications in response to DNA damage based on studies in yeast [114]. H3T58p has not been previously characterized. Additionally, we

investigated *in silico* potential phosphorylation sites on the surface of the nucleosome which could be easily accessible to kinases and phosphatases and found that S57 and T58 are located on the surface. Specifically, these adjacent residues occur in an accessible turn of a helix-turn-helix motif of H3 in close proximity to DNA, which suggests these sites may engage in regulatory phosphorylation and supports investigation into these sites in brain and AD pathology.

Initially, we screened human frontal cortex for phosphorylation but were unable to detect any phosphorylation in the human tissue. We believed this is due to loss of phosphorylation in the time frame between the death of the donor and when the brain tissue was frozen, referred to as the post-mortem interval (PMI). PMI for most of our brain tissue from human donors ranged from 6 to 10 h. During the PMI, phosphatases are still active and able to remove phosphoryl groups from histones, additionally, phosphorylation is a very labile PTM and these effects likely degraded the histone phosphorylation. We instead chose to use the 5XFAD mouse model of rapid amyloid deposition as our subject for investigation of H3 phosphorylation at S57 and T58 sites because the PMI for mice was within minutes.

5XFAD mice were also treated with a low dose of efavirenz (EFV), an FDA-approved reverse transcriptase inhibitor used for the treatment of HIV. At clinical levels for HIV treatment, EFV has been shown to increase expression of β-secretase, an enzyme responsible for processing amyloid precursor protein (APP), and increase levels of soluble Aβ in murine N2a cells expressing the

Swedish APP mutation [115]. At levels a hundred-fold lower than used for HIV, EFV stimulates activity of cytochrome P450 CYP46A1, a brain-specific cholesterol 24-hydroxylase, which increases cholesterol turnover in mouse brain [116]. Elevated cerebral activity of cytochrome P450 CYP46A1 allows for clearance of cholesterol from the brain and is shown to ameliorate cognitive impairment and amyloid pathology in mouse models of neurodegeneration [117,118]. Moreover, cholesterol metabolism is linked to AD with hypercholesterolemia increasing Aβ plaques and hypocholesterolemia reducing Aβ plaques in brain [119,120]. Other neuroprotective effects may occur with low dose EFV administration that may affect epigenetic indicators, namely PTMs of histones. It was therefore prudent to measure changes in histone H3 S57 and H3T58 phosphorylation for EFV-associated effects.

This study shows that phosphorylation of both S57 and T58 on histone H3 is lower in 5XFAD models of amyloid deposition in comparison to wild type controls. Since changes in PTMs of histones are established to influence genetic expression, our measurements of specific histone H3 residues S57 and T58 may provide insight into the epigenetic blockade phenomenon in the pathology of neurodegeneration. While EFV treatment did not have observable effects, this may indicate either: (i) the neuroprotective mechanism of EFV is unrelated to S57 and T58 phosphorylation; (ii) the proposed therapeutic dosage of EFV was insufficient to produce observable changes in measured phosphorylation, APP, and Aβ.

4.2 Methods

4.2.1 Mice

All animal-handling procedures and approvals are provided in Appendix A1.4. 5XFAD mice [22] were maintained by crossing 5XFAD hemizygous males on B6SJL background (The Jackson Laboratory) with B6SJL females (The Jackson Laboratory, stock 100012). Only F1 males homozygous with respect to the transgene were used. Wild type C57BL/6J mice (The Jackson Laboratory, stock 000664), a common laboratory strain that does not develop amyloid plaques, and the progenitor strain used to make transgenic 5XFAD, were used as a control. Mice were housed in the Animal Resource Center at Case Western Reserve University and maintained in a standard 12 h light/12 h dark cycle environment. Water and food were provided *ab libitum*. 5XFAD male mice (n=3) and C57BL/6J age- and sex-matched wild type controls (n=3) were sacrificed at 3 months of age to assess the differences. Additional age- and sex-matched 5XFAD mice were maintained with EFV treatment (n=3) and without treatment (n=3) for a three month period. For EFV treated mice, administration of EFV was commenced after a one week period of acclimation. EFV was administered through drinking water at a concentration of 1.68 mg/liter, which was provided *ad libitum*. Daily dose of EFV during the 3-month treatment period was 0.22 mg/kg.

4.2.2 Whole Mouse Brain Processing

Hemispheres of brains were harvested and flash-frozen in liquid nitrogen for storage at -80 °C. Left hemispheres of the brain were finely minced with a scalpel blade and homogenized in 25 mmol/L NH_4HCO_3 by sonication at 30 W

using five, 10 second continuous cycles (Sonicator 3000, Misonix Inc., Farmingdale, NY). Total protein concentration of the homogenate was measured using a DC protein assay kit in the presence of 1% sodium dodecyl sulfate (SDS) with bovine serum albumin as the standard. Homogenates were aliquoted and stored at -80 °C. Samples of 3 mg total protein were supplemented with 12 pmol APP QconCAT standard [70] and treated with 20 mmol/L dithiothreitol (DTT) and 1% SDS. After 1 h incubation at room temperature to reduce cysteines, 55 mmol/L iodoacetamide was added and incubated an additional 1 h to alkylate cysteines. Chloroform/methanol precipitation was used to isolate proteins. Protein pellets were then sonicated in 1 mL 25 mmol/L NH_4HCO_3/0.1% RapiGest SF surfactant and treated with trypsin at 25:1 protein:trypsin mass ratio overnight at 37 °C. After trypsinolysis, 0.5% trifluoroacetic acid (TFA) was added and incubated at 37 °C for 1 h to cleave acid-labile RapiGest SF surfactant, which was subsequently removed by centrifugation at 179,000 *g* for 30 min at 4 °C. Supernatants were dried in an Eppendorf AG Vacufuge (Hamburg, Germany), yielding final peptides for analysis.

4.2.3 LC-MS/MS Analysis

Dried peptides were reconstituted in 3% acetonitrile, 97% water, and 0.1% formic acid. Separation was performed on an Agilent Zorbax Eclipse Plus C18 RRHD column (2.1 mm x 50 mm, 1.8 µm particle) and MRM analysis was performed on an Agilent 6490 iFunnel Triple Quadrupole LC/MS system (Santa Clara, CA). Peptides were eluted at a flow rate of 200 µL/min using the following gradient of solvent B in solvent A: 3% B for 3 min, 3% to 30% B in 32 min, 30%

to 50% B in 5 min, and 50% to 3% B in 3 min. Solvent A was water containing 0.1% formic acid and solvent B was acetonitrile containing 0.1% formic acid. The acquisition method used the following parameters in positive mode: fragmentor 380 V, collision energy 20 V, dwell time 100 ms, cell accelerator 4 V, electron multiplier 500 V, and capillary voltage 3500 V. MRM transitions for 2+ charge precursor ions and 1+ charge product ions were predicted using PinPoint software (Thermo Fisher Scientific, Waltham, MA).

4.2.4 Data Analysis for APP and Aβ

Quantification of total APP and Aβ in mouse brain samples, using MRM with QconCAT as an internal standard [70], was performed to confirm that the 5XFAD model of amyloid pathogenesis produced significant Aβ in comparison to the control. The QconCAT standard used contained peptides for both APP and Aβ [70] and was supplemented into homogenates prior to processing to increase precision and accuracy of measurements. Based on sequence specificity and measured intensity, a single peptide, LVFFAEDVGSNK, was selected from Aβ and two peptides, VESLEQEAANER and AVIQHFQEK, were selected to measure total APP. APP is a large transmembrane protein that undergoes processing to release the fragment Aβ. Therefore, the Aβ amino acid sequence is part of the APP protein. Measurements for Aβ are inclusive of the Aβ fragment and unprocessed APP, which still contains Aβ. These peptides were included in a stable isotope labeled QconCAT standard, as previously described [70], which was supplemented into samples. Quantification of APP and Aβ was performed by calculating the ratio of peak areas for unlabeled biological peptides to labeled

standard peptides using MassHunter software (Agilent) multiplying by the ratio of known picomoles of standard to milligrams of total protein. Protein concentrations are presented as pmol/mg and represent the mean ± standard deviation (SD) of peptide transitions associated with each protein. Statistical significance of mean differences was calculated using Student's two-tailed *t*-test and was considered significant if $p \leq 0.05$. Transitions used for quantification of APP and Aβ are presented in Table 4.1.

4.2.5 Data Analysis for Phosphorylation

All selected MRM transitions were used to confirm the identity of each peptide for each LC-MS analysis and a representative transition for each peptide was chosen for quantification (Table 4.2). Quantitative transitions were stable in replicate injections and produced signal reasonable for comparison to other peptides. Additionally, the ratio of quantitative transitions to remaining transitions for each precursor was consistent across biological samples, indicating quantitative transitions were not biased. Peak areas of quantitative transitions were calculated using MassHunter software from Agilent. Peak areas of phosphorylated peptides were normalized to peak area of calibrant peptide, EIAQDFK. Triplicate biological replicates, each with triplicate analytical replicates, produced n=9 normalized ratios, which were averaged together and presented as mean ± standard deviation. Statistical significance of mean differences was calculated using Student's two-tailed *t*-test. An example of calculations from raw integrated peak areas to normalized and averaged values is presented in Table 4.3.

Table 4.1 - MRM transitions for quantification of APP and Aβ.

Isoform	Peptide		Precursor (m/z)	Product Ions (m/z)			
				1	2	3	4
Aβ	LVFFAEDVGSNK	L	663.3	748.3 (y_7)	819.4 (y_8)	966.5 (y_9)	1113.5 (y_{10})
		H	667.3	756.4 (y_7)	827.4 (y_8)	974.5 (y_9)	1121.5 (y_{10})
APP	VESLEQEAANER	L	687.8	689.3 (y_6)	817.4 (y_7)	946.4 (y_8)	1146.5 (y_{10})
		H	692.8	699.3 (y_6)	827.4 (y_7)	956.4 (y_8)	1156.5 (y_{10})
APP	AVIQHFQEK	L	550.3	688.3 (y_5)	816.4 (y_6)	929.5 (y_7)	
		H	554.3	696.4 (y_5)	824.4 (y_6)	937.5 (y_7)	

Two peptides were selected to represent total amyloid precursor protein (APP) and a single peptide for amyloid beta (Aβ). Measurements using peptide for Aβ are a sum of all Aβ-containing proteins, including unprocessed APP and various processed forms of Aβ. Unlabeled, light (L) transitions were used to measure protein in brain, labeled, heavy (H) transitions were used to measure standard protein supplemented into biological sample.

Table 4.2 - MRM transitions used in identification and quantification of histone PTMs.

Peptide	Precursor Ion (m/z)	Product Ion (m/z)	Ion
EIAQDFK	425.72	409.21	y3
EIAQDFK	425.72	537.27	y4
EIAQDFK	425.72	608.30	y5
EIAQDFK	425.72	721.39	y6
SpTELLIR and STpELLIR	456.23	407.25	neutral loss
SpTELLIR and STpELLIR	456.23	401.29	y3
SpTELLIR and STpELLIR	456.23	514.37	y4
SpTELLIR and STpELLIR	456.23	643.41	y5
STpELLIR	456.23	824.43	y6
SpTELLIR	456.23	744.46	y6
SpTpELLIR	496.22	447.23	neutral loss
SpTpELLIR	496.22	401.29	y3
SpTpELLIR	496.22	514.37	y4
SpTpELLIR	496.22	643.41	y5
SpTpELLIR	496.22	824.43	y6

Phosphorylation (p) is indicated following the modified amino acid. All precursor ions were +2 charge and product ions were +1 charge. Specific ion (y-ion or neutral loss ion) information is included for reference. Transitions shown in blue were used for quantification.

Table 4.3 - MRM data of H3S57 and H3T58 phosphorylation in control and 5XFAD mice.

		Peak Area			Normalized to H3		
Sample		**Trial 1**	**Trial 2**	**Trial 3**	**Trial 1**	**Trial 2**	**Trial 3**
Mixed WT A	S57p	62949	49770	49050	5.69	6.52	6.94
	T58p	9169	7010	6452	0.83	0.92	0.91
	S57p/T58p	18585	13222	12205	1.68	1.73	1.73
	H3	11072	7631	7065			
Mixed WT B	S57p	88595	115736	110106	6.89	7.03	7.36
	T58p	11625	14957	15864	0.90	0.91	1.06
	S57p/T58p	23837	29511	29437	1.85	1.79	1.97
	H3	12863	16462	14955			
Mixed WT C	S57p	26263	48344	43994	6.35	6.84	7.04
	T58p	4257	7240	6560	1.03	1.02	1.05
	S57p/T58p	9974	18475	16279	2.41	2.61	2.61
	H3	4137	7073	6245			
5XFAD A	S57p	62367	61164	56620	3.86	4.01	3.98
	T58p	7513	8176	7302	0.46	0.54	0.51
	S57p/T58p	19122	13566	15859	1.18	0.89	1.12
	H3	16175	15241	14210			
5XFAD B	S57p	25894	16284	14155	3.48	3.80	3.81
	T58p	3439	2203	1950	0.46	0.51	0.53
	S57p/T58p	14015	7230	6099	1.88	1.69	1.64
	H3	7437	4281	3714			
5XFAD C	S57p	74980	46733	48136	4.82	4.51	4.44
	T58p	8963	6741	6183	0.58	0.65	0.57
	S57p/T58p	24396	16013	15676	1.57	1.54	1.45
	H3	15546	10371	10835			

	Mix WT		5XFAD	
	AVG	**SD**	**AVG**	**SD**
S57p	6.74	0.49	4.08	0.42
T58p	0.96	0.08	0.53	0.06
S57p/T58p	2.04	0.39	1.44	0.32

Multiple reaction monitoring (MRM) data of phosphorylated serine 57 only (S57p), threonine 58 only (T58p), and both (S57p/T58p) are shown as raw peak area values and normalized to calibration peptide (H3) to account for loading variability and H3 abundance. Averages (AVG) and standard deviations (SD) were calculated using three analytical replicates from three mice for both mixed wild type control and 5XFAD (n=9).

4.3 Results and Discussion

4.3.1 Preparation of Brain Samples for Measurement

To minimize unwanted loss of phosphorylation, SDS was added to tissue homogenates at the very first step of sample processing to arrest enzymatic activity. Early addition of SDS also efficiently denatures proteins [121,122] and evenly exposes Cys residues in all samples to subsequent reduction and alkylation. The main H3 variants, H3.1, H3.2, and H3.3, all contain a cysteine at position 110 that is known to undergo disulfide bonding to form an H3 dimer. H3.1, in addition, contains a cysteine at position 96 that participates in disulfide bonding [123,124]. A challenge to processing brain tissue for MS analysis is its high lipid content, which can degrade chromatography performance and contribute to ion suppression. The whole brain is approximately 80% lipid by dry mass [96] and, therefore, necessitates removal of lipids. Chloroform/methanol precipitation of the protein efficiently removed lipids, SDS, salts, and by-products alkylation to yield a pure protein pellet. These two major steps, (i) early addition of SDS followed by reduction/alkylation of Cys residues and (ii) chloroform/methanol precipitation to increase protein purity, ensure sample quality compatible with LC-MS/MS analyses, while minimizing processing to maintain endogenous phosphorylation. Additionally, all samples were processed in parallel to ensure that no artificial loss of phosphorylation would create a bias between samples groups and that observed differences between groups were purely of biological origin.

4.3.2 Selection of Transitions for MRM

The main histone H3 variants, H3.1, H3.2, and H3.3, have very close homology, which is evidenced by their sequence alignment (Figure 4.1). Initially, all selected transitions for peptides containing only S57p, only T58p, or both S57p and T58p were used to identify and confirm retention times of peptides in each MS chromatogram (Figure 4.2). With the specificity of MRM and consensus of six or more transitions for each peptide, peptide identification was performed with certainty. The most abundant, unique transition for each peptide was then used for quantification using integrated peak area. By selecting the most abundant transition for quantification, peak area could be more reproducibly and accurately measured. Our measurements using this method of relative quantification enable comparison of the level of change in S57 and T58 phosphorylation in the AD model 5XFAD to control and to EFV-treated 5XFAD.

4.3.3 APP and Aβ in 5XFAD Brain

Mice with rapid amyloid deposition (5XFAD) [22] were compared to age- and sex-matched wild type C57BL/6J mice. 5XFAD provide an appropriate model for AD-related amyloid pathogenesis for the exploration of amyloid-associated changes [125]. Aβ was 460 ± 70 pmol/mg total protein in 5XFAD mouse brain, a 177-fold greater concentration than the 2.6 ± 0.2 pmol/mg in control (Figure 4.3). APP was 54 ± 3 pmol/mg in 5XFAD, 13-fold greater than the 4.1 ± 0.5 pmol/mg in control (Figure 4.3). The significant increase in APP and Aβ indicates the presence of amyloid pathology in the 5XFAD mouse brain.

H3.1	1	ARTKQTARKSTGGKAPRKQLATKAARKSAPATGGVKKPHRYRPGT	45
H3.2	1	ARTKQTARKSTGGKAPRKQLATKAARKSAPATGGVKKPHRYRPGT	45
H3.3	1	ARTKQTARKSTGGKAPRKQLATKAARKSAPSTGGVKKPHRYRPGT	45
H3.1	46	VALREIRRYQK**STELLIR**KLPFQRLVR**EIAQDFK**TDLRFQSSAVM	90
H3.2	46	VALREIRRYQK**STELLIR**KLPFQRLVR**EIAQDFK**TDLRFQSSAVM	90
H3.3	46	VALREIRRYQK**STELLIR**KLPFQRLVR**EIAQDFK**TDLRFQSAAIG	90
H3.1	91	ALQEACEAYLVGLFEDTNLCAIHAKRVTIMPKDIQLARRIRGERA	135
H3.2	91	ALQEASEAYLVGLFEDTNLCAIHAKRVTIMPKDIQLARRIRGERA	135
H3.3	91	ALQEASEAYLVGLFEDTNLCAIHAKRVTIMPKDIQLARRIRGERA	135

Figure 4.1 - Sequence alignment of mouse H3 variants.
Protein sequence alignment was performed using BLAST. Sequences shown in blue are peptides used for quantification. Amino acid residues shown in red indicate differences between histone variants to H3.1. Due to sequence homology of quantitative peptides used, data values obtained reflect changes in mouse H3 as a whole.

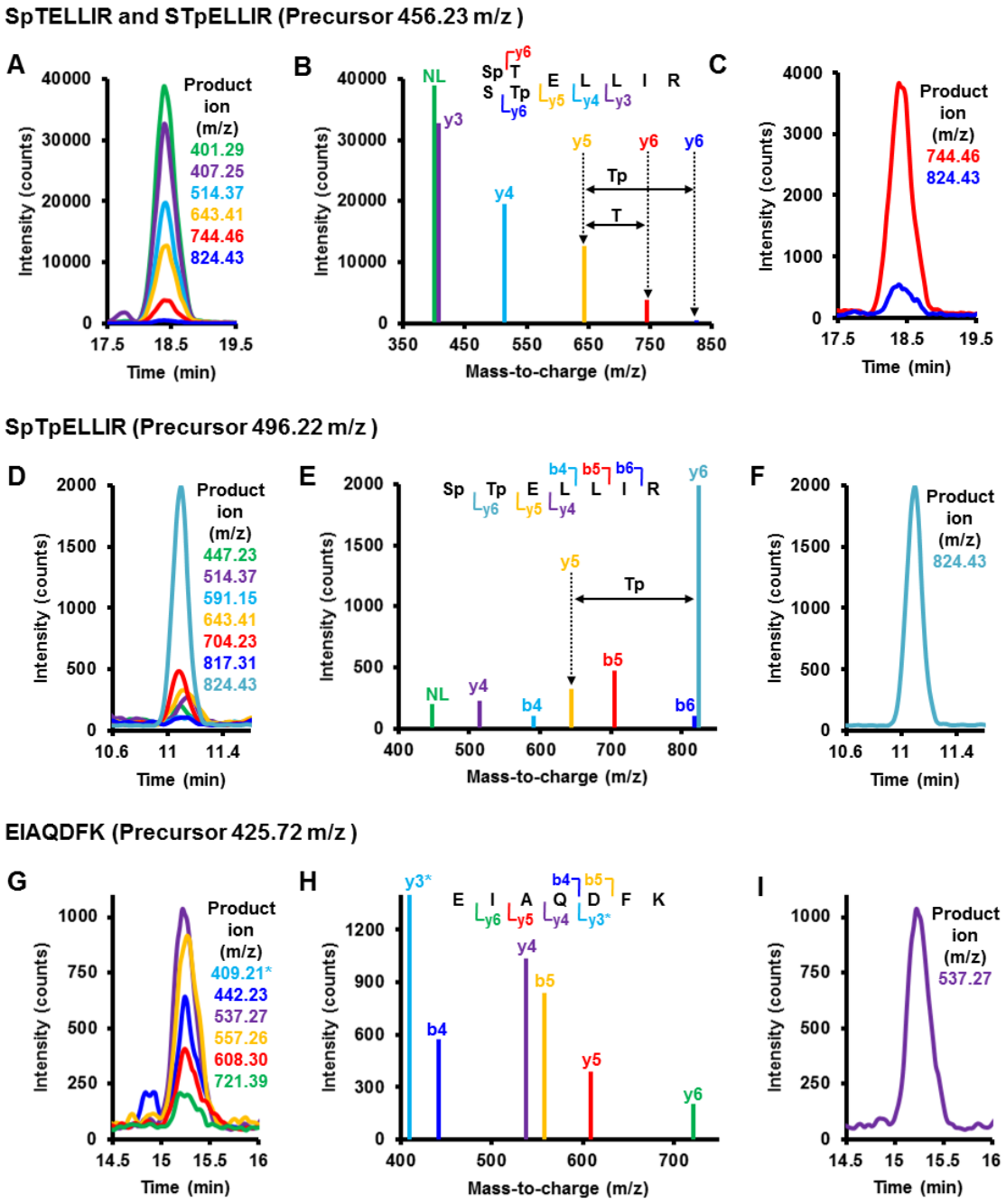

Figure 4.2 - Peptide identification by MRM and selection of transitions for quantification.

(A, D, F) Numerous transitions were monitored to determine retention time and confirm identity of each peptide. **(B, E, H)** Spectra of ions used to confirm identity and site of phosphorylation. **(C, F, I)** A single transition was selected from each peptide for quantification. *Transition 425.72→409.21 had high signal intensity and was removed from chromatogram **(G)** and reduced in spectrum **(H)** to better illustrate other monitored transitions.

Since the amino acid sequence for Aβ is present in both free Aβ and unprocessed APP, it is of interest to compare the level of Aβ to APP to verify that Aβ concentration increases were not largely attributed to unprocessed APP. Additionally, our inclusion of denaturants facilitated the unfolding and solubilization of Aβ for proteolysis, therefore our measurements represent the total amount of solubilized Aβ. In control mice, the 4.1 ± 0.5 pmol/mg of APP was similarly low in concentration to 2.6 ± 0.2 pmol/mg of Aβ. However, in 5XFAD, the 460 ± 70 pmol/mg of Aβ is nearly 9-fold greater than the 54 ± 3 pmol/mg of APP, indicating a large increase in Aβ not attributed to unprocessed APP. Our measurements confirm that 5XFAD mice produce significantly more Aβ than control mice in the brain (Figure 4.3). Our findings validated the use of 5XFAD as a model of rapid amyloid pathogenesis for subsequent quantification of phosphorylation of S57 and T58 residues.

5XFAD mice were treated with EFV for three months in parallel to untreated 5XFAD controls. EFV was previously shown to directly stimulate the activity of brain-specific cholesterol 24-hydroxylase, cytochrome P450 CYP46A1, and increase cholesterol turnover [116]. Cholesterol metabolism is closely associated with AD pathology; high levels of cholesterol in the brain increase susceptibility to AD and advance Aβ plaque formation, while depletion of brain cholesterol inhibits production of Aβ [119,120]. Since cholesterol turnover reduces cognitive impairment and amyloid pathology [117,118], EFV was chosen to evaluate its effect on amyloid formation.

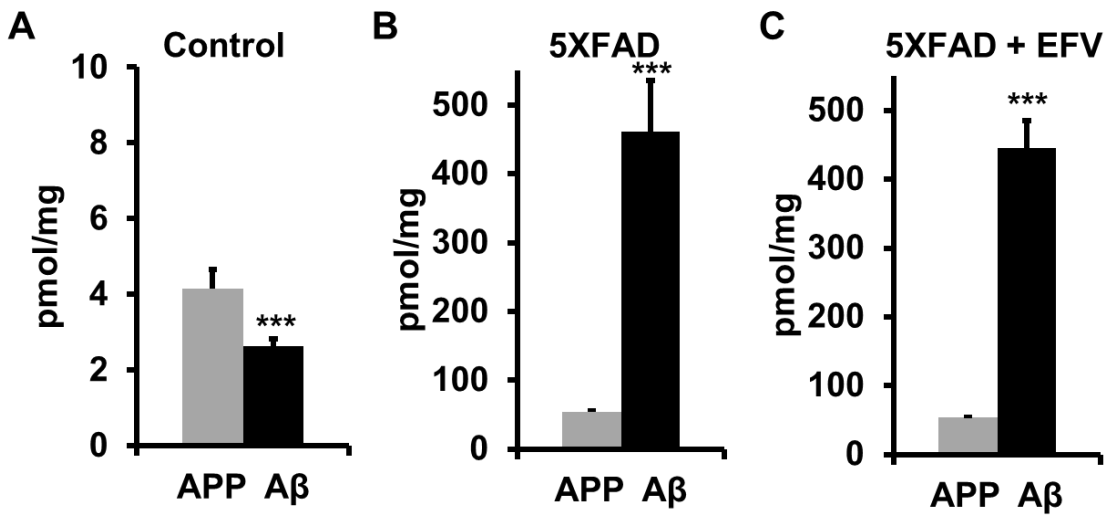

Figure 4.3 - APP and Aβ in control, 5XFAD, and EFV-treated 5XFAD.
Total amyloid precursor protein (APP) peptide AVIQHFQEK and amyloid beta (Aβ) peptide LVFFAEDVGSNK were measured in whole hemisphere homogenates from **(A)** wild type mice (n=3), **(B)** 5XFAD mice (n=3), and **(C)** EFV-treated 5XFAD mice (n=3). Measurements represent mean ± standard deviation of biological replicates (n=3) using three transitions for AVIQHFQEK and four transitions for LVFFAEDVGSNK for absolute quantification using QconCAT as internal standard. ***, $p < 0.001$.

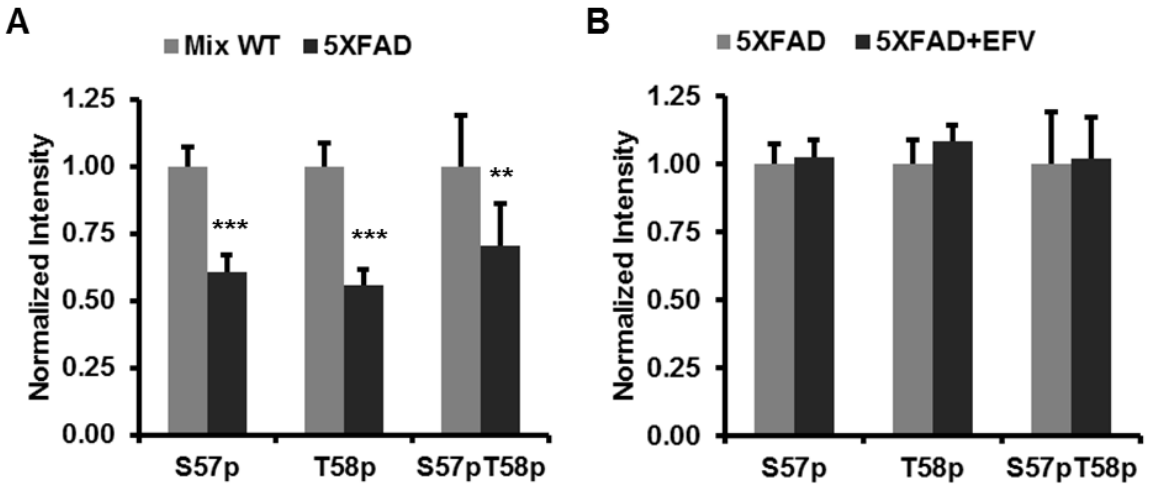

Figure 4.4 - S57 and T58 phosphorylation in mice.
(A) Effect of 5XFAD model on S57 and T58 phosphorylation. Phosphorylation was measured in whole hemisphere homogenates from mixed wild type mice (n=3) and 5XFAD mice (n=3). **(B)** Effect of efavirenz on S57 and T58 phosphorylation in 5XFAD mice. Phosphorylation was measured in whole hemisphere homogenates from 5XFAD mice (n=3) and 5XFAD mice treated with EFV (n=3). Measurements represent mean ± standard deviation of biological and analytical replicates (n=9) normalized to respective phosphorylation site in control. **, $p < 0.01$; ***, $p < 0.001$.

Despite implications of low-dose EFV mitigating effects of AD, EFV-treated 5XFAD had significantly more Aβ than APP and did not show statistically different levels of APP and Aβ compared to 5XFAD without treatment (Figure 4.3). While the proposed therapeutic low-dose EFV did not cause a reduction in Aβ, using greater dosages of EFV to reduce Aβ may not be a practical option for long-term treatment of AD.

4.3.4 S57 and T58 Phosphorylation of 5XFAD Brain

As compared to C57BL/6J mice, 5XFAD showed a 40% lower level of S57p, 45% lower level of T58p, and a 30% lower level of simultaneously phosphorylated S57p and T58p (Figure 4.4). The decrease in phosphorylation of S57 and T58 might have an impact on nucleosome stability. S57 is less than 11 Å from DNA and T58 is less than 9 Å from DNA in the crystal structure of the human nucleosome, PDB ID: 2CV5 [126] (Figure 4.5). These distances were measured with PyMOL Molecular Graphics System (Version 1.7.2, Schrödinger, LLC). Phosphorylation of S57 and T58 causes a significant increase in negative charge in close proximity to the negatively charged phosphate backbone of DNA (Figure 4.5C). Furthermore, both residues are on the histone surface and are positioned in a turn of a helix-turn-helix motif of the H3 polypeptide chain, highlighting the ease of access by modifying enzymes (Figure 4.6). Introduction of phosphoryl groups, about 2.5 Å in size, in close proximity to the negatively charged backbone of DNA can weaken DNA-histone interactions [113] (Figure 4.6). Conversely, dephosphorylation, as observed in 5XFAD (Figure 4.6C), can strengthen nucleosome stability and lead to condensed chromatin with reduced

gene expression [113], consistent with AD pathology [36,103]. Our measurements reveal dephosphorylation of S57 and T58 in 5XFAD, which may illustrate specific epigenetic changes that occur in AD.

The effect of EFV on histone phosphorylation was also measured. Low-dose EFV treatment of 5XFAD did not show statistically different levels of S57 and T58 phosphorylation compared to 5XFAD without treatment (Figure 4.4). Our findings may indicate that previously reported effects of EFV are not directly associated with S57 and T58 phosphorylation. Furthermore, unregulated production of Aβ in 5XFAD prior to EFV treatment may have detrimental effects on the mice, indicated by low levels of S57 and T58 phosphorylation, which persist after three months of EFV treatment. This is an interesting observation for AD pathology and may suggest that some epigenetic markers, such as histone PTMs, may be less reversible with mild drug treatment after onset of neurodegenerative disease. Conversely, it may be that the EFV dose was insufficient to generate changes in phosphorylation.

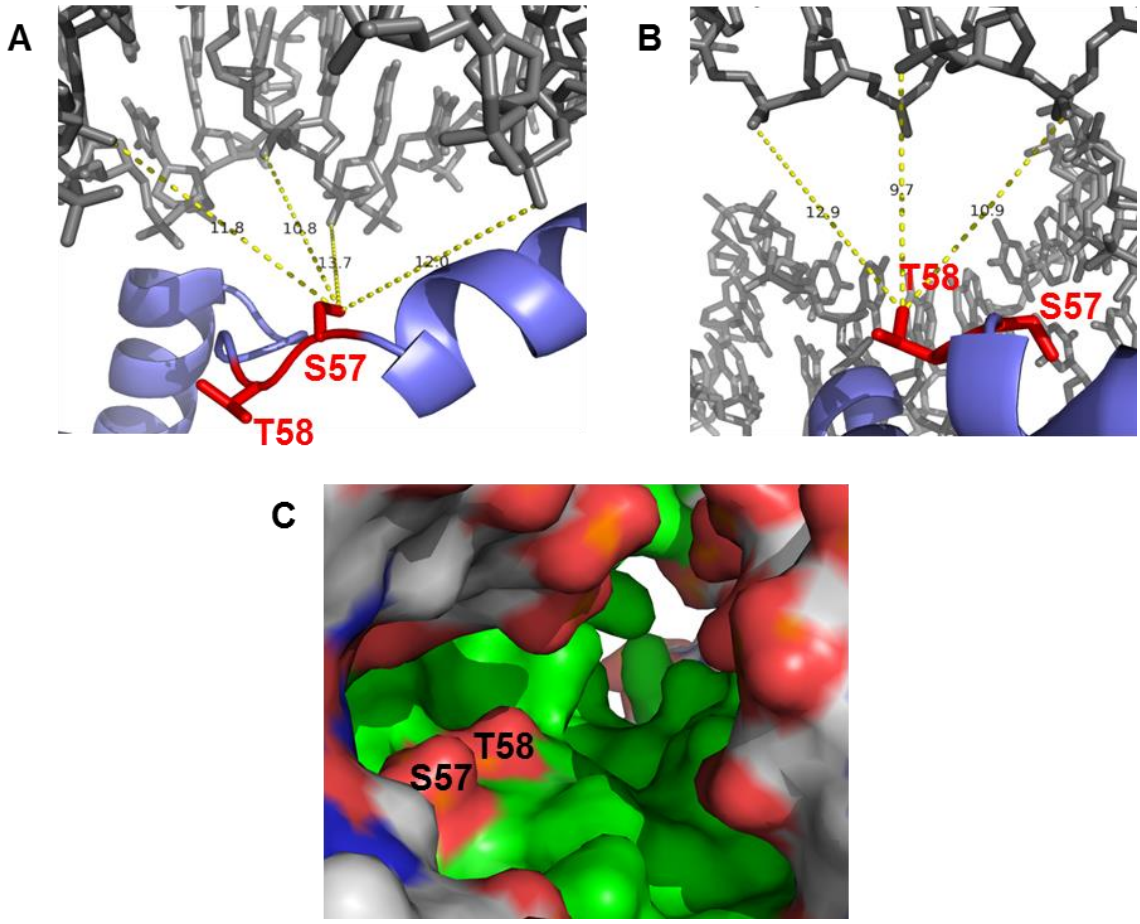

Figure 4.5 - Proximity of H3 S57 and T58 to DNA.
(A) S57 is less than 11 Å from DNA and **(B)** T58 is less than 9 Å from DNA. DNA is shown in gray, H3 in blue, and S57 and T58 sites in red. Distance measurements were performed in PyMOL Molecular Graphics System Version 1.7.2 using the crystal structure of the human nucleosome (PDB ID: 2CV5) [126]. **(C)** Surface view of phosphorylated S57 and T58 on histone core (green) in close proximity to the interface of the negatively charged phosphate backbone (red) of DNA (gray). All modeling was performed in PyMOL and insertion of phosphate groups was performed using a PyMOL plugin called PyTMs [127].

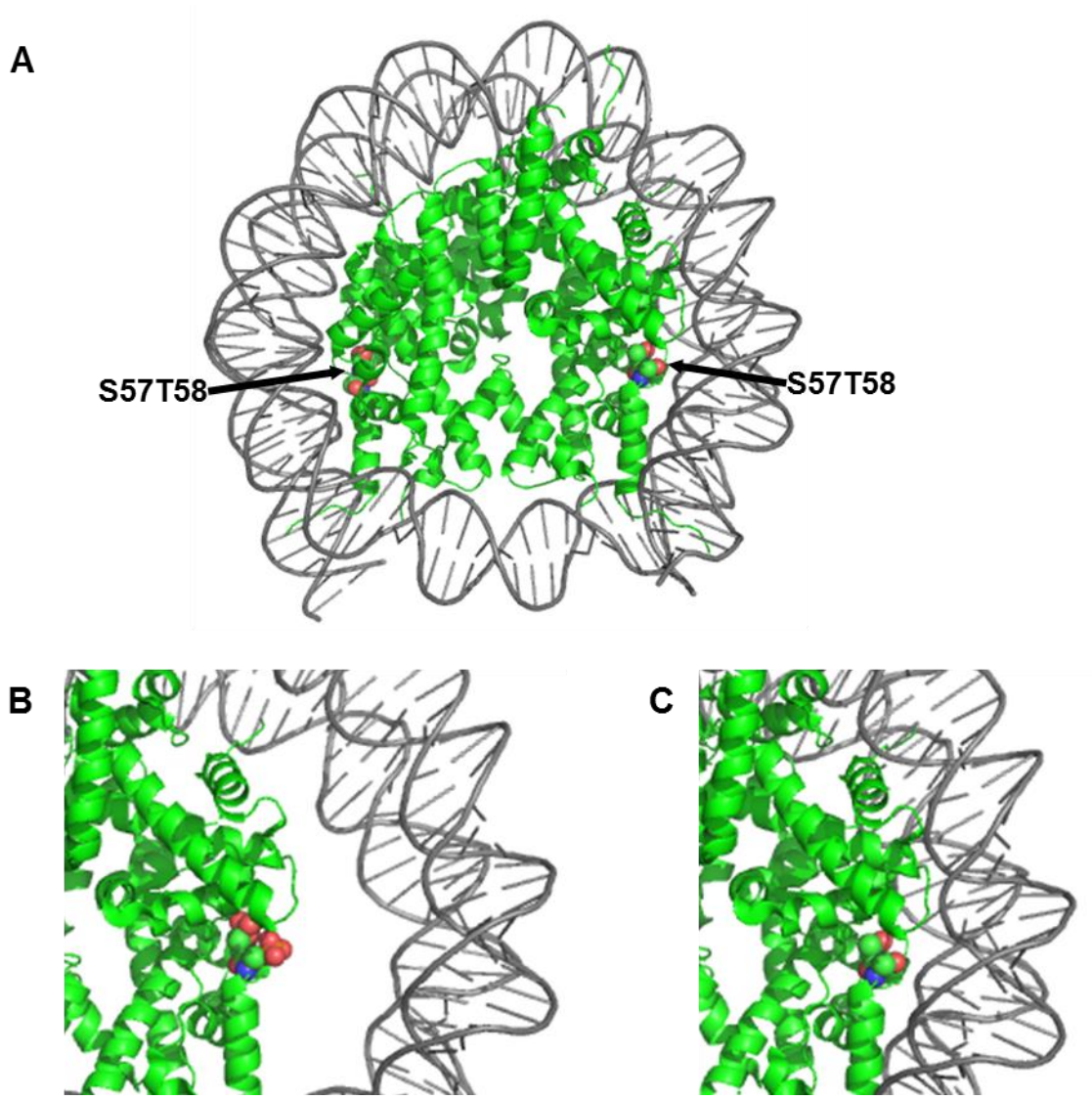

Figure 4.6 - Location of H3 residues S57 and T58 within nucleosome.
(A) Core histones (green), with flexible histone tails truncated in structure, is shown wrapped in DNA (gray). The S57T58 regions (spheres with oxygen in red and nitrogen in blue) are in the turn of a helix-turn-helix motif that brings the residues in close proximity to DNA and are easily accessible to kinases and phosphatases. **(B)** Phosphorylated S57 and T58 create a repulsive charge-charge interaction with negatively charged DNA, weakening the affinity of the nucleosome. **(C)** Dephosphorylation of S57 and T58 greatly reduces negative charge on the histone interface, strengthening the affinity of the DNA-histone interaction. Modeling was performed using PyMOL Molecular Graphics System Version 1.7.2 and the crystal structure of the human nucleosome (PDB ID: 2CV5) [126]. Insertion of phosphate groups was performed using the PyTMs plugin [127].

4.4 Conclusions

We demonstrated that MRM assay can provide relative quantification of phosphorylation of histone H3 residues S57 and T58 in lipid-rich, whole mouse brain homogenates. We showed that levels of S57p, T58p, and doubly phosphorylated S57 and T58 decrease in 5XFAD mice. This suggests these histone PTMs play an epigenetic role in AD pathology and may stabilize nucleosomes, causing decreased gene transcription. Additionally, we measured effect of low-dose EFV on S57p and T58p, which showed no statistically significant changes. Our measurements contribute to the overall understanding of AD pathology and may provide clinical targets for pharmaceutical intervention.

Chapter 5: Histone PTMs in AD-affected Human Frontal Cortex

This chapter contains data submitted to *Clinical Proteomics* for publication.

5.1 Introduction

We have identified several sites of histone PTMs in frontal cortex from human donors with AD that are differentially abundant compared to age-matched normal donors. The majority of PTM and protein measurements in AD research are performed in animal models of neurodegeneration, with few studies being performed using human brain. While we do not underestimate the potential of animal models, it is beneficial to obtain measurements, when possible, in human brain tissue affected by AD to confirm changes are truly indicative of AD pathology. With our multiple reaction monitoring (MRM) mass spectrometry method of PTM quantification, we were able to measure several histone PTMs in frontal cortex from humans. Frontal cortex is an ideal neural tissue for investigation of PTMs because it is responsible for short-term memory, cognition, and decision making, which are all affected by AD, and it is severely damaged in late AD [128]. Significant changes in methylation of H2B K108 and H4 R55 and ubiquitination of H2B K120 reported herein have not been previously reported in frontal cortex from human donors affected with AD. Structural and functional effects from these modifications likely have implications in AD pathology and may identify enzyme associated with these PTMs to be used as drug targets.

5.2 Methods

5.2.1 Human Tissue

Frozen samples of frontal cortex were obtained from Washington University School of Medicine Alzheimer's Disease Research Center (St. Louis, MO) as described in Appendix A1.3. Demographic information on the de-identified donors is summarized in Table 5.1.

Table 5.1 - Donor information.

Donor ID	Age (years)	Gender	Disease status	PMI (h)
1	90	F	Normal	9.5
2	87	M	Normal	6.3
3	80.7	F	Normal	5.5
4	86.9	M	Normal	11.6
5	87.2	M	Normal	12
6	92.1	F	Normal	6
11	79	M	Severe AD	6
12	73.6	F	Severe AD	4
13	81.2	F	Severe AD	4
14	91	F	Severe AD	4.5
15	72	M	Severe AD	1
16	84	F	Severe AD	4.5

Alzheimer's disease (AD) in frontal cortex was evaluated by the Clinical Dementia Rating (CDR) with no dementia representing normal brain and severe dementia representing severe AD-affected brain. Post mortem interval (PMI) is defined as the time between death and when the collected tissue was frozen. Frontal cortex was obtained from Washington University.

5.2.2 Purification of Histones from Frontal Cortex for PTM Screening

To reduce sample complexity for data-dependent screening for PTMs, histones were purified from tissue. Frontal cortex tissue from both AD-affected and normal donors were carefully cleaned from white matter and blood and 1.1 g of cortex was minced. Nuclei isolation and histone purification was performed as previously described [129] using nuclei isolation buffer (NIB-250) composed of 15 mmol/L Tris-HCl (pH 7.5), 15 mmol/L NaCl, 60 mmol/L KCl, 5 mmol/L $MgCl_2$, 1 mmol/L $CaCl_2$, and 250 mmol/L sucrose. Tissue was added to 10 mL of NIB-250 containing 10 mmol/L DTT, 10 mmol/L sodium butyrate, and 0.2% NP-40 and homogenized on ice with a glass/teflon dounce homogenizer using 10 strokes. Homogenate was incubated for 10 min on ice and then centrifuged at 1,000 *g* for 7 min at 4 °C. Pellet was washed with NIB containing 10 mmol/L DTT and 10 mmol/L sodium butyrate, but no NP-40. Pellet was supplemented with 8 mL 0.4 mol/L H_2SO_4 and incubated for 2 h at 4 °C with rotation. Sample was then centrifuged at 3,400 *g* for 5 min at 4 °C and resulting supernatant was supplemented in a 4:1 (volume ratio) with trichloroacetic acid and allowed to precipitate overnight at 4 °C.Pellet was washed with 12 mL of acetone acidified with 0.1% volume of hydrochloric acid and centrifuged for 5 min at 3,400 *g* at 4 °C. Pellet was washed with 12 mL of pure acetone and centrifuged for 5 min at 3,400 *g* at 4 °C. Pellet was air dried for 2 h at room temperature. 1 mL of water was added to the pellet and sample was gently rotated to allow for histones to be solubilized in the water. Sample was then centrifuged for 5 min at 3,400 *g* at room temperature and histones were collected in the supernatant. Histone

concentration was determined using the DC protein assay kit and bovine serum albumin as a standard. Histones were stored at -20 °C before further processing. The resulting 100 µL histone sample (15.5 µg) was supplemented with 100 µL of 25 mmol/L NH_4HCO_3 and 0.1% RapiGest SF (Waters, Milford, MA) then treated in a 25:1 mass ratio of histone to trypsin overnight at 37 °C. Following trypsinolysis, 0.5% trifluoroacetic acid (TFA) was added and incubated at 37 °C for 1 h to cleave acid-labile RapiGest. Samples were then centrifuged at 179,000 *g* for 30 min at 4 °C to remove precipitated surfactant. Supernatants were dried using a Vacufuge.

5.2.3 PTM Identification and Selection

Data-dependent acquisition of histone peptides was performed by LC-MS/MS using an Agilent 6550 QTOF. Peptides were eluted from an Agilent ProtID C18 nanochip (75 µm x 150 mm, 300 nm) over 120 min gradient from 3% to 35% acetonitrile containing 0.1% formic acid at a flow rate of 300 nL/min. Acquisition method in positive mode used capillary temperature 275 °C, fragmentor 180 V, capillary voltage 1950 V, a 300 m/z to 2000 m/z mass window at 8 spectra/s scan rate for precursor ions, 1.3 m/z isolation window, and a 80 m/z to 1700 m/z mass window at 3 spectra/s scan rate for product ions. Collision energy (CE) was determined using the formulas [95]:

For peptides with 2+ charge, $CE = \frac{3\,m/z}{100} + 1$

For peptides with 3+ charge or greater, $CE = \frac{3.6\,m/z}{100} - 4.8$

Data was searched against the SwissProt database for human proteins using both Mascot (MatrixScience) and MassMatrix [130] to identify histone peptides and PTMs. Search settings were: precursor mass tolerance, 0.05 Da; fragment mass tolerance, 0.05 Da; maximum missed cleavages, 4; variable modifications, acetylation of lysine, methylation of arginine and lysine, and ubiquitination of lysine; enzyme, trypsin. Both Mascot and MassMatrix were used together to reduce false positives based on individual searching algorithms. Identifications in consensus with both Mascot and MassMatrix were manually confirmed by spectra annotation and using LC retention time analysis [131] with MassMatrix. Fragmentation data was then used to develop a transition list for MRM.

5.2.4 Human Frontal Cortex Processing for Quantitative Measurements

For quantitative measurements, samples were minimally processed (i) to reduce loss of native PTMs and (ii) to reduce PTM artifacts caused by sample processing. Frontal cortex tissue was carefully cleaned from white matter and blood from AD-affected (n=6) and normal (n=6) donors. Tissue (0.2 g) was minced and then homogenized in 1 mL of 25 mmol/L NH_4HCO_3 by sonication at 50 W using four 10 s continuous cycles (Sonicator 3000, Misonix Inc., Farmingdale, NY). Homogenates were centrifuged at 2,000 *g* for 5 min to remove debris. Resulting supernatant was measured for total protein concentration using detergent-compatible DC protein assay kit in the presence of 1% SDS and bovine serum albumin as a standard. Homogenates were stored at -80 °C. Samples of 0.2 mg were supplemented with 20 mmol/L DTT and 1% SDS. After

1 h incubation at room temperature to reduce cysteines, 55 mmol/L iodoacetamide was added and incubated for an additional 1 h to alkylate cysteines. Protein was isolated by chloroform/methanol precipitation. Protein pellets were sonicated in 1 mL 25 mmol/L NH_4HCO_3 and 0.1% RapiGest SF and then treated with a 25:1 mass ratio of histone to trypsin overnight at 37 °C. Following trypsinolysis, 0.5% TFA was added and incubated at 37 °C for 1 h to cleave acid-labile RapiGest. Samples were then centrifuged at 179,000 *g* for 30 min at 4 °C to remove precipitated surfactant. Supernatants were dried using a Vacufuge.

5.2.5 PTM Quantification by Multiple Reaction Monitoring

Dried peptides were reconstituted in 3% acetonitrile, 97% water, and 0.1% formic acid. Separation was performed on an Agilent Zorbax Eclipse Plus C18 RRHD column (2.1 mm x 50 mm, 1.8 µm particle) and multiple reaction monitoring (MRM) analysis was performed on an Agilent 6490 iFunnel Triple Quadrupole LC/MS system (Santa Clara, CA). Peptides were eluted at a flow rate of 200 µL/min using the following gradient of solvent B in solvent A: 3% B for 3 min, 3% to 30% B in 32 min, 30% to 80% B in 5 min, and 80% to 3% B in 3 min. Solvent A was water containing 0.1% formic acid and solvent B was acetonitrile containing 0.1% formic acid. The acquisition method used the following parameters in positive mode: fragmentor 380 V, collision energy 25 V, cell accelerator 4 V, electron multiplier 600 V, and capillary voltage 3500 V. Selected transitions from fragmentation data were used to confirm the retention

time and identity during MRM analysis; the transition most appropriate for quantification for each peptide is listed in Table 5.2.

Chromatographic peaks were integrated for transitions selected for quantification and peak areas for peptides were divided by the peak area of a non-modified peptide for the respective histone (Table 5.2). Ratios of biological replicates and injection replicates were averaged and the average from the normal frontal cortex samples was used to normalize the control group to 1.00 and to normalize the AD-affected group for easy comparison of fold changes. Student's two-tailed *t*-test was performed to determine the level of statistical significance of changes between AD and normal groups.

Table 5.2 - Histone modifications and MRM transitions used for quantification.

Histone	Sequence	Precursor ion (m/z)	Product Ion (m/z)
H2A	**AGLQFPVGR**	472.796 (2+)	703.39 (1+, y6)
H2A (canonical)	VTIAQGGVLPNIQAVLLPK	966.08 (2+)	1092.68 (1+, y10)
H2A (1-A, 2-B, H2Ax)	LLGGVTIAQGGVLPNIQAVLLPK	757.80 (3+)	546.84 (2+, y10)
H2B	**EIQTAVR**	408.73 (2+)	446.27 (1+, y4)
H2B, K108-methylation	LLLPGELAKme	484.31 (2+)	736.46 (1+, b7)
H2B, K120-ubiquitination	AVTKubYTSSK	549.79 (2+)	827.43 (1+, y6)
H3	**DIQLAR**	358.21 (2+)	359.24 (1+, y3)
H3, K4-, K9-acetylation	KacQLATKacAAR	535.82 (2+)	772.47 (1+, y7)
H4	**VFLENVIR**	495.29 (2+)	501.31 (1+, y4)
H4, K8-, K12-, K16-acetylation	GGKacGLGKacGGAKacR	606.34 (2+)	927.54 (1+, y9)
H4, K12-, K16-acetylation	GLGKacGGAKacR	464.27 (2+)	530.30 (1+, y5)
H4, R55-methylation	ISGLIYEETRme	597.82 (2+)	290.18 (1+, y2)

Modifications (ac) acetylation, (me) methylation, and (ub) ubiquitination of peptides were measured and normalized to an unmodified peptide, shown in bold, from the respective histone.

5.3 Results and Discussion

5.3.1 Selection of Transitions for MRM

Initially, histones were purified from normal and AD-affected tissue to produce a sample with less complex matrix for improved identification of histone peptides in a discovery mode screening. While dynamic exclusion was used during MS acquisition, data-dependent analysis benefits from having enrichment of the histone targets, particularly when a histone PTM may be only a few percent of the total amount of the unmodified peptide. Once peptides were identified by Mascot and MassMatrix and manually confirmed using retention time analysis and spectra annotation, a transition list was created from abundant fragment ions, which was used for MRM. The optimized transitions used for quantification are in Table 5.2.

5.3.2 Preparation of Samples

For PTM screening, histones were extensively purified. However, it was preferable to minimally process the tissue samples for quantification to evaluate differences in AD versus normal frontal cortex because extensive processing may cause a loss in PTMs and also introduce processing artifacts, resulting in inaccuracy of measurements. These two major steps, (i) early addition of SDS followed by reduction/alkylation of Cys residues and (ii) chloroform/methanol precipitation to increase protein purity, ensure sample quality compatible with LC-MS/MS analyses, while minimizing processing to maintain endogenous PTMs.

5.3.3 Reproducibility and Data Quality

Selected transitions for quantification had good peak shape and intensity as is preferred for quantification (Figure 5.1). However, it is important to establish the level of variability in measurements to confirm that observed changes are attributed to true biological changes and not an artifact of LC-MS/MS performance or sample preparation. To demonstrate our data quality, we first performed six replicate injections of the same sample (Figure 5.2A) and measured modified H3 peptide KacQLATKacAAR as a ratio to non-modified H3 peptide DIQLAR. Measured ratios were nearly identical with negligible variation, demonstrating LC-MS/MS performance was precise and not a contributor to measurement variation. Second, we compared variability between six biological samples from normal frontal cortex using the ratio of non-modified H2B peptide EIQTAVR to H3 peptide DIQLAR (Figure 5.2B). Histones H2B and H3 are present in equal amounts as there is a 1:1 stoichiometry between core histones in the nucleosome. Therefore, H2B to H3 should not change between donors or sample preparations. Indeed, our measurements confirm that there is negligible variation in H2B/H3 between donors, demonstrating that our sample preparation results in precision of measurements. Lastly, we monitored the H3 peptide KacQLATKacAAR as a ratio to H3 peptide DIQLAR (Figure 5.2C) for the same six donors of normal frontal cortex and in the same LC-MS/MS runs as for Figure 5.2B. Detectable variability across donors for KacQLATKacAAR shows that variability in KacQLATKacAAR measurements is due to biological differences in PTM level between donors.

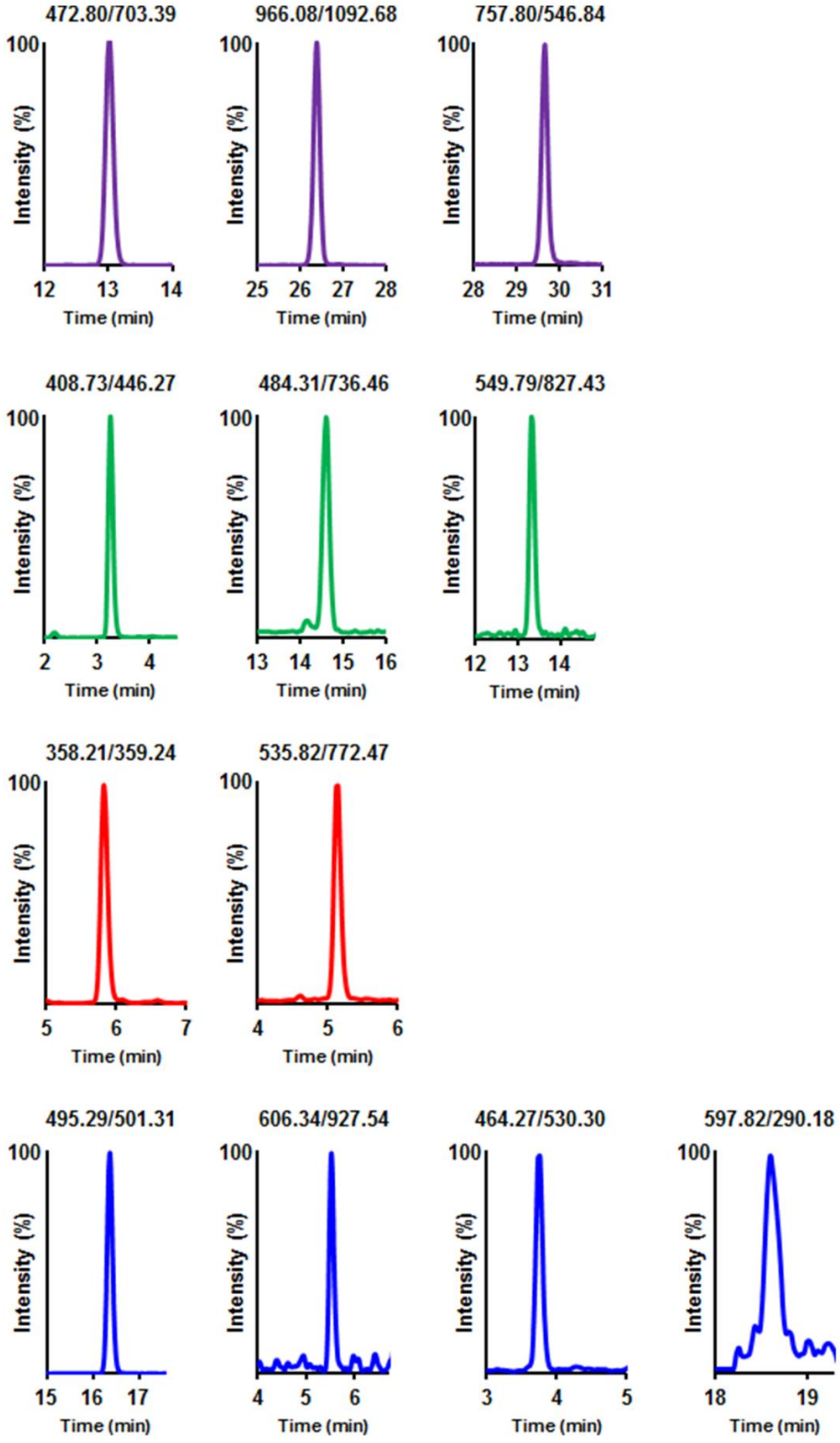

Figure 5.1 - Chromatograms of transitions used for quantification.
Transitions for H2A (purple), H2B (green), H3 (red), and H4 (blue) with non-modified peptides used for normalization in the first column.

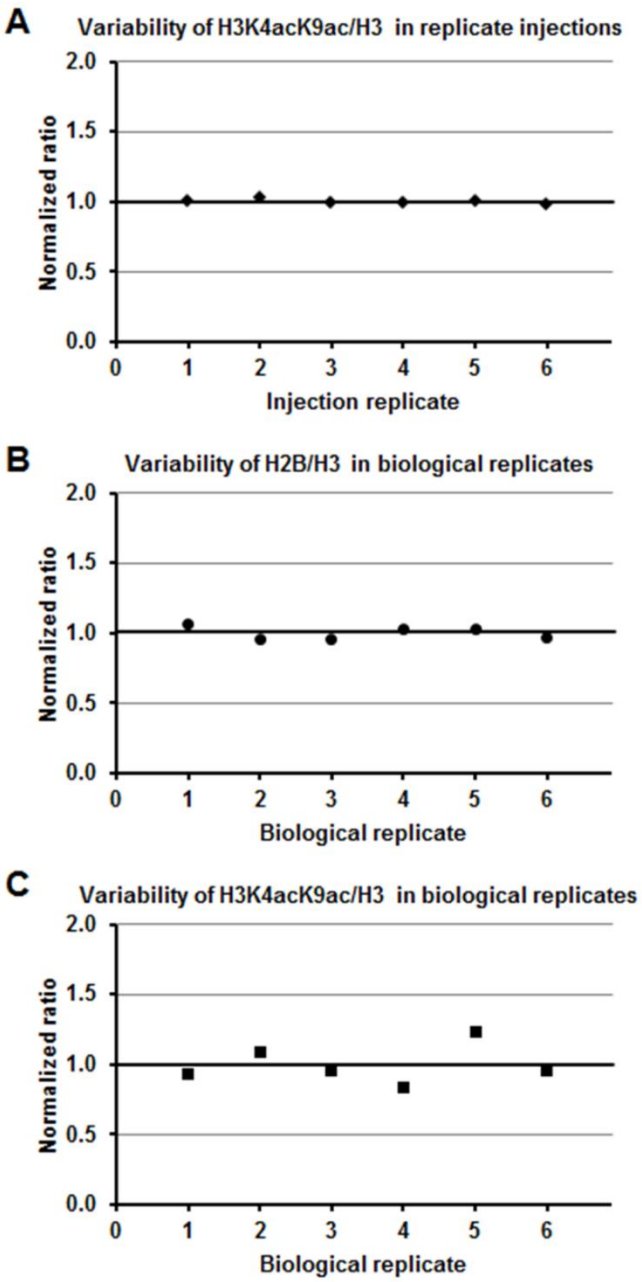

Figure 5.2 - Variability in replicate measurements.
(A) The ratio of modified H3 peptide KacQLATKacAAR to H3 was measured in 6 replicate injections of a frontal cortex sample from a normal donor and individual ratios were normalized to their average (n=6) and plotted to show the negligible variability between replicate injections. **(B)** The ratio of non-modified H2B to H3 plotted for biological replicates from normal donors (n=6) and normalized to the average, showing negligible variability between biological replicates for the stoichiometric H2B/H3 ratio. **(C)** The ratio of KacQLATKacAAR to H3 plotted for the average of two injections for each biological sample from normal donors (n=6) and normalized to the average for all measurements (n=12), showing variability in PTM is attributed to differences in donors and not due to inherent variability in MRM.

In summary, we established that measured differences between AD and control samples described herein are representative of biological variation and that our sample preparation and MRM assay is robust and precise.

5.3.4 Effect of Histone Used for Normalization

Changes in quantified histone PTMs between AD and normal frontal cortex from human donors are presented in Figure 5.3B. For quantification of histone PTMs, the peak areas of modified peptides were normalized to the peak areas of non-modified peptides from the respective histone. For example, ubiquitinated H2B peptide AVTKubYTSSK was normalized to H2B peptide EIQTAVR while acetylated H4 peptide GLGKacGGAKacR was normalized to H4 peptide VFLENVIR. While normalization of PTMs within a protein to the total amount of the protein is an accepted practice for quantification [132], it is typically not advisable to normalize PTMs within one protein to the total abundance of a different protein. Histones, however, are present in a stoichiometric 1:1:1:1 ratio of H2A:H2B:H3:H4 in the nucleosome. Due to their equal abundance, using a peptide from a single histone for normalization of all measured histone PTMs should generate similar quantification results and relative standard deviation (RSD) without a bias for using the respective histone that contains the PTM for normalization. We performed a series of normalizations, normalizing all measured PTMs to a single histone to evaluate the effect of normalization (Figure 5.3A). We were able to show that there is a close consensus in RSD between H2A, H2B, and H3 normalization. H4 normalization varied in RSD with H4 RSD matching that of the other histones or being more or less than that of the

other histones used for normalization. While H4 was often different than the consensus RSD for other histones, it did not show bias for H4 PTMs or PTMs of other histones. While the histone used for normalization should not have an effect, we would expect any effect on normalization to have a bias for normalizing PTMs to their respective histone, resulting in lower RSD for H4 PTMs to total H4 pairs. Additionally, no single histone showed a significantly different RSD when used for normalization. The average RSD when PTMs were normalized to their respective histones was 19%, while normalizing all PTMs to one histone yielded an average RSD of 19% for H2A, 20% for H2B, 19% for H3, and 22% for H4 . Overall, we were not able to observe any bias in histone normalization, which supports the stoichiometric relationship of histones in the nucleosome and the quality of our normalized measurements.

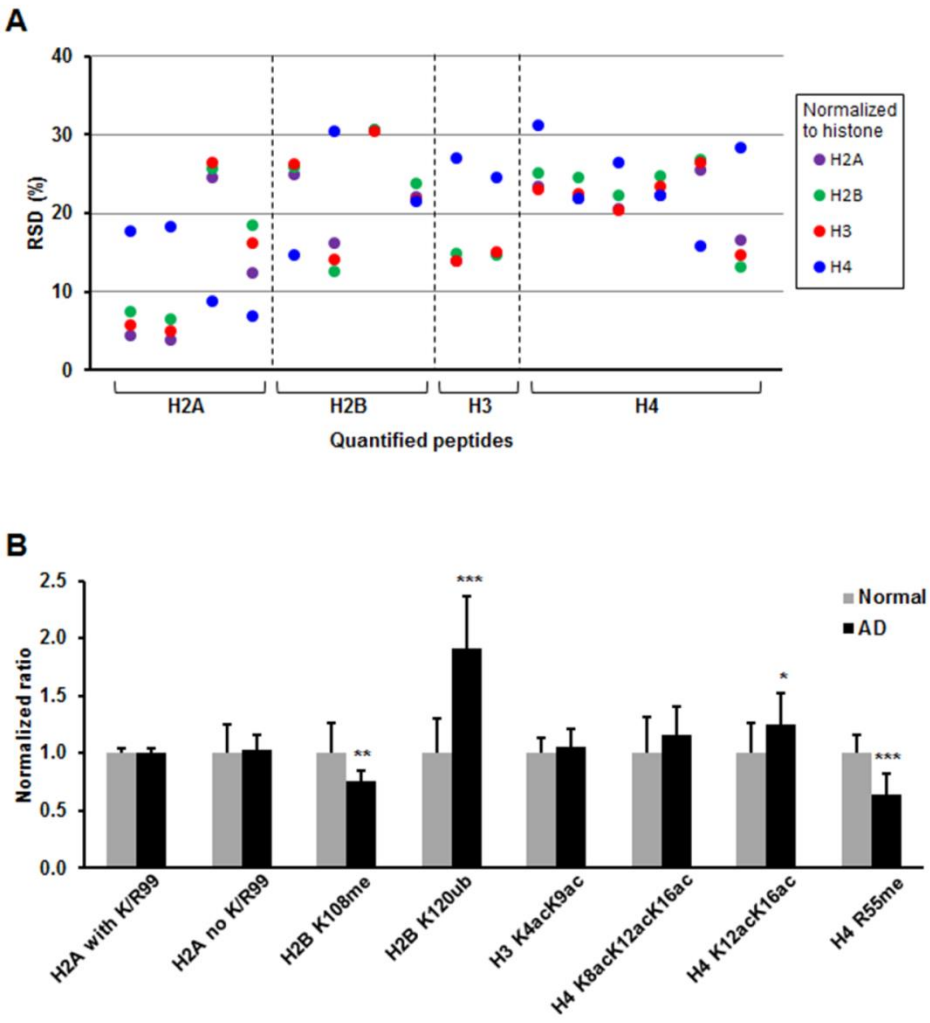

Figure 5.3 - Histone PTMs in frontal cortex.
(A) Measured peak areas of each quantified peptide were normalized to the peak area of different histone subunits. The relative standard deviation (n=12) for each quantified peptide in normal and AD frontal cortex is shown grouped by the histone in which the peptides are located. **(B)** Changes in histone PTMs in AD-affected human frontal cortex. Measurements were performed using human frontal cortex from normal (n=6) and AD-affected (n=6) donors (Additional file 1: Table S1) and two experimental replicates per donor (n=12 total measurements per condition). Q-peptide transitions are summarized in Table 1. Data presented as mean ± SD. PTMs are (ac) acetylation, (me) methylation, and (ub) ubquitination. * $p < 0.05$; ** $p < 0.01$; *** $p < 0.001$.

5.3.5 Implications of Histone PTMs in AD Human Frontal Cortex

Observed changes in histone PTMs in AD are presented in Figure 5.3B. In most sequence variants, histone H2A contains a lysine or arginine residue at position 99, however variants 1-A, 2-B, and H2Ax do not contain K/R99. Since K/R99 is a potential site for modification, the inability to regulate by K/R99 via a reduction in variants that contain this site could be of importance. We did not observe any differences in abundance in isoforms with K/R99 or without K/R99, indicating turnover of these variants is not present in AD pathology in the frontal cortex. Similarly, measurements for K4- and K9-acetylated H3 and K8-, K12-, and K16-acetylated H4 did not show statistically significant changes between AD and control. We did measure significant changes in PTMs of other sites that are associated with structural and functional implications related to AD.

K12- and K16-acetylated H4 increased 25% in AD. The increase in K12- and K16-acetylated H4 could be due to a loss in acetylation of K8, leading to tryptic cleavage after K8 and increasing the peptide ^{9}GLGKacGGAKacR^{17}. While we did not observe a change in ^{6}GGKacGLGKacGGAKacR^{17}, loss of K5 may have increased fragment 6-17, which was simultaneously undergoing a loss of K8, resulting in no net change in fragment 6-17. Global deaceylation of histones is associated with AD; however, our data suggests that deacetylation may be occurring more frequently at the N-terminus of the histone tail. The N-terminal regions of histones are rich in glycine residues, which provide a high degree of flexibility to histone tails and lack of tertiary structure. Additionally, the high abundance of basic residues lysine and arginine contribute to an overall positive

charge. Positively charged histone tails and negatively charged DNA form an electrostatic interaction that structurally results in the tail region wrapping along the DNA backbone, thereby forming a tight nucleosome structure [133]. The reduction in net charge, due to the DNA-histone tail interaction, and orientation of the extended tail against the nucleosome surface lead to denser, less transcriptionally active chromatin [133]. The loss of N-terminal acetylation induces this charge interaction and likely results in decreased gene expression in the AD frontal cortex. Deacetylation of histones is catalyzed by histone deacetylases (HDACs) and there is a growing interest in using HDAC inhibitors to slow aberrant deacetylation in brain [31]. Our previous work measured absolute concentrations of HDAC isoforms and identified specific isoforms associated with AD pathology in various neural tissues [53].

While HDAC has demonstrated potential as a prospective AD therapy, therapies targeting other histone-modifying enzymes have yet to come forward. Other PTMs, such as methylation, are modulated by enzymes with greater residue specificity than acetyltransferases and deacetylases. Often times, a methyltransferase or demethylase may only act on one site in a histone [39]. This specificity may correlate to improved efficacy and safety when targeting enzymes for specific methylation sites compared to HDAC inhibition alone. Additionally, they may be more efficacious as a combinatorial treatment. H2B methylation at K108 decreased 25% and H4 methylation at R55 decreased 35% in AD frontal cortex (Figure 5.3B). Both of these sites have been reported to be methylated in human cells [134]. To our knowledge, H2B K108 and H4 R55 methylation have

not been investigated in AD-affected human frontal cortex. Both H2B K108 and H4 R55 are located on the outermost surface of the nucleosome (Figure 5.4A) [126], suggesting their accessibility to methyltransferases and demethylases may incline them to be used as switches for transcriptional activity. Monomethylation is commonly a marker of transcription activation. Since AD is characterized by a global repression in gene expression, our observed decrease in several methylation sites strongly suggests their role in reducing transcription consistent with AD. H4 R55 participates in a complex hydrogen bond network in the nucleosome (Figure 5.4B) [126]. H4 residues Q27 and E52 and the I29 backbone form a hydrogen bond network that structurally thrusts N25 into a hydrogen bond with E73 on neighboring histone H3 [135]. By forming a hydrogen bonding network that increases affinity between H3 and H4, the nucleosome becomes structurally more stable. However, methylation of H4 R55 likely disrupts this bonding network, thereby lessening the H3-H4 interaction and weakening the nucleosome [135]. Our observed decrease in methylation of R55 may be a mechanism for increasing nucleosome stability and favoring denser chromatin, which decreases gene expression. Similarly, H2B K108 is central to a hydrogen bond network involving histones H2A, H2B, and H4 (Figure 5.4C) [126]. H2B K108 and E105 participate in intra-chain hydrogen bonding which structurally positions H2B residues for two interactions between neighboring histones favoring nucleosome stability. First, K108 forms a hydrogen bond with E105, pulling E105 away from close proximity to E93 on histone H2A.

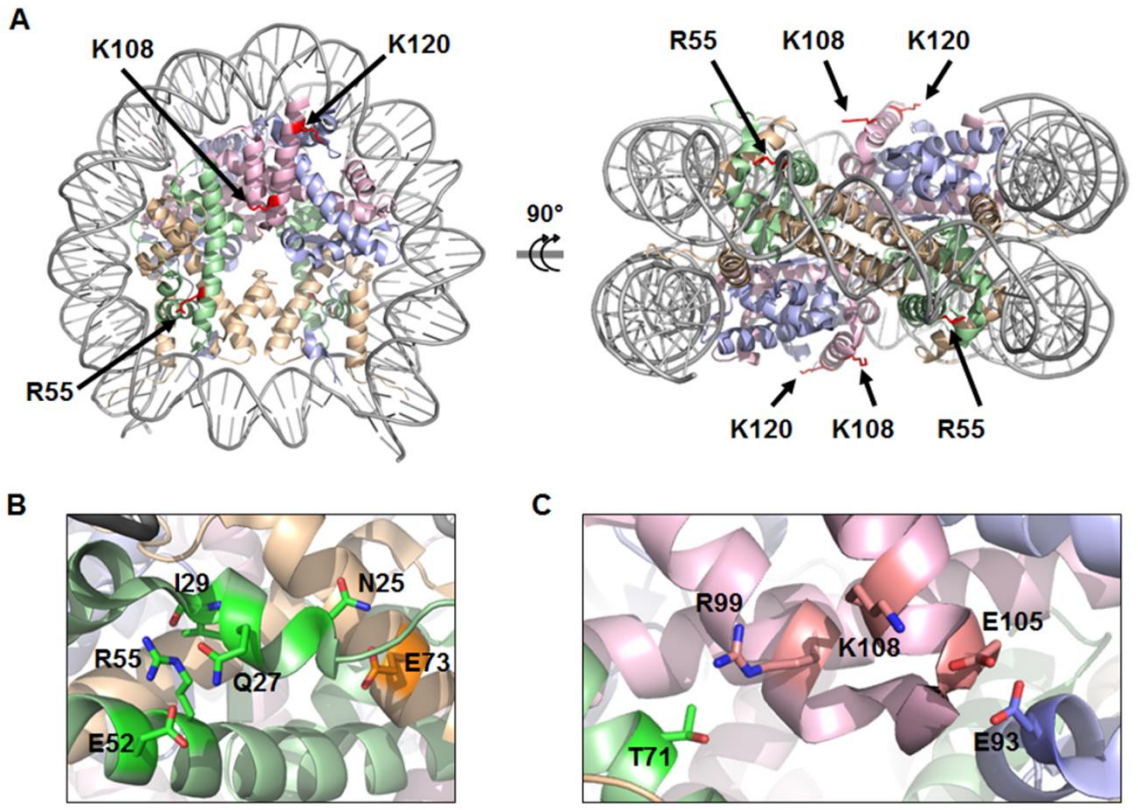

Figure 5.4 - Location of core PTMs on nucleosome surface.
H2A (blue), H2B (pink), H3 (yellow), and H4 (green) form an octamer in the nucleosome core, which is wrapped by DNA. Nucleosome crystal structure PDB ID: 2CV5 [126] was modified using PyMOL Molecular Graphics System (Version 1.7.2, Schrödinger, LLC). **(A)** Methylation sites R55 on H4 and K108 on H3 and ubiquitination site K120 on H2B are shown in red. **(B)** Hydrogen bond network of H4 R55. **(C)** Hydrogen bond network of H2B K108.

E105 and E93 can create electrostatic repulsion, however when E105 is distanced from E93 and hydrogen bonded to K108, this electrostatic repulsion is greatly reduced and H2A and H2B are able nestle together [126]. Second, the K108 hydrogen bond with E105 twists the helix-loop-helix, shown in Figure 5.4C, to position R99 on H2B directly facing T71 on H4 for a hydrogen bond. This hydrogen bond between residues on H2B and H4 strengthen the H2B-H4 stability. Methylation likely disturbs this H4-H2B-H2A inter-chain network and would favor disassembly of the nucleosome. The structural and functional effect of our observed decrease in methylation of H2B K108 is consistent with the decrease in H4 R55, suggesting methylation of histones is used to down regulate transcriptional activity and gene expression in AD pathology. Establishing specific sites of histone methylation and their modulation, as described herein, is important in characterizing AD pathology.

H2B ubiquitination at K120 increased 91% in AD (Figure 5.3B). K120 has been reported to be ubiquitinated in human cell culture and animal neural tissue [134,136,137], but we were unable to find reports measuring ubiquitination of this site in AD-affected human frontal cortex. Polyubiquitination of proteins is commonly to mark proteins for degradation; however, monoubiquitination of proteins is typically used for regulatory functions [46]. After trypsin digestion, a di-glycine remnant of ubiquitination remains on modified lysine residues, which does not allow for differentiation between mono- and polyubiquitination. Polyubiquitination of histones is less common, but has been suggested to affect the affinity of histone-histone interactions within the nucleosome [45].

Monoubiquitination of histones has been shown to indicate the presence of DNA damage [46,47] and to engage in “cross-talk” with methylation of other sites [136]. Ubiquitination of H2B K120 has been shown to be inversely related to methylation of H3 core residue K79 [136]. While we did not detect methylation of H3 K79, we did detect a decrease in methylation of other core residues H2B K108 and H4 R55. Additionally, site H2B K120 is an easily accessible site for ubiquitin ligases as it is located on the outermost surface of the nucleosome core and distant from the histone-DNA interface (Figure 5.4A) [126], an important consideration for a relatively large, 8.5 kDa PTM. Abnormal accumulation of ubiquitinated proteins other than histones in AD has been reported [138], suggesting ubiquitination in AD may extend beyond histones and the epigenome.

5.4 Conclusions

Histone PTMs have been implicated in many biological functions and diseases and serve an important role in epigenetic regulation of gene expression. Aberrant modulations in histone PTMs have been suggested to occur in brain as part of AD pathology. Histone PTMs that were found to be significantly different in AD frontal cortex were decreases in methylation of H2B K108 and H4 R55 and an increase in ubiquitination of H2B K120. Changes of these sites have not been previously reported in AD-affected frontal cortex in humans. Additionally, acetylated H4 peptide ^{9}GLGKacGGAKacR^{17} increased in abundance, which may indicate N-terminal loss of acetylation of K5 and K8. Structural effects induced by changes in these PTMs likely alter gene expression in the brain. Future work to evaluate the combinatorial effect of these PTMs on gene expression and other

specific functional roles may prove to be important in elucidating the pathology of AD. Moreover, the PTMs described herein could be used to identify specific histone-modifying enzymes to serve as drug targets for the treatment of AD, a disease which currently does not have any approved therapies to slow disease progression in humans.

Chapter 6: Conclusions and Significance

QconCATs are a unique standard for quantification containing Q-peptides. We have shown that incorporation of natural flanking sequences, while not directly used for quantification, appear to aid in the reliability of quantification. Based on our findings, the length of natural amino acid flanking sequences in the +0 to +6 amino acid residue range is not the only factor affecting trypsin cleavage. The amino acid composition within this range also affects the flanking sequence; however, our results are not entirely explained by Keil rules of trypsin cleavage. Future studies comparing the proximity of positively or negatively charged residues near the cleavage site and natural flanking sequence could increase our understanding of this phenomenon of cleavage variability. In light of the amino acid composition, it is best to provide more natural amino acids in the flanking residues when appropriate for improved quantification reliability.

Use of QconCATs for multiplexed quantification of HDAC isoforms were obtained in three different tissues: human frontal cortex, human retina, and whole mouse brain. This method of protein quantification is appropriate in diverse types of tissues, including tissues abundant in lipids. In human frontal cortex, HDAC1,2 decreased, HDAC5 increased, and HDAC6 had negligible change in concentration in AD. In human retina, the concentration of all detected HDACs decreased in both AD and AMD retina. In whole mouse brain, the profile varied from human brain with HDAC3 and HDAC4 abundance being greater in mouse. HDAC1,2 concentrations decreased in both human frontal cortex and retina, but showed no change in mouse. While mouse models are commonly used for

neurodegenerative research, disparity in HDAC profiles and changes in disease state compared to human frontal cortex tissue indicates that measurements in humans are beneficial when possible. This method of quantification is practical and useful tool for disease pathology and can be used for other tissues and disease conditions.

Relative quantification by MRM of histone PTMs in mouse and human brain revealed unique changes in AD pathology. Phosphorylation of histone H3 residues S57 and T58 decreased in 5XFAD mice, suggesting these histone PTMs play an epigenetic role in AD pathology and may stabilize nucleosomes. A mouse model was used for phosphorylation data because phosphorylation is a very labile modification that is lost during the lengthy post-mortem interval for human neural tissue. The effect of low-dose EFV, a stimulator of cholesterol hydroxylase CYP46A1 activity, on S57p and T58p showed no statistically significant changes in 5XFAD brain. In AD human frontal cortex, decreases in methylation of H2B K108 and H4 R55 and an increase in ubiquitination of H2B K120 were measured. Measurements of these sites have not been previously reported in AD-affected frontal cortex in humans. Acetylated H4 peptide ^{9}GLGKacGGAKacR^{17} increased concentration, which may indicate N-terminal loss of acetylation at K5 and K8.

Changes in PTMs can have structural effects which likely alter gene expression in the brain. We have proposed several structural mechanisms for how histone PTM modulation can affect gene expression. Future work could be performed to investigate the combinatorial effect of PTMs on gene expression.

My efforts to perform intact profiling of histone PTMs were unsuccessful. The heterogeneity of histone variants and complexity of PTM profiles proved challenging for spectral deconvolution software, which resulted in large variability of PTM abundances between software packages and acquisition conditions. Other research laboratories are developing in-house software to handle the challenges related to intact histone PTM profiling, which should prove helpful in future intact histone studies using MS.

Histone PTM measurements can describe specific functional roles, which could prove to be important in elucidating AD pathology. Perhaps more important is the use of histone PTMs to identify specific histone-modifying enzymes, which could serve as drug targets for AD treatments. Currently, there are no approved therapies to slow or prevent AD progression, highlighting the importance of drug target findings that may come from this body of research.

Appendix 1: Approvals and Funding

A1.1 Disclaimer

Certain commercial materials, instruments, and equipment are identified in this dissertation in order to specify the experimental procedure as completely as possible. In no case does such identification imply a recommendation or endorsement by the National Institute of Standards and Technology nor does it imply that the materials, instruments, or equipment identified are necessarily the best available for the purpose.

A1.2 Funding

Human frontal cortex was funded by the Washington University School of Medicine Alzheimer's Disease Research Center's National Institute of Aging grant (P50 AG005681). Retina studies were funded by the National Institutes of Health grant EY018383 (to I.A. Pikuleva). Mouse studies were funded by the U.S. Public Health Service grant GM062882 (to I.A. Pikuleva).

A1.3 Use of Human Tissue

Frozen samples of frontal cortex were obtained from Washington University School of Medicine Alzheimer's Disease Research Center (St. Louis, MO). Human frontal cortex was collected in accordance with guidance from the Washington University Human Research Protection Office (HRPO number: 89-0556). We consulted the Washington University HRPO, which determined that Institutional Review Board (IRB) oversight was not required for these studies and

waived the need for IRB approval. In the state of Missouri, individuals can give prospective consent for autopsy. Our participants provided this consent by signing the hospital's autopsy form. If the participant does not provide future consent before death, the DPOA or next of kin provide it after death. Human retina use conformed to the Declaration of Helsinki and had been approved by the Ethical Committee at Case Western Reserve University. Eyes were acquired, characterized and dissected as described [94]. The neural retina was isolated, flash-frozen in liquid nitrogen, and stored at -80 °C until analyzed. Handling of tissues for sample processing conformed to University of Maryland regulations. All data were analyzed anonymously.

A1.4 Use of Mice

All animal-handling procedures were performed at Case Western Reserve University and were approved by the Institutional Animal Care and Use Committee at Case Western Reserve University and conformed to the standards of the U.S. Public Health Service Policy on Humane Care and Use of Laboratory Animals and recommendations of the American Veterinary Association Panel on Euthanasia. Mice were housed in the Animal Resource Center at Case Western Reserve University and maintained in a standard 12 h light/12 h dark cycle environment. Water and food were provided *ab libitum*. Mice were sacrificed by cervical dislocation, and their brains were immediately isolated and frozen.

A1.5 General Materials

The DC Protein Assay kit was purchased from Bio-Rad Laboratories (Hercules, CA). RapiGest SF surfactant was from Waters (Milford, MA), Trypsin (T0303, Type IX-S from porcine pancreas) and all other chemicals were purchased from Sigma-Aldrich (St. Louis, MO).

Appendix 2: Additional Data

A2.1 Sequences of HDAC Isoforms and Variants

Isoform	Amino acids	UniProt Number	Sequence differences
HDAC1	482	Q13547	Canonical
HDAC2	488	Q92769	Canonical
HDAC3 Isoform 1	428	O15379-1	Canonical
HDAC3 Isoform 2	429	O15379-2	1-15: MAKTVAYFYDPDVGN → MIVFKPYQASQHDMCR
HDAC4	1084	P56524	Canonical
HDAC5 Isoform 1	1122	Q9UQL6-1	Canonical
HDAC5 Isoform 2	1037	Q9UQL6-2	684-768: Missing
HDAC5 Isoform 3	1123	Q9UQL6-3	7-7: S → SA
HDAC6	1215	Q9UBN7	Canonical
HDAC7 Isoform 1	952	Q8WUI4-1	Canonical
HDAC7 Isoform 2	480	Q8WUI4-2	1-472: Missing, 473-520: LAQGGHRPLS...TPARTLPFTT → MQACVGVRGV...WVPALTLAPA
HDAC7 Isoform 3	915	Q8WUI4-3	227-263: Missing
HDAC7 Isoform 4	922	Q8WUI4-4	227-256: Missing
HDAC7 Isoform 5	991	Q8WUI4-5	1-1: M → MHSPGADGTQVSPGAHYCSPTGAGCPRPCADTPGPQPQPM
HDAC7 Isoform 6	974	Q8WUI4-6	1-1: M → MHSPGAGCPRPCADTPGPQPQPM
HDAC7 Isoform 7	954	Q8WUI4-7	1-1: M → MHSPGADGTQVSPGAHYCSPTGAGCPRPCADTPGPQPQPM, 227-263: Missing
HDAC7 Isoform 8	1014	Q8WUI4-8	1-1: M → MSDLRKRELGALFTSRGTGGVEWDGTQVSPGAHYCSPTGAGCPRPCADTPGPQPQPM, 892-952: SKYWGCMQRL...LVEEEEPMNL → MGALTLSQIP...QGLTKKKWRQ
HDAC7 Isoform 9	425	Q8WUI4-9	1-527: Missing
HDAC7 Isoform 10	614	Q8WUI4-10	1-338: Missing
HDAC8 Isoform 1	377	Q9BY41-1	Canonical
HDAC8 Isoform 2	272	Q9BY41-2	248-272: LKEVYQAFNPKAVVLQLGADTIAGD → RTSCPKSRPVEAAAAACLPHLH SLV, 273-377: Missing
HDAC8 Isoform 3	163	Q9BY41-3	147-163: DEASGFCYLNDAVLGIL → RDVCVCGTLQGILKKSK, 164-377: Missing
HDAC8 Isoform 4	286	Q9BY41-4	56-146: Missing
HDAC8 Isoform 5	256	Q9BY41-5	246-272: SVLKEVYQAFNPKAVVLQLGADTIAGD → RYEPPAPNPGL, 273-377: Missing
HDAC9 Isoform 1	1011	Q9UKV0-1	Canonical
HDAC9 Isoform 2	923	Q9UKV0-2	487-574: Missing
HDAC9 Isoform 3	590	Q9UKV0-3	575-590: PFLEPTHTRALSVRQA → VIGKDLAPGFVIKVII, 591-1011: Missing
HDAC9 Isoform 4	879	Q9UKV0-4	861-879: GTGLGEGYNINIAWTGGLD → RFISLEPHFYLYLSGNCIA, 880-1011: Missing

HDAC9 Isoform 5	1066	Q9UKV0-5	1006-1011: MSLKFS → KYWKSVRMVAVPRGCALAGAQLQEETETVSALASLTVDVE QPFAQEDSRTAGEPMEEEPAL
HDAC9 Isoform 6	1025	Q9UKV0-6	88-88: K → KLQQ, 218-261: Missing, 1006-1011: MSLKFS → KYWKSVRMVAVPRGCALAGAQLQEETETVSALASLTVDVE QPFAQEDSRTAGEPMEEEPAL
HDAC9 Isoform 7	1069	Q9UKV0-7	88-88: K → KLQQ, 1006-1011: MSLKFS → KYWKSVRMVAVPRGCALAGAQLQEETETVSALASLTVDVE QPFAQEDSRTAGEPMEEEPAL
HDAC9 Isoform 8	588	Q9UKV0-8	1-1: M → MMSSPAQPDLMWNLVPWVLFCGCCRIFPDGVAGREQLLAQQRM, 218-261: Missing, 575-590: PFLEPTHTRALSVRQA → VIGKDLAPGFVIKVII, 591-1011: Missing
HDAC10 Isoform 1	669	Q969S8-1	Canonical
HDAC10 Isoform 2	649	Q969S8-2	252-271: Missing
HDAC10 Isoform 4	658	Q969S8-4	612-669: NSTPQLAGIL...MLQCHPHLVA → VSWAGWRCCG...GPGAEWRGTS
HDAC10 Isoform 5	396	Q969S8-5	252-301: Missing, 447-669: Missing
HDAC11 Isoform 1	347	Q96DB2-1	Canonical
HDAC11 Isoform 2	296	Q96DB2-2	1-28: Missing, 85-107: Missing

HDAC (*Homo sapiens*) Sequences (UniProtKB)

HDAC1

```
>sp|Q13547|HDAC1_HUMAN Histone deacetylase 1 OS=Homo sapiens GN=HDAC1
PE=1 SV=1
MAQTQGTRRKVCYYYDGDVGNYYYGQGHPMKPHRIRMTHNLLLNYGLYRKMEIYRPHKAN
AEEMTKYHSDDYIKFLRSIRPDNMSEYSKQMQRFNVGEDCPVFDGLFEFCQLSTGGSVAS
AVKLNKQQTDIAVNWAGGLHHAKKSEASGFCYVNDIVLAILELLKYHQRVLYIDIDIHHG
DGVEEAFYTTDRVMTVSFHKYGEYFPGTGDLRDIGAGKGKYYAVNYPLRDGIDDESYEAI
FKPVMSKVMEMFQPSAVVLQCGSDSLSGDRLGCFNLTIKGHAKCVEFVKSFNLPMLMLGG
GGYTIRNVARCWTYETAVALDTEIPNELPYNDYFEYFGPDFKLHISPSNMTNQNTNEYLE
KIKQRLFENLRMLPHAPGVQMQAIPEDAIPEESGDEDEDDPDKRISICSSDKRIACEEEF
SDSEEEGEGGRKNSSNFKKAKRVKTEDEKEKDPEEKKEVTEEEKTKEEKPEAKGVKEEVK
LA
```

HDAC2

```
>sp|Q92769|HDAC2_HUMAN Histone deacetylase 2 OS=Homo sapiens GN=HDAC2
PE=1 SV=2
MAYSQGGGKKKVCYYYDGDIGNYYYGQGHPMKPHRIRMTHNLLLNYGLYRKMEIYRPHKA
TAEEMTKYHSDEYIKFLRSIRPDNMSEYSKQMQRFNVGEDCPVFDGLFEFCQLSTGGSVA
GAVKLNRQQTDMAVNWAGGLHHAKKSEASGFCYVNDIVLAILELLKYHQRVLYIDIDIHH
GDGVEEAFYTTDRVMTVSFHKYGEYFPGTGDLRDIGAGKGKYYAVNFPMRDGIDDESYGQ
IFKPIISKVMEMYQPSAVVLQCGADSLSGDRLGCFNLTVKGHAKCVEVVKTFNLPLLMLG
GGGYTIRNVARCWTYETAVALDCEIPNELPYNDYFEYFGPDFKLHISPSNMTNQNTPEYM
EKIKQRLFENLRMLPHAPGVQMQAIPEDAVHEDSGDEDGEDPDKRISIRASDKRIACDEE
FSDSEDEGEGGRRNVADHKKGAKKARIEEDKKETEDKKTDVKEEDKSKDNSGEKTDTKGT
KSEQLSNP
```

HDAC3

```
>sp|O15379|HDAC3_HUMAN Histone deacetylase 3 OS=Homo sapiens GN=HDAC3
PE=1 SV=2
MAKTVAYFYDPDVGNFHYGAGHPMKPHRLALTHSLVLHYGLYKKMIVFKPYQASQHDMCR
FHSEDYIDFLQRVSPTNMQGFTKSLNAFNVGDDCPVFPGLFEFCSRYTGASLQGATQLNN
KICDIAINWAGGLHHAKKFEASGFCYVNDIVIGILELLKYHPRVLYIDIDIHHGDGVQEA
```

FYLTDRVMTVSFHKYGNYFFPGTGDMYEVGAESGRYYCLNVPLRDGIDDQSYKHLFQPVI
NQVVDFYQPTCIVLQCGADSLGCDRLGCFNLSIRGHGECVEYVKSFNIPLLVLGGGGYTV
RNVARCWTYETSLLVEEAISEELPYSEYFEYFAPDFTLHPDVSTRIENQNSRQYLDQIRQ
TIFENLKMLNHAPSVQIHDVPADLLTYDRTDEADAEERGPEENYSRPEAPNEFYDGDHDN
DKESDVEI

>sp|O15379-2|HDAC3_HUMAN Isoform 2 of Histone deacetylase 3 OS=Homo sapiens GN=HDAC3
MIVFKPYQASQHDMCRFHYGAGHPMKPHRLALTHSLVLHYGLYKKMIVFKPYQASQHDMC
RFHSEDYIDFLQRVSPTNMQGFTKSLNAFNVGDDCPVFPGLFEFCSRYTGASLQGATQLN
NKICDIAINWAGGLHHAKKFEASGFCYVNDIVIGILELLKYHPRVLYIDIDIHHGDGVQE
AFYLTDRVMTVSFHKYGNYFFPGTGDMYEVGAESGRYYCLNVPLRDGIDDQSYKHLFQPV
INQVVDFYQPTCIVLQCGADSLGCDRLGCFNLSIRGHGECVEYVKSFNIPLLVLGGGGYT
VRNVARCWTYETSLLVEEAISEELPYSEYFEYFAPDFTLHPDVSTRIENQNSRQYLDQIR
QTIFENLKMLNHAPSVQIHDVPADLLTYDRTDEADAEERGPEENYSRPEAPNEFYDGDHD
NDKESDVEI

HDAC4

>sp|P56524|HDAC4_HUMAN Histone deacetylase 4 OS=Homo sapiens GN=HDAC4 PE=1 SV=3
MSSQSHPDGLSGRDQPVELLNPARVNHMPSTVDVATALPLQVAPSAVPMDLRLDHQFSLP
VAEPALREQQLQQELLALKQKQQIQRQILIAEFQRQHEQLSRQHEAQLHEHIKQQQEMLA
MKHQQELLEHQRKLERHRQEQELEKQHREQKLQQLKNKEKGKESAVASTEVKMKLQEFVL
NKKKALAHRNLNHCISSDPRYWYGKTQHSSLDQSSPPQSGVSTSYNHPVLGMYDAKDDFP
LRKTASEPNLKLRSRLKQKVAERRSSPLLRRKDGPVVTALKKRPLDVTDSACSSAPGSGP
SSPNNSSGSVSAENGIAPAVPSIPAETSLAHRLVAREGSAAPLPLYTSPSLPNITLGLPA
TGPSAGTAGQQDAERLTLPALQQRLSLFPGTHLTPYLSTSPLERDGGAAHSPLLQHMVLL
EQPPAQAPLVTGLGALPLHAQSLVGADRVSPSIHKLRQHRPLGRTQSAPLPQNAQALQHL
VIQQQHQQFLEKHKQQFQQQQLQMNKIIPKPSEPARQPESHPEETEEELREHQALLDEPY
LDRLPGQKEAHAQAGVQVKQEPIESDEEEAEPPREVEPGQRQPSEQELLFRQQALLLEQQ
RIHQLRNYQASMEAAGIPVSFGGHRPLSRAQSSPASATFPVSVQEPPTKPRFTTGLVYDT
LMLKHQCTCGSSSSHPEHAGRIQSIWSRLQETGLRGKCECIRGRKATLEELQTVHSEAHT
LLYGTNPLNRQKLDSKKLLGSLASVFVRLPCGGVGVDSDTIWNEVHSAGAARLAVGCVVE
LVFKVATGELKNGFAVVRPPGHHAEESTPMGFCYFNSVAVAAKLLQQRLSVSKILIVDWD
VHHGNGTQQAFYSDPSVLYMSLHRYDDGNFFPGSGAPDEVGTGPGVGFNVNMAFTGGLDP
PMGDAEYLAAFRTVVMPIASEFAPDVVLVSSGFDAVEGHPTPLGGYNLSARCFGYLTKQL
MGLAGGRIVLALEGGHDLTAICDASEACVSALLGNELDPLPEKVLQQRPNANAVRSMEKV
MEIHSKYWRCLQRTTSTAGRSLIEAQTCENEEAETVTAMASLSVGVKPAEKRPDEEPMEE
EPPL

HDAC5

>sp|Q9UQL6|HDAC5_HUMAN Histone deacetylase 5 OS=Homo sapiens GN=HDAC5 PE=1 SV=2
MNSPNESDGMSGREPSLEILPRTSLHSIPVTVEVKPVLPRAMPSSMGGGGGGSPSPVELR
GALVGSVDPTLREQQLQQELLALKQQQQLQKQLLFAEFQKQHDHLTRQHEVQLQKHLKQQ
QEMLAAKQQQEMLAAKRQQELEQQRQREQQRQEELEKQRLEQQLLILRNKEKSKESAIAS
TEVKLRLQEFLLSKSKEPTPGGLNHSLPQHPKCWGAHHASLDQSSPPQSGPPGTPPSYKL
PLPGPYDSRDDFPLRKTASEPNLKVRSRLKQKVAERRSSPLLRRKDGTVISTFKKRAVEI
TGAGPGASSVCNSAPGSGPSSPNSSHSTIAENGFTGSVPNIPTEMLPQHRALPLDSSPNQ
FSLYTSPSLPNISLGLQATVTVTNSHLTASPKLSTQQEAERQALQSLRQGGTLTGKFMST
SSIPGCLLGVALEGDGSPHGHASLLQHVLLLEQARQQSTLIAVPLHGQSPLVTGERVATS
MRTVGKLPRHRPLSRTQSSPLPQSPQALQQLVMQQQHQQFLEKQKQQQLQLGKILTKTGE
LPRQPTTHPEETEEELTEQQEVLLGEGALTMPREGSTESESTQEDLEEEDEEDDGEEEED
CIQVKDEEGESGAEEGPDLEEPGAGYKKLFSDAQPLQPLQVYQAPLSLATVPHQALGRTQ
SSPAAPGGMKSPPDQPVKHLFTTGVVYDTFMLKHQCMCGNTHVHPEHAGRIQSIWSRLQE
TGLLSKCERIRGRKATLDEIQTVHSEYHTLLYGTSPLNRQKLDSKKLLGPISQKMYAVLP
CGGIGVDSDTVWNEMHSSSAVRMAVGCLLELAFKVAAGELKNGFAIIRPPGHHAEESTAM

GFCFFNSVAITAKLLQQKLNVGKVLIVDWDIHHGNGTQQAFYNDPSVLYISLHRYDNGNF
FPGSGAPEEVGGGPGVGYNVNVAWTGGVDPPIGDVEYLTAFRTVVMPIAHEFSPDVVLVS
AGFDAVEGHLSPLGGYSVTARCFGHLTRQLMTLAGGRVVLALEGGHDLTAICDASEACVS
ALLSVELQPLDEAVLQQKPNINAVATLEKVIEIQSKHWSCVQKFAAGLGRSLREAQAGET
EEAETVSAMALLSVGAEQAQAAAAREHSPRPAEEPMEQEPAL

>sp|Q9UQL6-2|HDAC5_HUMAN Isoform 2 of Histone deacetylase 5 OS=Homo sapiens GN=HDAC5
MNSPNESDGMSGREPSLEILPRTSLHSIPVTVEVKPVLPRAMPSSMGGGGGGSPSPVELR
GALVGSVDPTLREQQLQQELLALKQQQQLQKQLLFAEFQKQHDHLTRQHEVQLQKHLKQQ
QEMLAAKQQQEMLAAKRQQELEQQRQREQQRQEELEKQRLEQQLLILRNKEKSKESAIAS
TEVKLRLQEFLLSKSKEPTPGGLNHSLPQHPKCWGAHHASLDQSSPPQSGPPGTPPSYKL
PLPGPYDSRDDFPLRKTASEPNLKVRSRLKQKVAERRSSPLLRRKDGTVISTFKKRAVEI
TGAGPGASSVCNSAPGSGPSSPNSSHSTIAENGFTGSVPNIPTEMLPQHRALPLDSSPNQ
FSLYTSPSLPNISLGLQATVTVTNSHLTASPKLSTQQEAERQALQSLRQGGTLTGKFMST
SSIPGCLLGVALEGDGSPHGHASLLQHVLLLEQARQQSTLIAVPLHGQSPLVTGERVATS
MRTVGKLPRHRPLSRTQSSPLPQSPQALQQLVMQQQHQQFLEKQKQQQLQLGKILTKTGE
LPRQPTTHPEETEEELTEQQEVLLGEGALTMPREGSTESESTQEDLEEEDEEDDGEEEED
CIQVKDEEGESGAEEGPDLEEPGAGYKKLFSDAQPLQPLQVYQAPLSLATVPHQALGRTQ
SSPAAPGGMKSPPDQPVKHLFTTGPISQKMYAVLPCGGIGVDSDTVWNEMHSSSAVRMAV
GCLLELAFKVAAGELKNGFAIIRPPGHHAEESTAMGFCFFNSVAITAKLLQQKLNVGKVL
IVDWDIHHGNGTQQAFYNDPSVLYISLHRYDNGNFFPGSGAPEEVGGGPGVGYNVNVAWT
GGVDPPIGDVEYLTAFRTVVMPIAHEFSPDVVLVSAGFDAVEGHLSPLGGYSVTARCFGH
LTRQLMTLAGGRVVLALEGGHDLTAICDASEACVSALLSVELQPLDEAVLQQKPNINAVA
TLEKVIEIQSKHWSCVQKFAAGLGRSLREAQAGETEEAETVSAMALLSVGAEQAQAAAAR
EHSPRPAEEPMEQEPAL

>sp|Q9UQL6-3|HDAC5_HUMAN Isoform 3 of Histone deacetylase 5 OS=Homo sapiens GN=HDAC5
MNSPNESADGMSGREPSLEILPRTSLHSIPVTVEVKPVLPRAMPSSMGGGGGGSPSPVEL
RGALVGSVDPTLREQQLQQELLALKQQQQLQKQLLFAEFQKQHDHLTRQHEVQLQKHLKQ
QQEMLAAKQQQEMLAAKRQQELEQQRQREQQRQEELEKQRLEQQLLILRNKEKSKESAIA
STEVKLRLQEFLLSKSKEPTPGGLNHSLPQHPKCWGAHHASLDQSSPPQSGPPGTPPSYK
LPLPGPYDSRDDFPLRKTASEPNLKVRSRLKQKVAERRSSPLLRRKDGTVISTFKKRAVE
ITGAGPGASSVCNSAPGSGPSSPNSSHSTIAENGFTGSVPNIPTEMLPQHRALPLDSSPN
QFSLYTSPSLPNISLGLQATVTVTNSHLTASPKLSTQQEAERQALQSLRQGGTLTGKFMS
TSSIPGCLLGVALEGDGSPHGHASLLQHVLLLEQARQQSTLIAVPLHGQSPLVTGERVAT
SMRTVGKLPRHRPLSRTQSSPLPQSPQALQQLVMQQQHQQFLEKQKQQQLQLGKILTKTG
ELPRQPTTHPEETEEELTEQQEVLLGEGALTMPREGSTESESTQEDLEEEDEEDDGEEEE
DCIQVKDEEGESGAEEGPDLEEPGAGYKKLFSDAQPLQPLQVYQAPLSLATVPHQALGRT
QSSPAAPGGMKSPPDQPVKHLFTTGVVYDTFMLKHQCMCGNTHVHPEHAGRIQSIWSRLQ
ETGLLSKCERIRGRKATLDEIQTVHSEYHTLLYGTSPLNRQKLDSKKLLGPISQKMYAVL
PCGGIGVDSDTVWNEMHSSSAVRMAVGCLLELAFKVAAGELKNGFAIIRPPGHHAEESTA
MGFCFFNSVAITAKLLQQKLNVGKVLIVDWDIHHGNGTQQAFYNDPSVLYISLHRYDNGN
FFPGSGAPEEVGGGPGVGYNVNVAWTGGVDPPIGDVEYLTAFRTVVMPIAHEFSPDVVLV
SAGFDAVEGHLSPLGGYSVTARCFGHLTRQLMTLAGGRVVLALEGGHDLTAICDASEACV
SALLSVELQPLDEAVLQQKPNINAVATLEKVIEIQSKHWSCVQKFAAGLGRSLREAQAGE
TEEAETVSAMALLSVGAEQAQAAAAREHSPRPAEEPMEQEPAL

HDAC6

>sp|Q9UBN7|HDAC6_HUMAN Histone deacetylase 6 OS=Homo sapiens GN=HDAC6 PE=1 SV=2
MTSTGQDSTTTRQRRSRQNPQSPPQDSSVTSKRNIKKGAVPRSIPNLAEVKKKGKMKKLG
QAMEEDLIVGLQGMDLNLEAEALAGTGLVLDEQLNEFHCLWDDSFPEGPERLHAIKEQLI
QEGLLDRCVSFQARFAEKEELMLVHSLEYIDLMETTQYMNEGELRVLADTYDSVYLHPNS
YSCACLASGSVLRLVDAVLGAEIRNGMAIIRPPGHHAQHSLMDGYCMFNHVAVAARYAQQ
KHRIRRVLIVDWDVHHGQGTQFTFDQDPSVLYFSIHRYEQGRFWPHLKASNWSTTGFGQG

QGYTINVPWNQVGMRDADYIAAFLHVLLPVALEFQPQLVLVAAGFDALQGDPKGEMAATP
AGFAQLTHLLMGLAGGKLILSLEGGYNLRALAEGVSASLHTLLGDPCPMLESPGAPCRSA
QASVSCALEALEPFWEVLVRSTETVERDNMEEDNVEESEEEGPWEPPVLPILTWPVLQSR
TGLVYDQNMMNHCNLWDSHHPEVPQRILRIMCRLEELGLAGRCLTLTPRPATEAELLTCH
SAEYVGHLRATEKMKTRELHRESSNFDSIYICPSTFACAQLATGAACRLVEAVLSGEVLN
GAAVVRPPGHHAEQDAACGFCFFNSVAVAARHAQTISGHALRILIVDWDVHHGNGTQHMF
EDDPSVLYVSLHRYDHGTFFPMGDEGASSQIGRAAGTGFTVNVAWNGPRMGDADYLAAWH
RLVLPIAYEFNPELVLVSAGFDAARGDPLGGCQVSPEGYAHLTHLLMGLASGRIILILEG
GYNLTSISESMAACTRSLLGDPPPLLTLPRPPLSGALASITETIQVHRRYWRSLRVMKVE
DREGPSSSKLVTKKAPQPAKPRLAERMTTREKKVLEAGMGKVTSASFGEESTPGQTNSET
AVVALTQDQPSEAATGGATLAQTISEAAIGGAMLGQTTSEEAVGGATPDQTTSEETVGGA
ILDQTTSEDAVGGATLGQTTSEEAVGGATLAQTTSEAAMEGATLDQTTSEEAPGGTELIQ
TPLASSTDHQTPPTSPVQGTTPQISPSTLIGSLRTLELGSESQGASESQAPGEENLLGEA
AGGQDMADSMLMQGSRGLTDQAIFYAVTPLPWCPHLVAVCPIPAAGLDVTQPCGDCGTIQ
ENWVCLSCYQVYCGRYINGHMLQHHGNSGHPLVLSYIDLSAWCYYCQAYVHHQALLDVKN
IAHQNKFGEDMPHPH

HDAC7

>sp|Q8WUI4|HDAC7_HUMAN Histone deacetylase 7 OS=Homo sapiens GN=HDAC7
PE=1 SV=2
MDLRVGQRPPVEPPPEPTLLALQRPQRLHHHLFLAGLQQQRSVEPMRLSMDTPMPELQVG
PQEQELRQLLHKDKSKRSAVASSVVKQKLAEVILKKQQAALERTVHPNSPGIPYRTLEPL
ETEGATRSMLSSFLPPVPSLPSDPPEHFPLRKTVSEPNLKLRYKPKKSLERRKNPLLRKE
SAPPSLRRRPAETLGDSSPSSSSTPASGCSSPNDSEHGPNPILGSEALLGQRLRLQETSV
APFALPTVSLLPAITLGLPAPARADSDRRTHPTLGPRGPILGSPHTPLFLPHGLEPEAGG
TLPSRLQPILLLDPSGSHAPLLTVPGLGPLPFHFAQSLMTTERLSGSGLHWPLSRTRSEP
LPPSATAPPPPGPMQPRLEQLKTHVQVIKRSAKPSEKPRLRQIPSAEDLETDGGGPGQVV
DDGLEHRELGHGQPEARGPAPLQQHPQVLLWEQQRLAGRLPRGSTGDTVLLPLAQGGHRP
LSRAQSSPAAPASLSAPEPASQARVLSSSETPARTLPFTTGLIYDSVMLKHQCSCGDNSR
HPEHAGRIQSIWSRLQERGLRSQCECLRGRKASLEELQSVHSERHVLLYGTNPLSRLKLD
NGKLAGLLAQRMFVMLPCGGVGVDTDTIWNELHSSNAARWAAGSVTDLAFKVASRELKNG
FAVVRPPGHHADHSTAMGFCFFNSVAIACRQLQQQSKASKILIVDWDVHHGNGTQQTFYQ
DPSVLYISLHRHDDGNFFPGSGAVDEVGAGSGEGFNVNVAWAGGLDPPMGDPEYLAAFRI
VVMPIAREFSPDLVLVSAGFDAAEGHPAPLGGYHVSAKCFGYMTQQLMNLAGGAVVLALE
GGHDLTAICDASEACVAALLGNRVDPLSEEGWKQKPNLNAIRSLEAVIRVHSKYWGCMQR
LASCPDSWVPRVPGADKEEVEAVTALASLSVGILAEDRPSEQLVEEEEPMNL

>sp|Q8WUI4-2|HDAC7_HUMAN Isoform 2 of Histone deacetylase 7 OS=Homo
sapiens GN=HDAC7
MQACVGVRGVYPPGSMWVPAVAVLACSLQPRPWGVRTPWVPALTLAPAGLIYDSVMLKHQ
CSCGDNSRHPEHAGRIQSIWSRLQERGLRSQCECLRGRKASLEELQSVHSERHVLLYGTN
PLSRLKLDNGKLAGLLAQRMFVMLPCGGVGVDTDTIWNELHSSNAARWAAGSVTDLAFKV
ASRELKNGFAVVRPPGHHADHSTAMGFCFFNSVAIACRQLQQQSKASKILIVDWDVHHGN
GTQQTFYQDPSVLYISLHRHDDGNFFPGSGAVDEVGAGSGEGFNVNVAWAGGLDPPMGDP
EYLAAFRIVVMPIAREFSPDLVLVSAGFDAAEGHPAPLGGYHVSAKCFGYMTQQLMNLAG
GAVVLALEGGHDLTAICDASEACVAALLGNRVDPLSEEGWKQKPNLNAIRSLEAVIRVHS
KYWGCMQRLASCPDSWVPRVPGADKEEVEAVTALASLSVGILAEDRPSEQLVEEEEPMNL

>sp|Q8WUI4-3|HDAC7_HUMAN Isoform 3 of Histone deacetylase 7 OS=Homo
sapiens GN=HDAC7
MDLRVGQRPPVEPPPEPTLLALQRPQRLHHHLFLAGLQQQRSVEPMRLSMDTPMPELQVG
PQEQELRQLLHKDKSKRSAVASSVVKQKLAEVILKKQQAALERTVHPNSPGIPYRTLEPL
ETEGATRSMLSSFLPPVPSLPSDPPEHFPLRKTVSEPNLKLRYKPKKSLERRKNPLLRKE
SAPPSLRRRPAETLGDSSPSSSSTPASGCSSPNDSEHGPNPILGSEADSDRRTHPTLGPR
GPILGSPHTPLFLPHGLEPEAGGTLPSRLQPILLLDPSGSHAPLLTVPGLGPLPFHFAQS
LMTTERLSGSGLHWPLSRTRSEPLPPSATAPPPPGPMQPRLEQLKTHVQVIKRSAKPSEK
PRLRQIPSAEDLETDGGGPGQVVDDGLEHRELGHGQPEARGPAPLQQHPQVLLWEQQRLA

GRLPRGSTGDTVLLPLAQGGHRPLSRAQSSPAAPASLSAPEPASQARVLSSSETPARTLP
FTTGLIYDSVMLKHQCSCGDNSRHPEHAGRIQSIWSRLQERGLRSQCECLRGRKASLEEL
QSVHSERHVLLYGTNPLSRLKLDNGKLAGLLAQRMFVMLPCGGVGVDTDTIWNELHSSNA
ARWAAGSVTDLAFKVASRELKNGFAVVRPPGHHADHSTAMGFCFFNSVAIACRQLQQQSK
ASKILIVDWDVHHGNGTQQTFYQDPSVLYISLHRHDDGNFFPGSGAVDEVGAGSGEGFNV
NVAWAGGLDPPMGDPEYLAAFRIVVMPIAREFSPDLVLVSAGFDAAEGHPAPLGGYHVSA
KCFGYMTQQLMNLAGGAVVLALEGGHDLTAICDASEACVAALLGNRVDPLSEEGWKQKPN
LNAIRSLEAVIRVHSKYWGCMQRLASCPDSWVPRVPGADKEEVEAVTALASLSVGILAED
RPSEQLVEEEEPMNL

>sp|Q8WUI4-4|HDAC7_HUMAN Isoform 4 of Histone deacetylase 7 OS=Homo
sapiens GN=HDAC7
MDLRVGQRPPVEPPPEPTLLALQRPQRLHHHLFLAGLQQQRSVEPMRLSMDTPMPELQVG
PQEQELRQLLHKDKSKRSAVASSVVKQKLAEVILKKQQAALERTVHPNSPGIPYRTLEPL
ETEGATRSMLSSFLPPVPSLPSDPPEHFPLRKTVSEPNLKLRYKPKKSLERRKNPLLRKE
SAPPSLRRRPAETLGDSSPSSSSTPASGCSSPNDSEHGPNPILGSEGLPAPARADSDRRT
HPTLGPRGPILGSPHTPLFLPHGLEPEAGGTLPSRLQPILLLDPSGSHAPLLTVPGLGPL
PFHFAQSLMTTERLSGSGLHWPLSRTRSEPLPPSATAPPPPGPMQPRLEQLKTHVQVIKR
SAKPSEKPRLRQIPSAEDLETDGGGPGQVVDDGLEHRELGHGQPEARGPAPLQQHPQVLL
WEQQRLAGRLPRGSTGDTVLLPLAQGGHRPLSRAQSSPAAPASLSAPEPASQARVLSSSE
TPARTLPFTTGLIYDSVMLKHQCSCGDNSRHPEHAGRIQSIWSRLQERGLRSQCECLRGR
KASLEELQSVHSERHVLLYGTNPLSRLKLDNGKLAGLLAQRMFVMLPCGGVGVDTDTIWN
ELHSSNAARWAAGSVTDLAFKVASRELKNGFAVVRPPGHHADHSTAMGFCFFNSVAIACR
QLQQQSKASKILIVDWDVHHGNGTQQTFYQDPSVLYISLHRHDDGNFFPGSGAVDEVGAG
SGEGFNVNVAWAGGLDPPMGDPEYLAAFRIVVMPIAREFSPDLVLVSAGFDAAEGHPAPL
GGYHVSAKCFGYMTQQLMNLAGGAVVLALEGGHDLTAICDASEACVAALLGNRVDPLSEE
GWKQKPNLNAIRSLEAVIRVHSKYWGCMQRLASCPDSWVPRVPGADKEEVEAVTALASLS
VGILAEDRPSEQLVEEEEPMNL

>sp|Q8WUI4-5|HDAC7_HUMAN Isoform 5 of Histone deacetylase 7 OS=Homo
sapiens GN=HDAC7
MHSPGADGTQVSPGAHYCSPTGAGCPRPCADTPGPQPQPMDLRVGQRPPVEPPPEPTLLA
LQRPQRLHHHLFLAGLQQQRSVEPMRLSMDTPMPELQVGPQEQELRQLLHKDKSKRSAVA
SSVVKQKLAEVILKKQQAALERTVHPNSPGIPYRTLEPLETEGATRSMLSSFLPPVPSLP
SDPPEHFPLRKTVSEPNLKLRYKPKKSLERRKNPLLRKESAPPSLRRRPAETLGDSSPSS
SSTPASGCSSPNDSEHGPNPILGSEALLGQRLRLQETSVAPFALPTVSLLPAITLGLPAP
ARADSDRRTHPTLGPRGPILGSPHTPLFLPHGLEPEAGGTLPSRLQPILLLDPSGSHAPL
LTVPGLGPLPFHFAQSLMTTERLSGSGLHWPLSRTRSEPLPPSATAPPPPGPMQPRLEQL
KTHVQVIKRSAKPSEKPRLRQIPSAEDLETDGGGPGQVVDDGLEHRELGHGQPEARGPAP
LQQHPQVLLWEQQRLAGRLPRGSTGDTVLLPLAQGGHRPLSRAQSSPAAPASLSAPEPAS
QARVLSSSETPARTLPFTTGLIYDSVMLKHQCSCGDNSRHPEHAGRIQSIWSRLQERGLR
SQCECLRGRKASLEELQSVHSERHVLLYGTNPLSRLKLDNGKLAGLLAQRMFVMLPCGGV
GVDTDTIWNELHSSNAARWAAGSVTDLAFKVASRELKNGFAVVRPPGHHADHSTAMGFCF
FNSVAIACRQLQQQSKASKILIVDWDVHHGNGTQQTFYQDPSVLYISLHRHDDGNFFPGS
GAVDEVGAGSGEGFNVNVAWAGGLDPPMGDPEYLAAFRIVVMPIAREFSPDLVLVSAGFD
AAEGHPAPLGGYHVSAKCFGYMTQQLMNLAGGAVVLALEGGHDLTAICDASEACVAALLG
NRVDPLSEEGWKQKPNLNAIRSLEAVIRVHSKYWGCMQRLASCPDSWVPRVPGADKEEVE
AVTALASLSVGILAEDRPSEQLVEEEEPMNL

>sp|Q8WUI4-6|HDAC7_HUMAN Isoform 6 of Histone deacetylase 7 OS=Homo
sapiens GN=HDAC7
MHSPGAGCPRPCADTPGPQPQPMDLRVGQRPPVEPPPEPTLLALQRPQRLHHHLFLAGLQ
QQRSVEPMRLSMDTPMPELQVGPQEQELRQLLHKDKSKRSAVASSVVKQKLAEVILKKQQ
AALERTVHPNSPGIPYRTLEPLETEGATRSMLSSFLPPVPSLPSDPPEHFPLRKTVSEPN
LKLRYKPKKSLERRKNPLLRKESAPPSLRRRPAETLGDSSPSSSSTPASGCSSPNDSEHG
PNPILGSEALLGQRLRLQETSVAPFALPTVSLLPAITLGLPAPARADSDRRTHPTLGPRG
PILGSPHTPLFLPHGLEPEAGGTLPSRLQPILLLDPSGSHAPLLTVPGLGPLPFHFAQSL

MTTERLSGSGLHWPLSRTRSEPLPPSATAPPPPGPMQPRLEQLKTHVQVIKRSAKPSEKP
RLRQIPSAEDLETDGGGPGQVVDDGLEHRELGHGQPEARGPAPLQQHPQVLLWEQQRLAG
RLPRGSTGDTVLLPLAQGGHRPLSRAQSSPAAPASLSAPEPASQARVLSSSETPARTLPF
TTGLIYDSVMLKHQCSCGDNSRHPEHAGRIQSIWSRLQERGLRSQCECLRGRKASLEELQ
SVHSERHVLLYGTNPLSRLKLDNGKLAGLLAQRMFVMLPCGGVGVDTDTIWNELHSSNAA
RWAAGSVTDLAFKVASRELKNGFAVVRPPGHHADHSTAMGFCFFNSVAIACRQLQQQSKA
SKILIVDWDVHHGNGTQQTFYQDPSVLYISLHRHDDGNFFPGSGAVDEVGAGSGEGFNVN
VAWAGGLDPPMGDPEYLAAFRIVVMPIAREFSPDLVLVSAGFDAAEGHPAPLGGYHVSAK
CFGYMTQQLMNLAGGAVVLALEGGHDLTAICDASEACVAALLGNRVDPLSEEGWKQKPNL
NAIRSLEAVIRVHSKYWGCMQRLASCPDSWVPRVPGADKEEVEAVTALASLSVGILAEDR
PSEQLVEEEEPMNL

>sp|Q8WUI4-7|HDAC7_HUMAN Isoform 7 of Histone deacetylase 7 OS=Homo
sapiens GN=HDAC7
MHSPGADGTQVSPGAHYCSPTGAGCPRPCADTPGPQPQPMDLRVGQRPPVEPPPEPTLLA
LQRPQRLHHHLFLAGLQQQRSVEPMRLSMDTPMPELQVGPQEQELRQLLHKDKSKRSAVA
SSVVKQKLAEVILKKQQAALERTVHPNSPGIPYRTLEPLETEGATRSMLSSFLPPVPSLP
SDPPEHFPLRKTVSEPNLKLRYKPKKSLERRKNPLLRKESAPPSLRRRPAETLGDSSPSS
SSTPASGCSSPNDSEHGPNPILGSEADSDRRTHPTLGPRGPILGSPHTPLFLPHGLEPEA
GGTLPSRLQPILLLDPSGSHAPLLTVPGLGPLPFHFAQSLMTTERLSGSGLHWPLSRTRS
EPLPPSATAPPPPGPMQPRLEQLKTHVQVIKRSAKPSEKPRLRQIPSAEDLETDGGGPGQ
VVDDGLEHRELGHGQPEARGPAPLQQHPQVLLWEQQRLAGRLPRGSTGDTVLLPLAQGGH
RPLSRAQSSPAAPASLSAPEPASQARVLSSSETPARTLPFTTGLIYDSVMLKHQCSCGDN
SRHPEHAGRIQSIWSRLQERGLRSQCECLRGRKASLEELQSVHSERHVLLYGTNPLSRLK
LDNGKLAGLLAQRMFVMLPCGGVGVDTDTIWNELHSSNAARWAAGSVTDLAFKVASRELK
NGFAVVRPPGHHADHSTAMGFCFFNSVAIACRQLQQQSKASKILIVDWDVHHGNGTQQTF
YQDPSVLYISLHRHDDGNFFPGSGAVDEVGAGSGEGFNVNVAWAGGLDPPMGDPEYLAAF
RIVVMPIAREFSPDLVLVSAGFDAAEGHPAPLGGYHVSAKCFGYMTQQLMNLAGGAVVLA
LEGGHDLTAICDASEACVAALLGNRVDPLSEEGWKQKPNLNAIRSLEAVIRVHSKYWGCM
QRLASCPDSWVPRVPGADKEEVEAVTALASLSVGILAEDRPSEQLVEEEEPMNL

>sp|Q8WUI4-8|HDAC7_HUMAN Isoform 8 of Histone deacetylase 7 OS=Homo
sapiens GN=HDAC7
MSDLRKRELGALFTSRGTGGVEWDGTQVSPGAHYCSPTGAGCPRPCADTPGPQPQPMDLR
VGQRPPVEPPPEPTLLALQRPQRLHHHLFLAGLQQQRSVEPMRLSMDTPMPELQVGPQEQ
ELRQLLHKDKSKRSAVASSVVKQKLAEVILKKQQAALERTVHPNSPGIPYRTLEPLETEG
ATRSMLSSFLPPVPSLPSDPPEHFPLRKTVSEPNLKLRYKPKKSLERRKNPLLRKESAPP
SLRRRPAETLGDSSPSSSSTPASGCSSPNDSEHGPNPILGSEALLGQRLRLQETSVAPFA
LPTVSLLPAITLGLPAPARADSDRRTHPTLGPRGPILGSPHTPLFLPHGLEPEAGGTLPS
RLQPILLLDPSGSHAPLLTVPGLGPLPFHFAQSLMTTERLSGSGLHWPLSRTRSEPLPPS
ATAPPPPGPMQPRLEQLKTHVQVIKRSAKPSEKPRLRQIPSAEDLETDGGGPGQVVDDGL
EHRELGHGQPEARGPAPLQQHPQVLLWEQQRLAGRLPRGSTGDTVLLPLAQGGHRPLSRA
QSSPAAPASLSAPEPASQARVLSSSETPARTLPFTTGLIYDSVMLKHQCSCGDNSRHPEH
AGRIQSIWSRLQERGLRSQCECLRGRKASLEELQSVHSERHVLLYGTNPLSRLKLDNGKL
AGLLAQRMFVMLPCGGVGVDTDTIWNELHSSNAARWAAGSVTDLAFKVASRELKNGFAVV
RPPGHHADHSTAMGFCFFNSVAIACRQLQQQSKASKILIVDWDVHHGNGTQQTFYQDPSV
LYISLHRHDDGNFFPGSGAVDEVGAGSGEGFNVNVAWAGGLDPPMGDPEYLAAFRIVVMP
IAREFSPDLVLVSAGFDAAEGHPAPLGGYHVSAKCFGYMTQQLMNLAGGAVVLALEGGHD
LTAICDASEACVAALLGNRVDPLSEEGWKQKPNLNAIRSLEAVIRVHMGALTLSQIPGHG
SSQQQAGGAFSRPGHPCRAAVVMVNTGAACSAWPPVQTPGCLECQGLTKKKWRQ

>sp|Q8WUI4-9|HDAC7_HUMAN Isoform 9 of Histone deacetylase 7 OS=Homo
sapiens GN=HDAC7
MLKHQCSCGDNSRHPEHAGRIQSIWSRLQERGLRSQCECLRGRKASLEELQSVHSERHVL
LYGTNPLSRLKLDNGKLAGLLAQRMFVMLPCGGVGVDTDTIWNELHSSNAARWAAGSVTD
LAFKVASRELKNGFAVVRPPGHHADHSTAMGFCFFNSVAIACRQLQQQSKASKILIVDWD
VHHGNGTQQTFYQDPSVLYISLHRHDDGNFFPGSGAVDEVGAGSGEGFNVNVAWAGGLDP

PMGDPEYLAAFRIVVMPIAREFSPDLVLVSAGFDAAEGHPAPLGGYHVSAKCFGYMTQQL
MNLAGGAVVLALEGGHDLTAICDASEACVAALLGNRVDPLSEEGWKQKPNLNAIRSLEAV
IRVHSKYWGCMQRLASCPDSWVPRVPGADKEEVEAVTALASLSVGILAEDRPSEQLVEEE
EPMNL

>sp|Q8WUI4-10|HDAC7_HUMAN Isoform 10 of Histone deacetylase 7 OS=Homo
sapiens GN=HDAC7
MTTERLSGSGLHWPLSRTRSEPLPPSATAPPPPGPMQPRLEQLKTHVQVIKRSAKPSEKP
RLRQIPSAEDLETDGGGPGQVVDDGLEHRELGHGQPEARGPAPLQQHPQVLLWEQQRLAG
RLPRGSTGDTVLLPLAQGGHRPLSRAQSSPAAPASLSAPEPASQARVLSSSETPARTLPF
TTGLIYDSVMLKHQCSCGDNSRHPEHAGRIQSIWSRLQERGLRSQCECLRGRKASLEELQ
SVHSERHVLLYGTNPLSRLKLDNGKLAGLLAQRMFVMLPCGGVGVDTDTIWNELHSSNAA
RWAAGSVTDLAFKVASRELKNGFAVVRPPGHHADHSTAMGFCFFNSVAIACRQLQQQSKA
SKILIVDWDVHHGNGTQQTFYQDPSVLYISLHRHDDGNFFPGSGAVDEVGAGSGEGFNVN
VAWAGGLDPPMGDPEYLAAFRIVVMPIAREFSPDLVLVSAGFDAAEGHPAPLGGYHVSAK
CFGYMTQQLMNLAGGAVVLALEGGHDLTAICDASEACVAALLGNRVDPLSEEGWKQKPNL
NAIRSLEAVIRVHSKYWGCMQRLASCPDSWVPRVPGADKEEVEAVTALASLSVGILAEDR
PSEQLVEEEEPMNL

HDAC8

>sp|Q9BY41|HDAC8_HUMAN Histone deacetylase 8 OS=Homo sapiens GN=HDAC8
PE=1 SV=2
MEEPEEPADSGQSLVPVYIYSPEYVSMCDSLAKIPKRASMVHSLIEAYALHKQMRIVKPK
VASMEEMATFHTDAYLQHLQKVSQEGDDDHPDSIEYGLGYDCPATEGIFDYAAAIGGATI
TAAQCLIDGMCKVAINWSGGWHHAKKDEASGFCYLNDAVLGILRLRRKFERILYVDLDLH
HGDGVEDAFSFTSKVMTVSLHKFSPGFFPGTGDVSDVGLGKGRYYSVNVPIQDGIQDEKY
YQICESVLKEVYQAFNPKAVVLQLGADTIAGDPMCSFNMTPVGIGKCLKYILQWQLATLI
LGGGGYNLANTARCWTYLTGVILGKTLSSEIPDHEFFTAYGPDYVLEITPSCRPDRNEPH
RIQQILNYIKGNLKHVV

>sp|Q9BY41-2|HDAC8_HUMAN Isoform 2 of Histone deacetylase 8 OS=Homo
sapiens GN=HDAC8
MEEPEEPADSGQSLVPVYIYSPEYVSMCDSLAKIPKRASMVHSLIEAYALHKQMRIVKPK
VASMEEMATFHTDAYLQHLQKVSQEGDDDHPDSIEYGLGYDCPATEGIFDYAAAIGGATI
TAAQCLIDGMCKVAINWSGGWHHAKKDEASGFCYLNDAVLGILRLRRKFERILYVDLDLH
HGDGVEDAFSFTSKVMTVSLHKFSPGFFPGTGDVSDVGLGKGRYYSVNVPIQDGIQDEKY
YQICESVRTSCPKSRPVEAAAAACLPHLHSLV

>sp|Q9BY41-3|HDAC8_HUMAN Isoform 3 of Histone deacetylase 8 OS=Homo
sapiens GN=HDAC8
MEEPEEPADSGQSLVPVYIYSPEYVSMCDSLAKIPKRASMVHSLIEAYALHKQMRIVKPK
VASMEEMATFHTDAYLQHLQKVSQEGDDDHPDSIEYGLGYDCPATEGIFDYAAAIGGATI
TAAQCLIDGMCKVAINWSGGWHHAKKRDVCVCGTLQGILKKSK

>sp|Q9BY41-4|HDAC8_HUMAN Isoform 4 of Histone deacetylase 8 OS=Homo
sapiens GN=HDAC8
MEEPEEPADSGQSLVPVYIYSPEYVSMCDSLAKIPKRASMVHSLIEAYALHKQMRDEASG
FCYLNDAVLGILRLRRKFERILYVDLDLHHGDGVEDAFSFTSKVMTVSLHKFSPGFFPGT
GDVSDVGLGKGRYYSVNVPIQDGIQDEKYYQICESVLKEVYQAFNPKAVVLQLGADTIAG
DPMCSFNMTPVGIGKCLKYILQWQLATLILGGGGYNLANTARCWTYLTGVILGKTLSSEI
PDHEFFTAYGPDYVLEITPSCRPDRNEPHRIQQILNYIKGNLKHVV

>sp|Q9BY41-5|HDAC8_HUMAN Isoform 5 of Histone deacetylase 8 OS=Homo
sapiens GN=HDAC8
MEEPEEPADSGQSLVPVYIYSPEYVSMCDSLAKIPKRASMVHSLIEAYALHKQMRIVKPK
VASMEEMATFHTDAYLQHLQKVSQEGDDDHPDSIEYGLGYDCPATEGIFDYAAAIGGATI
TAAQCLIDGMCKVAINWSGGWHHAKKDEASGFCYLNDAVLGILRLRRKFERILYVDLDLH

HGDGVEDAFSFTSKVMTVSLHKFSPGFFPGTGDVSDVGLGKGRYYSVNVPIQDGIQDEKY
YQICERYEPPAPNPGL

HDAC9

>sp|Q9UKV0|HDAC9_HUMAN Histone deacetylase 9 OS=Homo sapiens GN=HDAC9
PE=1 SV=2
MHSMISSVDVKSEVPVGLEPISPLDLRTDLRMMMPVVDPVVREKQLQQELLLIQQQQQIQ
KQLLIAEFQKQHENLTRQHQAQLQEHIKELLAIKQQQELLEKEQKLEQQRQEQEVERHRR
EQQLPPLRGKDRGRERAVASTEVKQKLQEFLLSKSATKDTPTNGKNHSVSRHPKLWYTAA
HHTSLDQSSPPLSGTSPSYKYTLPGAQDAKDDFPLRKTASEPNLKVRSRLKQKVAERRSS
PLLRRKDGNVVTSFKKRMFEVTESSVSSSSPGSGPSSPNNGPTGSVTENETSVLPPTPHA
EQMVSQQRILIHEDSMNLLSLYTSPSLPNITLGLPAVPSQLNASNSLKEKQKCETQTLRQ
GVPLPGQYGGSIPASSSHPHVTLEGKPPNSSHQALLQHLLLKEQMRQQKLLVAGGVPLHP
QSPLATKERISPGIRGTHKLPRHRPLNRTQSAPLPQSTLAQLVIQQQHQQFLEKQKQYQQ
QIHMNKLLSKSIEQLKQPGSHLEEAEEELQGDQAMQEDRAPSSGNSTRSDSSACVDDTLG
QVGAVKVKEEPVDSDEDAQIQEMESGEQAAFMQQPFLEPTHTRALSVRQAPLAAVGMDGL
EKHRLVSRTHSSPAASVLPHPAMDRPLQPGSATGIAYDPLMLKHQCVCGNSTTHPEHAGR
IQSIWSRLQETGLLNKCERIQGRKASLEEIQLVHSEHHSLLYGTNPLDGQKLDPRILLGD
DSQKFFSSLPCGGLGVDSDTIWNELHSSGAARMAVGCVIELASKVASGELKNGFAVVRPP
GHHAEESTAMGFCFFNSVAITAKYLRDQLNISKILIVDLDVHHGNGTQQAFYADPSILYI
SLHRYDEGNFFPGSGAPNEVGTGLGEGYNINIAWTGGLDPPMGDVEYLEAFRTIVKPVAK
EFDPDMVLVSAGFDALEGHTPPLGGYKVTAKCFGHLTKQLMTLADGRVVLALEGGHDLTA
ICDASEACVNALLGNELEPLAEDILHQSPNMNAVISLQKIIEIQSMSLKFS

>sp|Q9UKV0-2|HDAC9_HUMAN Isoform 2 of Histone deacetylase 9 OS=Homo
sapiens GN=HDAC9
MHSMISSVDVKSEVPVGLEPISPLDLRTDLRMMMPVVDPVVREKQLQQELLLIQQQQQIQ
KQLLIAEFQKQHENLTRQHQAQLQEHIKELLAIKQQQELLEKEQKLEQQRQEQEVERHRR
EQQLPPLRGKDRGRERAVASTEVKQKLQEFLLSKSATKDTPTNGKNHSVSRHPKLWYTAA
HHTSLDQSSPPLSGTSPSYKYTLPGAQDAKDDFPLRKTASEPNLKVRSRLKQKVAERRSS
PLLRRKDGNVVTSFKKRMFEVTESSVSSSSPGSGPSSPNNGPTGSVTENETSVLPPTPHA
EQMVSQQRILIHEDSMNLLSLYTSPSLPNITLGLPAVPSQLNASNSLKEKQKCETQTLRQ
GVPLPGQYGGSIPASSSHPHVTLEGKPPNSSHQALLQHLLLKEQMRQQKLLVAGGVPLHP
QSPLATKERISPGIRGTHKLPRHRPLNRTQSAPLPQSTLAQLVIQQQHQQFLEKQKQYQQ
QIHMNKPFLEPTHTRALSVRQAPLAAVGMDGLEKHRLVSRTHSSPAASVLPHPAMDRPLQ
PGSATGIAYDPLMLKHQCVCGNSTTHPEHAGRIQSIWSRLQETGLLNKCERIQGRKASLE
EIQLVHSEHHSLLYGTNPLDGQKLDPRILLGDDSQKFFSSLPCGGLGVDSDTIWNELHSS
GAARMAVGCVIELASKVASGELKNGFAVVRPPGHHAEESTAMGFCFFNSVAITAKYLRDQ
LNISKILIVDLDVHHGNGTQQAFYADPSILYISLHRYDEGNFFPGSGAPNEVGTGLGEGY
NINIAWTGGLDPPMGDVEYLEAFRTIVKPVAKEFDPDMVLVSAGFDALEGHTPPLGGYKV
TAKCFGHLTKQLMTLADGRVVLALEGGHDLTAICDASEACVNALLGNELEPLAEDILHQS
PNMNAVISLQKIIEIQSMSLKFS

>sp|Q9UKV0-3|HDAC9_HUMAN Isoform 3 of Histone deacetylase 9 OS=Homo
sapiens GN=HDAC9
MHSMISSVDVKSEVPVGLEPISPLDLRTDLRMMMPVVDPVVREKQLQQELLLIQQQQQIQ
KQLLIAEFQKQHENLTRQHQAQLQEHIKELLAIKQQQELLEKEQKLEQQRQEQEVERHRR
EQQLPPLRGKDRGRERAVASTEVKQKLQEFLLSKSATKDTPTNGKNHSVSRHPKLWYTAA
HHTSLDQSSPPLSGTSPSYKYTLPGAQDAKDDFPLRKTASEPNLKVRSRLKQKVAERRSS
PLLRRKDGNVVTSFKKRMFEVTESSVSSSSPGSGPSSPNNGPTGSVTENETSVLPPTPHA
EQMVSQQRILIHEDSMNLLSLYTSPSLPNITLGLPAVPSQLNASNSLKEKQKCETQTLRQ
GVPLPGQYGGSIPASSSHPHVTLEGKPPNSSHQALLQHLLLKEQMRQQKLLVAGGVPLHP
QSPLATKERISPGIRGTHKLPRHRPLNRTQSAPLPQSTLAQLVIQQQHQQFLEKQKQYQQ
QIHMNKLLSKSIEQLKQPGSHLEEAEEELQGDQAMQEDRAPSSGNSTRSDSSACVDDTLG
QVGAVKVKEEPVDSDEDAQIQEMESGEQAAFMQQVIGKDLAPGFVIKVII

>sp|Q9UKV0-4|HDAC9_HUMAN Isoform 4 of Histone deacetylase 9 OS=Homo sapiens GN=HDAC9
MHSMISSVDVKSEVPVGLEPISPLDLRTDLRMMMPVVDPVVREKQLQQELLLIQQQQQIQ
KQLLIAEFQKQHENLTRQHQAQLQEHIKELLAIKQQQELLEKEQKLEQQRQEQEVERHRR
EQQLPPLRGKDRGRERAVASTEVKQKLQEFLLSKSATKDTPTNGKNHSVSRHPKLWYTAA
HHTSLDQSSPPLSGTSPSYKYTLPGAQDAKDDFPLRKTASEPNLKVRSRLKQKVAERRSS
PLLRRKDGNVVTSFKKRMFEVTESSVSSSSPGSGPSSPNNGPTGSVTENETSVLPPTPHA
EQMVSQQRILIHEDSMNLLSLYTSPSLPNITLGLPAVPSQLNASNSLKEKQKCETQTLRQ
GVPLPGQYGGSIPASSSHPHVTLEGKPPNSSHQALLQHLLLKEQMRQQKLLVAGGVPLHP
QSPLATKERISPGIRGTHKLPRHRPLNRTQSAPLPQSTLAQLVIQQQHQQFLEKQKQYQQ
QIHMNKLLSKSIEQLKQPGSHLEEAEEELQGDQAMQEDRAPSSGNSTRSDSSACVDDTLG
QVGAVKVKEEPVDSDEDAQIQEMESGEQAAFMQQPFLEPTHTRALSVRQAPLAAVGMDGL
EKHRLVSRTHSSPAASVLPHPAMDRPLQPGSATGIAYDPLMLKHQCVCGNSTTHPEHAGR
IQSIWSRLQETGLLNKCERIQGRKASLEEIQLVHSEHHSLLYGTNPLDGQKLDPRILLGD
DSQKFFSSLPCGGLGVDSDTIWNELHSSGAARMAVGCVIELASKVASGELKNGFAVVRPP
GHHAEESTAMGFCFFNSVAITAKYLRDQLNISKILIVDLDVHHGNGTQQAFYADPSILYI
SLHRYDEGNFFPGSGAPNEVRFISLEPHFYLYLSGNCIA

>sp|Q9UKV0-5|HDAC9_HUMAN Isoform 5 of Histone deacetylase 9 OS=Homo sapiens GN=HDAC9
MHSMISSVDVKSEVPVGLEPISPLDLRTDLRMMMPVVDPVVREKQLQQELLLIQQQQQIQ
KQLLIAEFQKQHENLTRQHQAQLQEHIKELLAIKQQQELLEKEQKLEQQRQEQEVERHRR
EQQLPPLRGKDRGRERAVASTEVKQKLQEFLLSKSATKDTPTNGKNHSVSRHPKLWYTAA
HHTSLDQSSPPLSGTSPSYKYTLPGAQDAKDDFPLRKTASEPNLKVRSRLKQKVAERRSS
PLLRRKDGNVVTSFKKRMFEVTESSVSSSSPGSGPSSPNNGPTGSVTENETSVLPPTPHA
EQMVSQQRILIHEDSMNLLSLYTSPSLPNITLGLPAVPSQLNASNSLKEKQKCETQTLRQ
GVPLPGQYGGSIPASSSHPHVTLEGKPPNSSHQALLQHLLLKEQMRQQKLLVAGGVPLHP
QSPLATKERISPGIRGTHKLPRHRPLNRTQSAPLPQSTLAQLVIQQQHQQFLEKQKQYQQ
QIHMNKLLSKSIEQLKQPGSHLEEAEEELQGDQAMQEDRAPSSGNSTRSDSSACVDDTLG
QVGAVKVKEEPVDSDEDAQIQEMESGEQAAFMQQPFLEPTHTRALSVRQAPLAAVGMDGL
EKHRLVSRTHSSPAASVLPHPAMDRPLQPGSATGIAYDPLMLKHQCVCGNSTTHPEHAGR
IQSIWSRLQETGLLNKCERIQGRKASLEEIQLVHSEHHSLLYGTNPLDGQKLDPRILLGD
DSQKFFSSLPCGGLGVDSDTIWNELHSSGAARMAVGCVIELASKVASGELKNGFAVVRPP
GHHAEESTAMGFCFFNSVAITAKYLRDQLNISKILIVDLDVHHGNGTQQAFYADPSILYI
SLHRYDEGNFFPGSGAPNEVGTGLGEGYNINIAWTGGLDPPMGDVEYLEAFRTIVKPVAK
EFDPDMVLVSAGFDALEGHTPPLGGYKVTAKCFGHLTKQLMTLADGRVVLALEGGHDLTA
ICDASEACVNALLGNELEPLAEDILHQSPNMNAVISLQKIIEIQSKYWKSVRMVAVPRGC
ALAGAQLQEETETVSALASLTVDVEQPFAQEDSRTAGEPMEEEPAL

>sp|Q9UKV0-6|HDAC9_HUMAN Isoform 6 of Histone deacetylase 9 OS=Homo sapiens GN=HDAC9
MHSMISSVDVKSEVPVGLEPISPLDLRTDLRMMMPVVDPVVREKQLQQELLLIQQQQQIQ
KQLLIAEFQKQHENLTRQHQAQLQEHIKLQQELLAIKQQQELLEKEQKLEQQRQEQEVER
HRREQQLPPLRGKDRGRERAVASTEVKQKLQEFLLSKSATKDTPTNGKNHSVSRHPKLWY
TAAHHTSLDQSSPPLSGTSPSYKYTLPGAQDAKDDFPLRKTESSVSSSSPGSGPSSPNNG
PTGSVTENETSVLPPTPHAEQMVSQQRILIHEDSMNLLSLYTSPSLPNITLGLPAVPSQL
NASNSLKEKQKCETQTLRQGVPLPGQYGGSIPASSSHPHVTLEGKPPNSSHQALLQHLLL
KEQMRQQKLLVAGGVPLHPQSPLATKERISPGIRGTHKLPRHRPLNRTQSAPLPQSTLAQ
LVIQQQHQQFLEKQKQYQQQIHMNKLLSKSIEQLKQPGSHLEEAEEELQGDQAMQEDRAP
SSGNSTRSDSSACVDDTLGQVGAVKVKEEPVDSDEDAQIQEMESGEQAAFMQQPFLEPTH
TRALSVRQAPLAAVGMDGLEKHRLVSRTHSSPAASVLPHPAMDRPLQPGSATGIAYDPLM
LKHQCVCGNSTTHPEHAGRIQSIWSRLQETGLLNKCERIQGRKASLEEIQLVHSEHHSLL
YGTNPLDGQKLDPRILLGDDSQKFFSSLPCGGLGVDSDTIWNELHSSGAARMAVGCVIEL
ASKVASGELKNGFAVVRPPGHHAEESTAMGFCFFNSVAITAKYLRDQLNISKILIVDLDV
HHGNGTQQAFYADPSILYISLHRYDEGNFFPGSGAPNEVGTGLGEGYNINIAWTGGLDPP
MGDVEYLEAFRTIVKPVAKEFDPDMVLVSAGFDALEGHTPPLGGYKVTAKCFGHLTKQLM
TLADGRVVLALEGGHDLTAICDASEACVNALLGNELEPLAEDILHQSPNMNAVISLQKII

EIQSKYWKSVRMVAVPRGCALAGAQLQEETETVSALASLTVDVEQPFAQEDSRTAGEPME
EEPAL

>sp|Q9UKV0-7|HDAC9_HUMAN Isoform 7 of Histone deacetylase 9 OS=Homo sapiens GN=HDAC9
MHSMISSVDVKSEVPVGLEPISPLDLRTDLRMMMPVVDPVVREKQLQQELLLIQQQQQIQ
KQLLIAEFQKQHENLTRQHQAQLQEHIKLQQELLAIKQQQELLEKEQKLEQQRQEQEVER
HRREQQLPPLRGKDRGRERAVASTEVKQKLQEFLLSKSATKDTPTNGKNHSVSRHPKLWY
TAAHHTSLDQSSPPLSGTSPSYKYTLPGAQDAKDDFPLRKTASEPNLKVRSRLKQKVAER
RSSPLLRRKDGNVVTSFKKRMFEVTESSVSSSSPGSGPSSPNNGPTGSVTENETSVLPPT
PHAEQMVSQQRILIHEDSMNLLSLYTSPSLPNITLGLPAVPSQLNASNSLKEKQKCETQT
LRQGVPLPGQYGGSIPASSSHPHVTLEGKPPNSSHQALLQHLLLKEQMRQQKLLVAGGVP
LHPQSPLATKERISPGIRGTHKLPRHRPLNRTQSAPLPQSTLAQLVIQQQHQQFLEKQKQ
YQQQIHMNKLLSKSIEQLKQPGSHLEEAEEELQGDQAMQEDRAPSSGNSTRSDSSACVDD
TLGQVGAVKVKEEPVDSDEDAQIQEMESGEQAAFMQQPFLEPTHTRALSVRQAPLAAVGM
DGLEKHRLVSRTHSSPAASVLPHPAMDRPLQPGSATGIAYDPLMLKHQCVCGNSTTHPEH
AGRIQSIWSRLQETGLLNKCERIQGRKASLEEIQLVHSEHHSLLYGTNPLDGQKLDPRIL
LGDDSQKFFSSLPCGGLGVDSDTIWNELHSSGAARMAVGCVIELASKVASGELKNGFAVV
RPPGHHAEESTAMGFCFFNSVAITAKYLRDQLNISKILIVDLDVHHGNGTQQAFYADPSI
LYISLHRYDEGNFFPGSGAPNEVGTGLGEGYNINIAWTGGLDPPMGDVEYLEAFRTIVKP
VAKEFDPDMVLVSAGFDALEGHTPPLGGYKVTAKCFGHLTKQLMTLADGRVVLALEGGHD
LTAICDASEACVNALLGNELEPLAEDILHQSPNMNAVISLQKIIEIQSKYWKSVRMVAVP
RGCALAGAQLQEETETVSALASLTVDVEQPFAQEDSRTAGEPMEEEPAL

>sp|Q9UKV0-8|HDAC9_HUMAN Isoform 8 of Histone deacetylase 9 OS=Homo sapiens GN=HDAC9
MMSSPAQPDLMWNLVPWVLFCGCCRIFPDGVAGREQLLAQQRMHSMISSVDVKSEVPVGL
EPISPLDLRTDLRMMMPVVDPVVREKQLQQELLLIQQQQQIQKQLLIAEFQKQHENLTRQ
HQAQLQEHIKELLAIKQQQELLEKEQKLEQQRQEQEVERHRREQQLPPLRGKDRGRERAV
ASTEVKQKLQEFLLSKSATKDTPTNGKNHSVSRHPKLWYTAAHHTSLDQSSPPLSGTSPS
YKYTLPGAQDAKDDFPLRKTESSVSSSSPGSGPSSPNNGPTGSVTENETSVLPPTPHAEQ
MVSQQRILIHEDSMNLLSLYTSPSLPNITLGLPAVPSQLNASNSLKEKQKCETQTLRQGV
PLPGQYGGSIPASSSHPHVTLEGKPPNSSHQALLQHLLLKEQMRQQKLLVAGGVPLHPQS
PLATKERISPGIRGTHKLPRHRPLNRTQSAPLPQSTLAQLVIQQQHQQFLEKQKQYQQQI
HMNKLLSKSIEQLKQPGSHLEEAEEELQGDQAMQEDRAPSSGNSTRSDSSACVDDTLGQV
GAVKVKEEPVDSDEDAQIQEMESGEQAAFMQQVIGKDLAPGFVIKVII

HDAC10

>sp|Q969S8|HDA10_HUMAN Histone deacetylase 10 OS=Homo sapiens GN=HDAC10 PE=1 SV=1
MGTALVYHEDMTATRLLWDDPECEIERPERLTAALDRLRQRGLEQRCLRLSAREASEEEL
GLVHSPEYVSLVRETQVLGKEELQALSGQFDAIYFHPSTFHCARLAAGAGLQLVDAVLTG
AVQNGLALVRPPGHHGQRAAANGFCVFNNVAIAAAHAKQKHGLHRILVVDWDVHHGQGIQ
YLFEDDPSVLYFSWHRYEHGRFWPFLRESDADAVGRGQGLGFTVNLPWNQVGMGNADYVA
AFLHLLLPLAFEFDPELVLVSAGFDSAIGDPEGQMQATPECFAHLTQLLQVLAGGRVCAV
LEGGYHLESLAESVCMTVQTLLGDPAPPLSGPMAPCQSALESIQSARAAQAPHWKSLQQQ
DVTAVPMSPSSHSPEGRPPPLLPGGPVCKAAASAPSSLLDQPCLCPAPSVRTAVALTTPD
ITLVLPPDVIQQEASALREETEAWARPHESLAREEALTALGKLLYLLDGMLDGQVNSGIA
ATPASAAAATLDVAVRRGLSHGAQRLLCVALGQLDRPPDLAHDGRSLWLNIRGKEAAALS
MFHVSTPLPVMTGGFLSCILGLVLPLAYGFQPDLVLVALGPGHGLQGPHAALLAAMLRGL
AGGRVLALLEENSTPQLAGILARVLNGEAPPSLGPSSVASPEDVQALMYLRGQLEPQWKM
LQCHPHLVA

>sp|Q969S8-2|HDA10_HUMAN Isoform 2 of Histone deacetylase 10 OS=Homo sapiens GN=HDAC10
MGTALVYHEDMTATRLLWDDPECEIERPERLTAALDRLRQRGLEQRCLRLSAREASEEEL
GLVHSPEYVSLVRETQVLGKEELQALSGQFDAIYFHPSTFHCARLAAGAGLQLVDAVLTG

AVQNGLALVRPPGHHGQRAAANGFCVFNNVAIAAAHAKQKHGLHRILVVDWDVHHGQGIQ
YLFEDDPSVLYFSWHRYEHGRFWPFLRESDADAVGRGQGLGFTVNLPWNQVGMGNADYVA
AFLHLLLPLAFEGQMQATPECFAHLTQLLQVLAGGRVCAVLEGGYHLESLAESVCMTVQT
LLGDPAPPLSGPMAPCQSALESIQSARAAQAPHWKSLQQQDVTAVPMSPSSHSPEGRPPP
LLPGGPVCKAAASAPSSLLDQPCLCPAPSVRTAVALTTPDITLVLPPDVIQQEASALREE
TEAWARPHESLAREEALTALGKLLYLLDGMLDGQVNSGIAATPASAAAATLDVAVRRGLS
HGAQRLLCVALGQLDRPPDLAHDGRSLWLNIRGKEAAALSMFHVSTPLPVMTGGFLSCIL
GLVLPLAYGFQPDLVLVALGPGHGLQGPHAALLAAMLRGLAGGRVLALLEENSTPQLAGI
LARVLNGEAPPSLGPSSVASPEDVQALMYLRGQLEPQWKMLQCHPHLVA

>sp|Q969S8-4|HDA10_HUMAN Isoform 4 of Histone deacetylase 10 OS=Homo sapiens GN=HDAC10
MGTALVYHEDMTATRLLWDDPECEIERPERLTAALDRLRQRGLEQRCLRLSAREASEEEL
GLVHSPEYVSLVRETQVLGKEELQALSGQFDAIYFHPSTFHCARLAAGAGLQLVDAVLTG
AVQNGLALVRPPGHHGQRAAANGFCVFNNVAIAAAHAKQKHGLHRILVVDWDVHHGQGIQ
YLFEDDPSVLYFSWHRYEHGRFWPFLRESDADAVGRGQGLGFTVNLPWNQVGMGNADYVA
AFLHLLLPLAFEFDPELVLVSAGFDSAIGDPEGQMQATPECFAHLTQLLQVLAGGRVCAV
LEGGYHLESLAESVCMTVQTLLGDPAPPLSGPMAPCQSALESIQSARAAQAPHWKSLQQQ
DVTAVPMSPSSHSPEGRPPPLLPGGPVCKAAASAPSSLLDQPCLCPAPSVRTAVALTTPD
ITLVLPPDVIQQEASALREETEAWARPHESLAREEALTALGKLLYLLDGMLDGQVNSGIA
ATPASAAAATLDVAVRRGLSHGAQRLLCVALGQLDRPPDLAHDGRSLWLNIRGKEAAALS
MFHVSTPLPVMTGGFLSCILGLVLPLAYGFQPDLVLVALGPGHGLQGPHAALLAAMLRGL
AGGRVLALLEEVSWAGWRCCGVGRGKGPVTASVFAPGPELHTPASRDPGPGAEWRGTS

>sp|Q969S8-5|HDA10_HUMAN Isoform 5 of Histone deacetylase 10 OS=Homo sapiens GN=HDAC10
MGTALVYHEDMTATRLLWDDPECEIERPERLTAALDRLRQRGLEQRCLRLSAREASEEEL
GLVHSPEYVSLVRETQVLGKEELQALSGQFDAIYFHPSTFHCARLAAGAGLQLVDAVLTG
AVQNGLALVRPPGHHGQRAAANGFCVFNNVAIAAAHAKQKHGLHRILVVDWDVHHGQGIQ
YLFEDDPSVLYFSWHRYEHGRFWPFLRESDADAVGRGQGLGFTVNLPWNQVGMGNADYVA
AFLHLLLPLAFEGGYHLESLAESVCMTVQTLLGDPAPPLSGPMAPCQSALESIQSARAAQ
APHWKSLQQQDVTAVPMSPSSHSPEGRPPPLLPGGPVCKAAASAPSSLLDQPCLCPAPSV
RTAVALTTPDITLVLPPDVIQQEASALREETEAWAR

HDAC11

>sp|Q96DB2|HDA11_HUMAN Histone deacetylase 11 OS=Homo sapiens GN=HDAC11 PE=1 SV=1
MLHTTQLYQHVPETRWPIVYSPRYNITFMGLEKLHPFDAGKWGKVINFLKEEKLLSDSML
VEAREASEEDLLVVHTRRYLNELKWSFAVATITEIPPVIFLPNFLVQRKVLRPLRTQTGG
TIMAGKLAVERGWAINVGGGFHHCSSDRGGGFCAYADITLAIKFLFERVEGISRATIIDL
DAHQGNGHERDFMDDKRVYIMDVYNRHIYPGDRFAKQAIRRKVELEWGTEDDEYLDKVER
NIKKSLQEHLPDVVVYNAGTDILEGDRLGGLSISPAGIVKRDELVFRMVRGRRVPILMVT
SGGYQKRTARIIADSILNLFGLGLIGPESPSVSAQNSDTPLLPPAVP

>sp|Q96DB2-2|HDA11_HUMAN Isoform 2 of Histone deacetylase 11 OS=Homo sapiens GN=HDAC11
MGLEKLHPFDAGKWGKVINFLKEEKLLSDSMLVEAREASEEDLLVVHTRRYLNELKRKVL
RPLRTQTGGTIMAGKLAVERGWAINVGGGFHHCSSDRGGGFCAYADITLAIKFLFERVEG
ISRATIIDLDAHQGNGHERDFMDDKRVYIMDVYNRHIYPGDRFAKQAIRRKVELEWGTED
DEYLDKVERNIKKSLQEHLPDVVVYNAGTDILEGDRLGGLSISPAGIVKRDELVFRMVRG
RRVPILMVTSGGYQKRTARIIADSILNLFGLGLIGPESPSVSAQNSDTPLLPPAVP

References

[1] O. Cairó, External measures of cognition, Front. Hum. Neurosci. 5 (2011) 108. doi:10.3389/fnhum.2011.00108.

[2] S. Herculano-Houzel, The remarkable, yet not extraordinary, human brain as a scaled-up primate brain and its associated cost, Proc. Natl. Acad. Sci. U. S. A. 109 Suppl 1 (2012) 10661–10668. doi:10.1073/pnas.1201895109.

[3] J.T. Pedersen, N.H.H. Heegaard, Analysis of protein aggregation in neurodegenerative disease, Anal. Chem. 85 (2013) 4215–4227. doi:10.1021/ac400023c.

[4] F. Chiti, C.M. Dobson, Protein misfolding, functional amyloid, and human disease, Annu. Rev. Biochem. 75 (2006) 333–366. doi:10.1146/annurev.biochem.75.101304.123901.

[5] P. Westermark, M.D. Benson, J.N. Buxbaum, A.S. Cohen, B. Frangione, S.-I. Ikeda, et al., Amyloid: toward terminology clarification. Report from the Nomenclature Committee of the International Society of Amyloidosis, Amyloid Int. J. Exp. Clin. Investig. Off. J. Int. Soc. Amyloidosis. 12 (2005) 1–4. doi:10.1080/13506120500032196.

[6] Y.S. Eisele, T. Bolmont, M. Heikenwalder, F. Langer, L.H. Jacobson, Z.-X. Yan, et al., Induction of cerebral beta-amyloidosis: intracerebral versus systemic Abeta inoculation, Proc. Natl. Acad. Sci. U. S. A. 106 (2009) 12926–12931. doi:10.1073/pnas.0903200106.

[7] K. Lundmark, G.T. Westermark, A. Olsén, P. Westermark, Protein fibrils in nature can enhance amyloid protein A amyloidosis in mice: Cross-seeding as a disease mechanism, Proc. Natl. Acad. Sci. U. S. A. 102 (2005) 6098–6102. doi:10.1073/pnas.0501814102.

[8] M. Tanaka, Y. Komi, Layers of structure and function in protein aggregation, Nat. Chem. Biol. 11 (2015) 373–377. doi:10.1038/nchembio.1818.

[9] M.I. Smith, J.S. Sharp, C.J. Roberts, Insulin Fibril Nucleation: The Role of Prefibrillar Aggregates, Biophys. J. 95 (2008) 3400–3406. doi:10.1529/biophysj.108.131482.

[10] L. Li, T.A. Darden, L. Bartolotti, D. Kominos, L.G. Pedersen, An atomic model for the pleated beta-sheet structure of Abeta amyloid protofilaments, Biophys. J. 76 (1999) 2871–2878. doi:10.1016/S0006-3495(99)77442-4.

[11] C. Haass, D.J. Selkoe, Soluble protein oligomers in neurodegeneration: lessons from the Alzheimer's amyloid beta-peptide, Nat. Rev. Mol. Cell Biol. 8 (2007) 101–112. doi:10.1038/nrm2101.

[12] A.T. Alexandrescu, Amyloid accomplices and enforcers, Protein Sci. Publ. Protein Soc. 14 (2005) 1–12. doi:10.1110/ps.04887005.

[13] Alzheimer's Association, 2015 Alzheimer's disease facts and figures, Alzheimers Dement. J. Alzheimers Assoc. 11 (2015) 332–384.

[14] J.C. Morris, The Clinical Dementia Rating (CDR): current version and scoring rules, Neurology. 43 (1993) 2412–2414.

[15] B.T. Hyman, C.H. Phelps, T.G. Beach, E.H. Bigio, N.J. Cairns, M.C. Carrillo, et al., National Institute on Aging-Alzheimer's Association guidelines for the neuropathologic assessment of Alzheimer's disease, Alzheimers Dement. J. Alzheimers Assoc. 8 (2012) 1–13. doi:10.1016/j.jalz.2011.10.007.

[16] D.J. Selkoe, Alzheimer's disease: genes, proteins, and therapy, Physiol. Rev. 81 (2001) 741–766.

[17] Z. Yang, A Dominant Role for FE65 (APBB1) in Nuclear Signaling, J. Biol. Chem. 281 (2006) 4207–4214. doi:10.1074/jbc.M508445200.
[18] R. Roncarati, N. Sestan, M.H. Scheinfeld, B.E. Berechid, P.A. Lopez, O. Meucci, et al., The gamma-secretase-generated intracellular domain of beta-amyloid precursor protein binds Numb and inhibits Notch signaling, Proc. Natl. Acad. Sci. 99 (2002) 7102–7107. doi:10.1073/pnas.102192599.
[19] M.E. Fortini, Gamma-secretase-mediated proteolysis in cell-surface-receptor signalling, Nat. Rev. Mol. Cell Biol. 3 (2002) 673–684. doi:10.1038/nrm910.
[20] S. Bray, H. Musisi, M. Bienz, Bre1 is required for Notch signaling and histone modification, Dev. Cell. 8 (2005) 279–286. doi:10.1016/j.devcel.2004.11.020.
[21] D. Edbauer, E. Winkler, J.T. Regula, B. Pesold, H. Steiner, C. Haass, Reconstitution of gamma-secretase activity, Nat. Cell Biol. 5 (2003) 486–488. doi:10.1038/ncb960.
[22] H. Oakley, S.L. Cole, S. Logan, E. Maus, P. Shao, J. Craft, et al., Intraneuronal beta-amyloid aggregates, neurodegeneration, and neuron loss in transgenic mice with five familial Alzheimer's disease mutations: potential factors in amyloid plaque formation, J. Neurosci. Off. J. Soc. Neurosci. 26 (2006) 10129–10140. doi:10.1523/JNEUROSCI.1202-06.2006.
[23] N. Oikawa, N. Kimura, K. Yanagisawa, Alzheimer-type tau pathology in advanced aged nonhuman primate brains harboring substantial amyloid deposition, Brain Res. 1315 (2010) 137–149. doi:10.1016/j.brainres.2009.12.005.
[24] L. Forny-Germano, N.M. Lyra e Silva, A.F. Batista, J. Brito-Moreira, M. Gralle, S.E. Boehnke, et al., Alzheimer's disease-like pathology induced by amyloid-β oligomers in nonhuman primates, J. Neurosci. Off. J. Soc. Neurosci. 34 (2014) 13629–13643. doi:10.1523/JNEUROSCI.1353-14.2014.
[25] C.A. Lemere, Developing novel immunogens for a safe and effective Alzheimer's disease vaccine, Prog. Brain Res. 175 (2009) 83–93. doi:10.1016/S0079-6123(09)17506-4.
[26] F. Bard, C. Cannon, R. Barbour, R.L. Burke, D. Games, H. Grajeda, et al., Peripherally administered antibodies against amyloid beta-peptide enter the central nervous system and reduce pathology in a mouse model of Alzheimer disease, Nat. Med. 6 (2000) 916–919. doi:10.1038/78682.
[27] J. McLaurin, M.E. Kierstead, M.E. Brown, C.A. Hawkes, M.H.L. Lambermon, A.L. Phinney, et al., Cyclohexanehexol inhibitors of Abeta aggregation prevent and reverse Alzheimer phenotype in a mouse model, Nat. Med. 12 (2006) 801–808. doi:10.1038/nm1423.
[28] P.S. Aisen, S. Gauthier, B. Vellas, R. Briand, D. Saumier, J. Laurin, et al., Alzhemed: a potential treatment for Alzheimer's disease, Curr. Alzheimer Res. 4 (2007) 473–478.
[29] A. Geling, H. Steiner, M. Willem, L. Bally-Cuif, C. Haass, A gamma-secretase inhibitor blocks Notch signaling in vivo and causes a severe neurogenic phenotype in zebrafish, EMBO Rep. 3 (2002) 688–694. doi:10.1093/embo-reports/kvf124.
[30] S. Weggen, J.L. Eriksen, P. Das, S.A. Sagi, R. Wang, C.U. Pietrzik, et al., A subset of NSAIDs lower amyloidogenic Abeta42 independently of cyclooxygenase activity, Nature. 414 (2001) 212–216. doi:10.1038/35102591.
[31] K. Xu, X.-L. Dai, H.-C. Huang, Z.-F. Jiang, Targeting HDACs: a promising therapy for Alzheimer's disease, Oxid. Med. Cell. Longev. 2011 (2011) 143269. doi:10.1155/2011/143269.
[32] A. Fischer, F. Sananbenesi, A. Mungenast, L.-H. Tsai, Targeting the correct HDAC(s) to treat cognitive disorders, Trends Pharmacol. Sci. 31 (2010) 605–617. doi:10.1016/j.tips.2010.09.003.

[33] M.E. Ketelaar, E.M.W. Hofstra, M.R. Hayden, What monozygotic twins discordant for phenotype illustrate about mechanisms influencing genetic forms of neurodegeneration, Clin. Genet. 81 (2012) 325–333. doi:10.1111/j.1399-0004.2011.01795.x.
[34] S. Sidoli, L. Cheng, O.N. Jensen, Proteomics in chromatin biology and epigenetics: Elucidation of post-translational modifications of histone proteins by mass spectrometry, J. Proteomics. 75 (2012) 3419–3433. doi:10.1016/j.jprot.2011.12.029.
[35] A. Izzo, R. Schneider, Chatting histone modifications in mammals, Brief. Funct. Genomics. 9 (2010) 429–443. doi:10.1093/bfgp/elq024.
[36] F. Sananbenesi, A. Fischer, The epigenetic bottleneck of neurodegenerative and psychiatric diseases, Biol. Chem. 390 (2009) 1145–1153. doi:10.1515/BC.2009.131.
[37] C.P. Fitzsimons, E. van Bodegraven, M. Schouten, R. Lardenoije, K. Kompotis, G. Kenis, et al., Epigenetic regulation of adult neural stem cells: implications for Alzheimer's disease, Mol. Neurodegener. 9 (2014) 25. doi:10.1186/1750-1326-9-25.
[38] M.J. Millan, The epigenetic dimension of Alzheimer's disease: causal, consequence, or curiosity?, Dialogues Clin. Neurosci. 16 (2014) 373–393.
[39] E.L. Greer, Y. Shi, Histone methylation: a dynamic mark in health, disease and inheritance, Nat. Rev. Genet. 13 (2012) 343–357. doi:10.1038/nrg3173.
[40] O.J. Rando, Combinatorial complexity in chromatin structure and function: revisiting the histone code, Curr. Opin. Genet. Dev. 22 (2012) 148–155. doi:10.1016/j.gde.2012.02.013.
[41] A.L. Clayton, S. Rose, M.J. Barratt, L.C. Mahadevan, Phosphoacetylation of histone H3 on c-fos- and c-jun-associated nucleosomes upon gene activation, EMBO J. 19 (2000) 3714–3726. doi:10.1093/emboj/19.14.3714.
[42] M.J. Hendzel, Y. Wei, M.A. Mancini, A. Van Hooser, T. Ranalli, B.R. Brinkley, et al., Mitosis-specific phosphorylation of histone H3 initiates primarily within pericentromeric heterochromatin during G2 and spreads in an ordered fashion coincident with mitotic chromosome condensation, Chromosoma. 106 (1997) 348–360.
[43] Y. Wei, C.A. Mizzen, R.G. Cook, M.A. Gorovsky, C.D. Allis, Phosphorylation of histone H3 at serine 10 is correlated with chromosome condensation during mitosis and meiosis in Tetrahymena, Proc. Natl. Acad. Sci. U. S. A. 95 (1998) 7480–7484.
[44] S.H. Baek, When Signaling Kinases Meet Histones and Histone Modifiers in the Nucleus, Mol. Cell. 42 (2011) 274–284. doi:10.1016/j.molcel.2011.03.022.
[45] W. Li, S. Nagaraja, G.P. Delcuve, M.J. Hendzel, J.R. Davie, Effects of histone acetylation, ubiquitination and variants on nucleosome stability, Biochem. J. 296 (Pt 3) (1993) 737–744.
[46] V.M. Weake, J.L. Workman, Histone ubiquitination: triggering gene activity, Mol. Cell. 29 (2008) 653–663. doi:10.1016/j.molcel.2008.02.014.
[47] S. Bergink, F.A. Salomons, D. Hoogstraten, T.A.M. Groothuis, H. de Waard, J. Wu, et al., DNA damage triggers nucleotide excision repair-dependent monoubiquitylation of histone H2A, Genes Dev. 20 (2006) 1343–1352. doi:10.1101/gad.373706.
[48] H. Lindner, B. Sarg, H. Grunicke, W. Helliger, Age-dependent deamidation of H1(0); histones in chromatin of mammalian tissues, J. Cancer Res. Clin. Oncol. 125 (1999) 182–186. doi:10.1007/s004320050261.

[49] G.L. Cuthbert, S. Daujat, A.W. Snowden, H. Erdjument-Bromage, T. Hagiwara, M. Yamada, et al., Histone deimination antagonizes arginine methylation, Cell. 118 (2004) 545–553. doi:10.1016/j.cell.2004.08.020.
[50] N.A. Filenko, C. Kolar, J.T. West, S.A. Smith, Y.I. Hassan, G.E.O. Borgstahl, et al., The role of histone H4 biotinylation in the structure of nucleosomes, PloS One. 6 (2011) e16299. doi:10.1371/journal.pone.0016299.
[51] J.L. García-Giménez, G. Olaso, S.B. Hake, C. Bönisch, S.M. Wiedemann, J. Markovic, et al., Histone h3 glutathionylation in proliferating Mammalian cells destabilizes nucleosomal structure, Antioxid. Redox Signal. 19 (2013) 1305–1320. doi:10.1089/ars.2012.5021.
[52] B. Liu, Y. Lin, A. Darwanto, X. Song, G. Xu, K. Zhang, Identification and characterization of propionylation at histone H3 lysine 23 in mammalian cells, J. Biol. Chem. 284 (2009) 32288–32295. doi:10.1074/jbc.M109.045856.
[53] K.W. Anderson, J. Chen, M. Wang, N. Mast, I.A. Pikuleva, I.V. Turko, Quantification of Histone Deacetylase Isoforms in Human Frontal Cortex, Human Retina, and Mouse Brain, PloS One. 10 (2015) e0126592. doi:10.1371/journal.pone.0126592.
[54] K.W. Anderson, N. Mast, I.A. Pikuleva, I.V. Turko, Histone H3 Ser57 and Thr58 phosphorylation in the brain of 5XFAD mice, FEBS Open Bio. 5 (2015) 550–556. doi:10.1016/j.fob.2015.06.009.
[55] W. Yuan, K.W. Anderson, S. Li, J.L. Edwards, Subsecond absolute quantitation of amine metabolites using isobaric tags for discovery of pathway activation in Mammalian cells, Anal. Chem. 84 (2012) 2892–2899. doi:10.1021/ac203453t.
[56] R. Bąchor, P. Mielczarek, M. Rudowska, J. Silberring, Z. Szewczuk, Sensitive detection of charge derivatized peptides at the attomole level using nano-LC-ESI–MRM analysis, Int. J. Mass Spectrom. 362 (2014) 32–38. doi:10.1016/j.ijms.2014.02.018.
[57] C. Fenselau, A review of quantitative methods for proteomic studies, J. Chromatogr. B Analyt. Technol. Biomed. Life. Sci. 855 (2007) 14–20. doi:10.1016/j.jchromb.2006.10.071.
[58] J. Chen, I.V. Turko, Trends in QconCATs for targeted proteomics, Trends Anal. Chem. 57 (2014) 1–5. doi:10.1016/j.trac.2013.12.013.
[59] J.M. Pratt, D.M. Simpson, M.K. Doherty, J. Rivers, S.J. Gaskell, R.J. Beynon, Multiplexed absolute quantification for proteomics using concatenated signature peptides encoded by QconCAT genes, Nat. Protoc. 1 (2006) 1029–1043. doi:10.1038/nprot.2006.129.
[60] D.M. Simpson, R.J. Beynon, QconCATs: design and expression of concatenated protein standards for multiplexed protein quantification, Anal. Bioanal. Chem. 404 (2012) 977–989. doi:10.1007/s00216-012-6230-1.
[61] C.S.F. Cheung, K.W. Anderson, M. Wang, I.V. Turko, Natural flanking sequences for peptides included in a quantification concatamer internal standard, Anal. Chem. 87 (2015) 1097–1102. doi:10.1021/ac503697j.
[62] R.J. Beynon, M.K. Doherty, J.M. Pratt, S.J. Gaskell, Multiplexed absolute quantification in proteomics using artificial QCAT proteins of concatenated signature peptides, Nat. Methods. 2 (2005) 587–589. doi:10.1038/nmeth774.
[63] S.J. Hubbard, The structural aspects of limited proteolysis of native proteins, Biochim. Biophys. Acta. 1382 (1998) 191–206.
[64] C.-Y. Yen, S. Russell, A.M. Mendoza, K. Meyer-Arendt, S. Sun, K.J. Cios, et al., Improving sensitivity in shotgun proteomics using a peptide-centric database with reduced complexity: protease cleavage and SCX elution rules from data mining of MS/MS spectra, Anal. Chem. 78 (2006) 1071–1084. doi:10.1021/ac051127f.

[65] R. Thomson, T.C. Hodgman, Z.R. Yang, A.K. Doyle, Characterizing proteolytic cleavage site activity using bio-basis function neural networks, Bioinforma. Oxf. Engl. 19 (2003) 1741–1747.
[66] C. Lawless, S.J. Hubbard, Prediction of missed proteolytic cleavages for the selection of surrogate peptides for quantitative proteomics, Omics J. Integr. Biol. 16 (2012) 449–456. doi:10.1089/omi.2011.0156.
[67] K. Kito, K. Ota, T. Fujita, T. Ito, A synthetic protein approach toward accurate mass spectrometric quantification of component stoichiometry of multiprotein complexes, J. Proteome Res. 6 (2007) 792–800. doi:10.1021/pr060447s.
[68] D. Nanavati, M. Gucek, J.L.S. Milne, S. Subramaniam, S.P. Markey, Stoichiometry and absolute quantification of proteins with mass spectrometry using fluorescent and isotope-labeled concatenated peptide standards, Mol. Cell. Proteomics MCP. 7 (2008) 442–447. doi:10.1074/mcp.M700345-MCP200.
[69] J. Chen, M. Wang, I.V. Turko, Mass spectrometry quantification of clusterin in the human brain, Mol. Neurodegener. 7 (2012) 41. doi:10.1186/1750-1326-7-41.
[70] J. Chen, M. Wang, I.V. Turko, Quantification of amyloid precursor protein isoforms using quantification concatamer internal standard, Anal. Chem. 85 (2013) 303–307. doi:10.1021/ac3033239.
[71] J. Chen, R.Y.-C. Huang, I.V. Turko, Mass spectrometry assessment of ubiquitin carboxyl-terminal hydrolase L1 partitioning between soluble and particulate brain homogenate fractions, Anal. Chem. 85 (2013) 6011–6017. doi:10.1021/ac400831z.
[72] W.-L. Liao, I.V. Turko, Strategy combining separation of isotope-labeled unfolded proteins and matrix-assisted laser desorption/ionization mass spectrometry analysis enables quantification of a wide range of serum proteins, Anal. Biochem. 377 (2008) 55–61. doi:10.1016/j.ab.2008.03.016.
[73] E.L. Kilpatrick, W.-L. Liao, J.E. Camara, I.V. Turko, D.M. Bunk, Expression and characterization of 15N-labeled human C-reactive protein in Escherichia coli and Pichia pastoris for use in isotope-dilution mass spectrometry, Protein Expr. Purif. 85 (2012) 94–99. doi:10.1016/j.pep.2012.06.019.
[74] W.-L. Liao, G.-Y. Heo, N.G. Dodder, I.A. Pikuleva, I.V. Turko, Optimizing the conditions of a multiple reaction monitoring assay for membrane proteins: quantification of cytochrome P450 11A1 and adrenodoxin reductase in bovine adrenal cortex and retina, Anal. Chem. 82 (2010) 5760–5767. doi:10.1021/ac100811x.
[75] J. Rivers, D.M. Simpson, D.H.L. Robertson, S.J. Gaskell, R.J. Beynon, Absolute multiplexed quantitative analysis of protein expression during muscle development using QconCAT, Mol. Cell. Proteomics MCP. 6 (2007) 1416–1427. doi:10.1074/mcp.M600456-MCP200.
[76] C.-D. Chen, C.-L. Wang, C.-J. Yu, K.-Y. Chien, Y.-T. Chen, M.-C. Chen, et al., Targeted proteomics pipeline reveals potential biomarkers for the diagnosis of metastatic lung cancer in pleural effusion, J. Proteome Res. 13 (2014) 2818–2829. doi:10.1021/pr4012377.
[77] E. Vandermarliere, M. Mueller, L. Martens, Getting intimate with trypsin, the leading protease in proteomics, Mass Spectrom. Rev. 32 (2013) 453–465. doi:10.1002/mas.21376.
[78] UniProt Consortium, Activities at the Universal Protein Resource (UniProt), Nucleic Acids Res. 42 (2014) D191–198. doi:10.1093/nar/gkt1140.
[79] M. Kilgore, C.A. Miller, D.M. Fass, K.M. Hennig, S.J. Haggarty, J.D. Sweatt, et al., Inhibitors of class 1 histone deacetylases reverse contextual memory deficits in a mouse model of Alzheimer's disease, Neuropsychopharmacol. Off. Publ. Am. Coll. Neuropsychopharmacol. 35 (2010) 870–880. doi:10.1038/npp.2009.197.

[80] R.M. Stilling, A. Fischer, The role of histone acetylation in age-associated memory impairment and Alzheimer's disease, Neurobiol. Learn. Mem. 96 (2011) 19–26. doi:10.1016/j.nlm.2011.04.002.
[81] C. Simões-Pires, V. Zwick, A. Nurisso, E. Schenker, P.-A. Carrupt, M. Cuendet, HDAC6 as a target for neurodegenerative diseases: what makes it different from the other HDACs?, Mol. Neurodegener. 8 (2013) 7. doi:10.1186/1750-1326-8-7.
[82] M.A. Castello, S. Soriano, On the origin of Alzheimer's disease. Trials and tribulations of the amyloid hypothesis, Ageing Res. Rev. 13 (2014) 10–12. doi:10.1016/j.arr.2013.10.001.
[83] J.M. Levenson, K.J. O'Riordan, K.D. Brown, M.A. Trinh, D.L. Molfese, J.D. Sweatt, Regulation of histone acetylation during memory formation in the hippocampus, J. Biol. Chem. 279 (2004) 40545–40559. doi:10.1074/jbc.M402229200.
[84] A. Fischer, F. Sananbenesi, X. Wang, M. Dobbin, L.-H. Tsai, Recovery of learning and memory is associated with chromatin remodelling, Nature. 447 (2007) 178–182. doi:10.1038/nature05772.
[85] R.C. Agis-Balboa, Z. Pavelka, C. Kerimoglu, A. Fischer, Loss of HDAC5 impairs memory function: implications for Alzheimer's disease, J. Alzheimers Dis. 33 (2013) 35–44. doi:10.3233/JAD-2012-121009.
[86] R. Sando, N. Gounko, S. Pieraut, L. Liao, J. Yates III, A. Maximov, HDAC4 governs a transcriptional program essential for synaptic plasticity and memory, Cell. 151 (2012) 821–834. doi:10.1016/j.cell.2012.09.037.
[87] T. Kawabata, K. Nishida, K. Takasugi, H. Ogawa, K. Sada, Y. Kadota, et al., Increased activity and expression of histone deacetylase 1 in relation to tumor necrosis factor-alpha in synovial tissue of rheumatoid arthritis, Arthritis Res. Ther. 12 (2010) R133. doi:10.1186/ar3071.
[88] A.K.B. Lucio-Eterovic, M.A.A. Cortez, E.T. Valera, F.J.N. Motta, R.G.P. Queiroz, H.R. Machado, et al., Differential expression of 12 histone deacetylase (HDAC) genes in astrocytomas and normal brain tissue: class II and IV are hypoexpressed in glioblastomas, BMC Cancer. 8 (2008) 243. doi:10.1186/1471-2407-8-243.
[89] R.S. Broide, J.M. Redwine, N. Aftahi, W. Young, F.E. Bloom, C.J. Winrow, Distribution of histone deacetylases 1-11 in the rat brain, J. Mol. Neurosci. MN. 31 (2007) 47–58.
[90] H.-H. Yeh, M. Tian, R. Hinz, D. Young, A. Shavrin, U. Mukhapadhyay, et al., Imaging epigenetic regulation by histone deacetylases in the brain using PET/MRI with ^{18}F-FAHA, NeuroImage. 64 (2013) 630–639. doi:10.1016/j.neuroimage.2012.09.019.
[91] J. Chen, M. Wang, I.V. Turko, Quantification of amyloid precursor protein isoforms using quantification concatamer internal standard, Anal. Chem. 85 (2013) 303–307. doi:10.1021/ac3033239.
[92] M. Wang, J. Chen, I.V. Turko, 15N-labeled full-length apolipoprotein E4 as an internal standard for mass spectrometry quantification of apolipoprotein E isoforms, Anal. Chem. 84 (2012) 8340–8344. doi:10.1021/ac3018873.
[93] J. Chen, I.A. Pikuleva, I.V. Turko, Mass spectrometry quantification of PICALM and AP180 in human frontal cortex and neural retina, Anal. Biochem. 442 (2013) 253–258. doi:10.1016/j.ab.2013.08.005.
[94] W. Zheng, R.E. Reem, S. Omarova, S. Huang, P.L. DiPatre, C.D. Charvet, et al., Spatial distribution of the pathways of cholesterol homeostasis in human retina, PloS One. 7 (2012) e37926. doi:10.1371/journal.pone.0037926.
[95] B. MacLean, D.M. Tomazela, S.E. Abbatiello, S. Zhang, J.R. Whiteaker, A.G. Paulovich, et al., Effect of collision energy optimization on the measurement of

peptides by selected reaction monitoring (SRM) mass spectrometry, Anal. Chem. 82 (2010) 10116–10124. doi:10.1021/ac102179j.
[96] J.S. O'Brien, E.L. Sampson, Lipid composition of the normal human brain: gray matter, white matter, and myelin, J. Lipid Res. 6 (1965) 537–544.
[97] C. Urbich, L. Rössig, D. Kaluza, M. Potente, J.-N. Boeckel, A. Knau, et al., HDAC5 is a repressor of angiogenesis and determines the angiogenic gene expression pattern of endothelial cells, Blood. 113 (2009) 5669–5679. doi:10.1182/blood-2009-01-196485.
[98] C. Cook, T.F. Gendron, K. Scheffel, Y. Carlomagno, J. Dunmore, M. DeTure, et al., Loss of HDAC6, a novel CHIP substrate, alleviates abnormal tau accumulation, Hum. Mol. Genet. 21 (2012) 2936–2945. doi:10.1093/hmg/dds125.
[99] G. Li, H. Jiang, M. Chang, H. Xie, L. Hu, HDAC6 α-tubulin deacetylase: a potential therapeutic target in neurodegenerative diseases, J. Neurol. Sci. 304 (2011) 1–8. doi:10.1016/j.jns.2011.02.017.
[100] M. Jakovcevski, R. Bharadwaj, J. Straubhaar, G. Gao, D.P. Gavin, I. Jakovcevski, et al., Prefrontal cortical dysfunction after overexpression of histone deacetylase 1, Biol. Psychiatry. 74 (2013) 696–705. doi:10.1016/j.biopsych.2013.03.020.
[101] L. Zhang, S. Sheng, C. Qin, The role of HDAC6 in Alzheimer's disease, J. Alzheimers Dis. JAD. 33 (2013) 283–295. doi:10.3233/JAD-2012-120727.
[102] M. Gonzalez-Zuñiga, P.S. Contreras, L.D. Estrada, D. Chamorro, A. Villagra, S. Zanlungo, et al., c-Abl stabilizes HDAC2 levels by tyrosine phosphorylation repressing neuronal gene expression in Alzheimer's disease, Mol. Cell. 56 (2014) 163–173. doi:10.1016/j.molcel.2014.08.013.
[103] J. Gräff, D. Rei, J.-S. Guan, W.-Y. Wang, J. Seo, K.M. Hennig, et al., An epigenetic blockade of cognitive functions in the neurodegenerating brain, Nature. 483 (2012) 222–226. doi:10.1038/nature10849.
[104] K. Kaarniranta, A. Salminen, A. Haapasalo, H. Soininen, M. Hiltunen, Age-related macular degeneration (AMD): Alzheimer's disease in the eye?, J. Alzheimers Dis. 24 (2011) 615–631. doi:10.3233/JAD-2011-101908.
[105] K. Ohno-Matsui, Parallel findings in age-related macular degeneration and Alzheimer's disease, Prog. Retin. Eye Res. 30 (2011) 217–238. doi:10.1016/j.preteyeres.2011.02.004.
[106] S. Tiwari, S. Dharmarajan, M. Shivanna, D.C. Otteson, T.L. Belecky-Adams, Histone deacetylase expression patterns in developing murine optic nerve, BMC Dev. Biol. 14 (2014) 30. doi:10.1186/1471-213X-14-30.
[107] Y. Wang, Y.-L. Zhang, K. Hennig, J.P. Gale, Y. Hong, A. Cha, et al., Class I HDAC imaging using [(3)H]CI-994 autoradiography, Epigenetics Off. J. DNA Methylation Soc. 8 (2013) 756–764. doi:10.4161/epi.25202.
[108] R. Loury, P. Sassone-Corsi, Histone phosphorylation: how to proceed, Methods San Diego Calif. 31 (2003) 40–48.
[109] O. Ogawa, X. Zhu, H.-G. Lee, A. Raina, M.E. Obrenovich, R. Bowser, et al., Ectopic localization of phosphorylated histone H3 in Alzheimer's disease: a mitotic catastrophe?, Acta Neuropathol. (Berl.). 105 (2003) 524–528. doi:10.1007/s00401-003-0684-3.
[110] P. Cheung, C.D. Allis, P. Sassone-Corsi, Signaling to chromatin through histone modifications, Cell. 103 (2000) 263–271.
[111] P.J. Hurd, A.J. Bannister, K. Halls, M.A. Dawson, M. Vermeulen, J.V. Olsen, et al., Phosphorylation of histone H3 Thr-45 is linked to apoptosis, J. Biol. Chem. 284 (2009) 16575–16583. doi:10.1074/jbc.M109.005421.

[112] S.L. Hammond, S.D. Byrum, S. Namjoshi, H.K. Graves, B.K. Dennehey, A.J. Tackett, et al., Mitotic phosphorylation of histone H3 threonine 80, Cell Cycle Georget. Tex. 13 (2014) 440–452. doi:10.4161/cc.27269.
[113] J.A. North, S. Javaid, M.B. Ferdinand, N. Chatterjee, J.W. Picking, M. Shoffner, et al., Phosphorylation of histone H3(T118) alters nucleosome dynamics and remodeling, Nucleic Acids Res. 39 (2011) 6465–6474. doi:10.1093/nar/gkr304.
[114] D.F. Zielinska, F. Gnad, M. Jedrusik-Bode, J.R. Wiśniewski, M. Mann, Caenorhabditis elegans has a phosphoproteome atypical for metazoans that is enriched in developmental and sex determination proteins, J. Proteome Res. 8 (2009) 4039–4049. doi:10.1021/pr900384k.
[115] L.A.M. Brown, J. Jin, D. Ferrell, E. Sadic, D. Obregon, A.J. Smith, et al., Efavirenz promotes β-secretase expression and increased Aβ1-40,42 via oxidative stress and reduced microglial phagocytosis: implications for HIV associated neurocognitive disorders (HAND), PloS One. 9 (2014) e95500. doi:10.1371/journal.pone.0095500.
[116] N. Mast, Y. Li, M. Linger, M. Clark, J. Wiseman, I.A. Pikuleva, Pharmacologic stimulation of cytochrome P450 46A1 and cerebral cholesterol turnover in mice, J. Biol. Chem. 289 (2014) 3529–3538. doi:10.1074/jbc.M113.532846.
[117] E. Hudry, D. Van Dam, W. Kulik, P.P. De Deyn, F.S. Stet, O. Ahouansou, et al., Adeno-associated virus gene therapy with cholesterol 24-hydroxylase reduces the amyloid pathology before or after the onset of amyloid plaques in mouse models of Alzheimer's disease, Mol. Ther. J. Am. Soc. Gene Ther. 18 (2010) 44–53. doi:10.1038/mt.2009.175.
[118] E.Y. Bryleva, M.A. Rogers, C.C.Y. Chang, F. Buen, B.T. Harris, E. Rousselet, et al., ACAT1 gene ablation increases 24(S)-hydroxycholesterol content in the brain and ameliorates amyloid pathology in mice with AD, Proc. Natl. Acad. Sci. U. S. A. 107 (2010) 3081–3086. doi:10.1073/pnas.0913828107.
[119] L.M. Refolo, B. Malester, J. LaFrancois, T. Bryant-Thomas, R. Wang, G.S. Tint, et al., Hypercholesterolemia accelerates the Alzheimer's amyloid pathology in a transgenic mouse model, Neurobiol. Dis. 7 (2000) 321–331. doi:10.1006/nbdi.2000.0304.
[120] M. Simons, P. Keller, B. De Strooper, K. Beyreuther, C.G. Dotti, K. Simons, Cholesterol depletion inhibits the generation of beta-amyloid in hippocampal neurons, Proc. Natl. Acad. Sci. U. S. A. 95 (1998) 6460–6464.
[121] T.-H. Liao, Reversible Inactivation of Pancreatic Deoxyribonuclease A by Sodium Dodecyl Sulfate, J. Biol. Chem. 250 (1975) 3831–3836.
[122] M.D. Womack, D.A. Kendall, R.C. MacDonald, Detergent effects on enzyme activity and solubilization of lipid bilayer membranes, Biochim. Biophys. Acta. 733 (1983) 210–215.
[123] S.B. Hake, C.D. Allis, Histone H3 variants and their potential role in indexing mammalian genomes: the "H3 barcode hypothesis," Proc. Natl. Acad. Sci. U. S. A. 103 (2006) 6428–6435. doi:10.1073/pnas.0600803103.
[124] R.D. Camerini-Otero, G. Felsenfeld, Histone H3 disulfide dimers and nucleosome structure, Proc. Natl. Acad. Sci. U. S. A. 74 (1977) 5519–5523.
[125] I. Hong, T. Kang, Y. Yoo, R. Park, J. Lee, S. Lee, et al., Quantitative proteomic analysis of the hippocampus in the 5XFAD mouse model at early stages of Alzheimer's disease pathology, J. Alzheimers Dis. JAD. 36 (2013) 321–334. doi:10.3233/JAD-130311.
[126] Y. Tsunaka, N. Kajimura, S. Tate, K. Morikawa, Alteration of the nucleosomal DNA path in the crystal structure of a human nucleosome core particle, Nucleic Acids Res. 33 (2005) 3424–3434. doi:10.1093/nar/gki663.

[127] A. Warnecke, T. Sandalova, A. Achour, R.A. Harris, PyTMs: a useful PyMOL plugin for modeling common post-translational modifications, BMC Bioinformatics. 15 (2014) 370. doi:10.1186/s12859-014-0370-6.
[128] P.M. Thompson, K.M. Hayashi, G. de Zubicaray, A.L. Janke, S.E. Rose, J. Semple, et al., Dynamics of gray matter loss in Alzheimer's disease, J. Neurosci. Off. J. Soc. Neurosci. 23 (2003) 994–1005.
[129] C. Wu, C.D. Allis, Nucleosomes, histones & chromatin. Part A Part A, Elsevier/Academic Press, Amsterdam, Netherland; Boston, Mass., 2012. http://public.eblib.com/choice/publicfullrecord.aspx?p=1019660 (accessed May 8, 2015).
[130] H. Xu, M.A. Freitas, A mass accuracy sensitive probability based scoring algorithm for database searching of tandem mass spectrometry data, BMC Bioinformatics. 8 (2007) 133. doi:10.1186/1471-2105-8-133.
[131] H. Xu, M.A. Freitas, Automated diagnosis of LC-MS/MS performance, Bioinforma. Oxf. Engl. 25 (2009) 1341–1343. doi:10.1093/bioinformatics/btp155.
[132] V. Mayya, K. Rezual, L. Wu, M.B. Fong, D.K. Han, Absolute quantification of multisite phosphorylation by selective reaction monitoring mass spectrometry: determination of inhibitory phosphorylation status of cyclin-dependent kinases, Mol. Cell. Proteomics MCP. 5 (2006) 1146–1157. doi:10.1074/mcp.T500029-MCP200.
[133] V. Morales, H. Richard-Foy, Role of histone N-terminal tails and their acetylation in nucleosome dynamics, Mol. Cell. Biol. 20 (2000) 7230–7237.
[134] H.C. Beck, E.C. Nielsen, R. Matthiesen, L.H. Jensen, M. Sehested, P. Finn, et al., Quantitative proteomic analysis of post-translational modifications of human histones, Mol. Cell. Proteomics MCP. 5 (2006) 1314–1325. doi:10.1074/mcp.M600007-MCP200.
[135] E. Montellier, F. Boussouar, S. Rousseaux, K. Zhang, T. Buchou, F. Fenaille, et al., Chromatin-to-nucleoprotamine transition is controlled by the histone H2B variant TH2B, Genes Dev. 27 (2013) 1680–1692. doi:10.1101/gad.220095.113.
[136] A. Darwanto, M.P. Curtis, M. Schrag, W. Kirsch, P. Liu, G. Xu, et al., A modified "cross-talk" between histone H2B Lys-120 ubiquitination and H3 Lys-79 methylation, J. Biol. Chem. 285 (2010) 21868–21876. doi:10.1074/jbc.M110.126813.
[137] R.Y. Tweedie-Cullen, J.M. Reck, I.M. Mansuy, Comprehensive mapping of post-translational modifications on synaptic, nuclear, and histone proteins in the adult mouse brain, J. Proteome Res. 8 (2009) 4966–4982. doi:10.1021/pr9003739.
[138] S.N. Thomas, D. Cripps, A.J. Yang, Proteomic analysis of protein phosphorylation and ubiquitination in Alzheimer's disease, Methods Mol. Biol. Clifton NJ. 566 (2009) 109–121. doi:10.1007/978-1-59745-562-6_8.